Activity-based Sulfatase and Affinity-based Metalloprotease Probes:

Ready for Take-off

Dissertation

presented to the Department of Chemistry
Bielefeld University

in partial fulfillment of the requirements for
the degree of *Doctor rerum naturalium* (Dr. rer. nat.)

by

Janina Lenger

May 2011

1^{st} reviewer: Prof. Dr. Norbert Sewald
Bioorganic and Organic Chemistry
Bielefeld University

2^{nd} reviewer: Prof. Dr. Thomas Dierks
Biochemistry I
Bielefeld Universtiy

Information, no matter how beautifully it is packaged or repackaged, does not equal an idea. Information is nothing more than the raw stuff that might lead you to something new. Having lots of it doesn't make you any cleverer. You can segment it, dimension it or color-code it if the mood takes you. But until it's seeded with an idea that leads into action, it's just a lump of words and figures.

John Hunt, the art of the idea

Acknowledgment

Accomplishing one of my goals in life, my dissertation, I want to acknowledge the contributions, encouragement, and support of many colleagues and friends:

I am grateful for the amount of trust my supervisor Norbert Sewald rewarded me with over the past years. Thank you for giving me the space I needed to grow and gain confidence in myself. I sincerely recognize all the decisions you let me make and your trust in my capability as a scientist. This dissertation was extremely dependent on finding cooperation partners, and you considered and approved all of them. I thank you for proposing me to the Studienstiftung des deutschen Volkes which supported me financially during the past years.

I also want to thank Thomas Dierks who was always interested in and enthusiastic about our project. Without your help concerning my lab internship at The Scripps Research Institute scientifically and administratively, this stay would not have been the success it was. I also thank you for taking over the chore of reviewing this dissertation. Your co-workers Eva C. Ennemann and Dr. Marc-André Frese have greatly contributed to the sulfatase part of my PhD. I especially thank Eva for all her help in the lab and being a friend during our studies at Bielefeld University.

The interdisciplinary character of my projects demanded the collaboration of different specialists who taught me a lot about the methods they use and also the way they conduct research: Dr. R.A.L. van der Hoorn and Dr. F. Kaschani from the MPI for Plant Breeding Research, Cologne: Thank you for giving me the opportunity to join your lab and for your help concerning plant biochemical and ABP methods. The way you focus your research on outcome was eye-opening. Renier, thank you so much

for supervising me during the week I spent writing our manuscript in Cologne.

Prof. Dr. H. Köster, Dr. C. Dalhoff, T. Lenz and Dr. O. Gräbner at caprotec bioanalytics GmbH, Berlin: I am very grateful for our fruitful cooperation that led to the release of the Marimastat-Kit. It was a valuable experience for me to work in an industrial research environment.

Prof. Dr. C.-H. Wong, Dr. S.R. Hanson and T. Gresham with The Scripps Research Institute in La Jolla, USA: Thank you so much for opening your lab to me. It was thrilling to be part of this inspiring community. To Sarah I am indebted for sharing her CySA- as well as life-experience with me. It was incredibly exciting for me to discuss and talk to you: there should be more women like you in science! Your help concerning language and finding the right words together with the fact that you generously discussed your insights with me helped getting this thing done with! Tanya: thank you so much for your help during visa application and getting started. I never met an administrative staff member like you!

For countless NMR and MS service measurements I want to thank K.-P. Mester, S. Heitkamp, O. Kollas and Dr. M. Letzel. I am especially grateful to Dr. A. Mix, L. Nagel and Dr. K. Gaus for measuring time-dependent ^{19}F-NMR spectra. Dr. R. Hoffrogge, B. Müller and S. Albaum from the faculty of technology have helped me with LC-MS/MS- and QuPE-analysis of sulfatase samples. Thanks so much for being patient and helpful in explaining these things to a computer-idiot like me. To Prof. Dr. K.-J. Dietz I am indebted to for organizing *Nicotiana benthamiana* plants for me at the University's green house.

This big THANK YOU is for all the students, apprentices and technicians who contributed to this PhD by working in my lab (in the order of appearance): D. Urbisch, A. Niess, A. Muschinski, S. Rasche (I am so happy to have had you in my lab: you taught me more than I was able

to teach you!), M. Höfener (for cool stuff daily, and being the sunshine of the lab), C. Sollert (for introducing me to some great music and speaking swedish at times), K.-K. Prior (for sticking with it even though things got very repetitive), L. Brokmann, T. Preuße, and M. Schröder (for making me feel very young and very old at the same time). I also want to thank all current, and past members of my group. It was great working with you. Luckily, some of you became close friends: Carolin and Patrik Plattner who I extremely miss to talk to on a daily basis. It's been fun cooking, eating and drinking with you! Anna Norgren the one I can always trust since she's a doctor (sometimes a bit touretty though). I miss laughing with you, and hopefully we will be able to continue our long-distance friendship. And of course Ansgar Zobel, Michi Höfener and Felix Mertink who always find encouraging words of wisdom, humor, and *Feierabendbier*. You all helped me cope with the everyday ups and downs.

There are many friends that accompanied me during the past years, and I would not have made it to this point without the possibility of forgetting all about work once in a while. I thank all of you!

Der größte Dank geht jedoch an meine Eltern, meine Brüder Thorsten und Marcus, meine Schwägerinnen Daniela und Dagny sowie meine großartigen Neffen: Ole, Leo, Mats und Noa. Ihr alle habt mir gezeigt, dass es wichtigere Dinge als meine Promotion gibt: die Liebe und den Zusammenhalt unserer Familie. Auch meiner Schwiegerfamilie in spe Vlado, Milka, Daniel und Mareike möchte ich für all ihren Rückhalt und die ständige Bestätigung danken. Ich bin froh, dass Olli so eine tolle Sippschaft hat, die mich von Anfang an wie eine Tochter/Schwester aufgenommen hat. Ich liebe Euch alle sehr!

Abschließend möchte ich mich bei meinem Freund Oliver Tosic bedanken. Ich freue mich auf unsere Zukunft und bin Dir unendlich dankbar für einfach alles. Niemand sieht mich wie Du.

Parts of this work have been published in:

J. Lenger, M. Schröder, E.C. Ennemann, B. Müller, C.-H. Wong, T. Noll, T. Dierks, S.R. Hanson, N. Sewald, Evaluation of Sulfatase-Directed Quinone Methide Traps for Proteomics, *Bioorg. Med. Chem.*, doi:10.1016/j.bmc.2011.04.044.

J. Lenger, F. Kaschani, T. Lenz, C. Dalhoff, H. Köster, N. Sewald, R.A.L. van der Hoorn, Labeling and Enrichment of Arabidopsis thaliana Matrix Metalloproteases Using an Acitve-Site Directed, Marimastat-based Photoreactive Probe, *Bioorg. Med. Chem.* **2011**, accepted.

Abbreviations

2D	two-dimensional
4-MUS	4-methylumbilleferyl sulfate
A	adenine, alanine
ABP	activity-based proteomics
ACN	acetonitrile
AH	addition-hydrolysis
Alloc	allyloxycarbonyl
APCI	atmospheric pressure chemical ionization
APS	ammonium persulfate
ar	aryl
ARS	aryl sulfatase
At	*Arabidopsis thaliana*
BCI	Biochemistry I
Boc_2O	di-*tert*-butyldicarbonate
BODIPY	dipyrromethene boron difluoride
bp	base pairs
BSA	bovine serum albumine
C	cytosine, cysteine
calcd.	calculated
CCD	charged coupled device
CCMS	capture compound mass spectrometry
cDNA	complementary DNA
CE	collision energy
CNBr	cyanogenbromide
cpm	counts per minute
CuAAC	Cu(I) catalyzed [3+2] azide-alkyne cycloaddition

Cy	cyanine
CySA	cyclic sulfamate
δ	chemical shift (NMR-spectroscopy)
d	doublet (NMR-spectroscopy)
DAST	diethylaminosulfur trifluoride
DBU	1,8-diazabicyclo[5.4.0]undec-7-ene
DCM	dichloromethane
DFPS	difluoromethylphenyl sulfate
^{3}DHEAS	^{3}H-dehydroepiandrosterone-3-sulfate
DIPEA	*N*,*N*-diisopropylethylamine
DMF	dimethylformamide
DMAP	dimethylaminopyridine
DMSO	dimethylsulfoxide
DNA	deoxyribonucleic acid
dNTP	deoxynucleoside triphosphate
DTT	dithiothreitol
E	glutamate
EA	ethylacetate
ECL	enhanced chemoluminescence
ECM	extracellular matrix
E. coli	*Escherichia coli*
EDC	*N*-ethyl-*N'*-(3-dimethylaminopropyl)-carbodiimid
EDTA	ethylendiamine tetraacetic acid
Enz	enzyme
ER	endoplasmic reticulum
ESI	electrospray ionization
EtOH	ethanol
Et_2O	diethylether
eq.	equivalents

FA	formic acid
FDR	false discovery rate
FGE	formylglycine generating enzyme
FGly	formylglycine
Fmoc	9-fluorenylmethoxycarbonyl
FRET	Förster resonance energy transfer
FT	fourier transform
g	earth's gravity, g = 9.8 m/s^2
G	guanine, glycine
GE	gel electrophoresis
GFP	green fluorescent protein
GPI	glycosylphosphoinositol
H	histidine
HA	hemagglutinin
HFIP	hexafluoroisopropanol
HOBt	1-Hydroxy-1-*H*-benzotriazol
HPLC	high performance liquid chromatography
HRP	horseradish peroxidase
IC_{50}	inhibitor concentration at 50 % residual enzyme activity
ICR	ion cyclotron resonance
IEF	isoelectric focussing
IPG	immobilized pH gradient
J	scalare coupling constant (NMR spectroscopy)
KARS	*Klebsiella pneumoniae* aryl sulfatase
L	Lysine
λ	wavelength
LB	lysogeny broth
LC	liquid chromatography
LiSA	linear sulfamate

Lys	lysine
m	multiplet (NMR-spectroscopy)
MALDI-ToF	matrix assisted laser desorption ionisation time of flight
MCS	multiple cloning site
MeOH	methanol
MFPS	monofluoromethylphenyl sulfate
MMP	matrix metalloprotease
MP	metalloprotease
MPI	Max Planck Institute
MS	mass spectrometry
NHS	*N*-hydroxysuccinimide
NMM	*N*-methylmorpholine
NMMP	*Nicotiana benthamiana* MMP
NMR	nuclear magnetic resonance
OAc	acetyl
OD_{600}	optical density at a wavelength of 600 nm
on	overnight
P	proline
PARS	*Pseudomonas aeruginosa* aryl sulfatase
PBS	phosphate buffered saline
PCR	polymerase chain reaction
*p*NCS	*para*-nitrocatechol sulfate
ppm	parts per million
PVDF	polyvinylidene fluoride
PyBOP	benzotriazol-1-yl-oxytripyrrolidinophosphonium hexafluorophosphate
QM	quinone methide
R	arginine
RECK	reversion-inducing cysteine-rich protein with Kazal motifs
RP	reversed phase

rpm	rotations per minute
rt	room temperature
s	singlet (NMR-spectroscopy)
S	serine
SDS	sodium dodecyl sulfate
STS	steroid sulfatase
t	triplet (NMR-spectroscopy)
T	thymine, threonine
TAE	tris acetate EDTA buffer
Taq	*Thermus aquaticus*
TBS	tris buffered saline
TBTA	tris-[(1-benzylic-1*H*-1,2,3-triazole-4-yl)methyl]-amine
TBTU	*O*-(benzotriazole-1-yl)-*N*,*N*,*N*′,*N*′-tetramethyluronium tetrafluoroborate
TCA	trichloroacetic acid
TCE	trichloroethyl
TE	transesterification-elimination
TEA	triethylamine
TEMED	*N*,*N*,*N*′,*N*′-tetramethylethylene diamine
TFA	trifluoroacetic acid
THF	tetrahydrofurane
TIMP	tissue inhibitor of metalloprotease
TLC	thin layer chromatography
TM	transmembrane
TMS	tetramethylsilane
Tris	tris-(hydroxymethyl)-aminomethane
TSRI	The Scripps Research Institute
U	unit(s), uracil
UV	ultraviolet

v/v	volume per volume
WB	western blotting
w/v	weight per volume
X	variable amino acid

Contents

1 Abstract

Recent advances in genome sequencing and annotation have provided major challenges of assigning functions to the magnitude of predicted novel proteins. In addition, disorders and pathological conditions need to be related to the responsible protein misregulations. As the analysis and characterization of low abundant proteins or protein families from complex mixtures is still out of reach using standard proteomics methods like 2D-GE/MS or LC-MS/MS, new techniques to circumvent problems with proteome complexity are of high value.

In this work these challenges are approached by selectively addressing enzyme classes based on their activity or affinity profiles for the creation of subproteomes.[1] Over the past decade activity-based proteomics (ABP) has developed into a powerful method for the comparison of different proteome states,[2] inhibitor screenings[3] and discovery of novel enzymes.[4] Our focus was on matrix metalloproteases (MMPs) and sulfatases since the activity of both protein families is post-translationally regulated *in vivo*, and changes in their respective activity levels are responsible for several pathological conditions.[5,6]

Sulfatases

Sulfatases cleave a wide variety of sulfate esters with substrate specificities ranging from sulfated lipids over sulfated steroids to complex sulfated proteoglycans. Their physiological involvement in processes like hormone-dependent cancer, cell signaling and pathogen infection has only recently been revealed.[7] Probes with two different mechanism-based

targeting groups were synthesized, biochemically evaluated and applied to address this enzyme class with emerging impact.

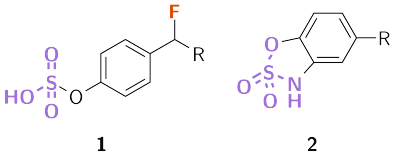

Figure 1.1: Structures of QM precursor probe **1** and cyclic sulfamate **2**.

The first activity-based inhibitor we assessed was the previously reported quinone methide (QM) precursor **1**.[8,9] Upon **sulfate** cleavage by a sulfatase, **fluoride** is eliminated and a quinone methide species generated. This electrophilic intermediate is then supposedly attacked by a nucleophile of the sulfatase active site to induce inactivation and labeling. ^{19}F-NMR and inhibition studies as well as labeling experiments with human and bacterial sulfatases were conducted. All studies demonstrated a high turnover rate of QM precursor probes in combination with unspecifically labeled background proteins.

To overcome these problems, **cyclic sulfamates** (CySAs) **2** were investigated for their inhibitory potential against a panel of human and bacterial sulfatases. The CySA binding mechanism was partially elucidated by chemoselective labeling of the sulfatase active site residue formylglycine (FGly). Additionally CySA probes were able to label sulfatases with improved selectivity compared to quinone methide type probes. A novel bioorthogonal *in situ* labeling procedure utilizing copper catalyzed azide-alkyne cycloaddition (CuAAC) was implemented for this probe class.

Matrix metalloproteases

Human MMPs play a role in cancer-related processes like metastasis and angiogenesis as well as in normal and pathological tissue remodeling (e.g. wound healing, placenta reduction after child birth or rheumatoid arthritis).[10] So far MMPs have mostly been studied using traditional biochemical methods such as zymography for visualization of activity states in physiological fluids like blood, plasma or synovia.[11] In contrast to the magnitude of zymography-based studies, there are only few examples for affinity-based photoinduced covalent MMP labeling,[12–17] the charac-

terization of reversibly binding MMP probes[18,19] and inhibitor affinity chromatography of MMPs from synovia.[20]

The concept of photoreactive affinity-based probes was applied to the selective labeling of *Arabidopsis thaliana* MMPs (At-MMPs). Of the five At-MMPs which were discovered by homology searches using human MMP-7[21] four At-MMPs were transiently expressed via *Agrobacterium tumefaciens* infiltration of *Nicotiana benthamiana* leaves. Infected leaves showed a phenotype which was a first strong indicator for metalloprotease activity. Protein expression was reviewed and optimized by western blotting of the leaf extracts using a hemagglutinin (HA) tag.

The well-known hydroxamic acid marimastat[22] was chosen for this affinity-based approach since the high homology between human MMP-7 and the At-MMPs might render them susceptible to this inhibitor. Marimastat affinity labeling of At-MMPs was realized by application of a tool developed in cooperation with caprotec bioanalytics GmbH, Berlin. They attached a **marimastat-based affinity probe** synthesized in our laboratory[19,23,24] to a **perfluorinated aryl azide** photoreactive group and **biotin** as reporter group. Probe **3** binds to MMPs based on the reversible marimastat moiety, and upon UV-irradiation the photoreactive group establishes a covalent bond to the captured protein. The protein-probe complex can then be extracted by streptavidin pull-down. Probe **3** was validated by IC_{50}-value determination for the inhibition of human MMP-2 following a previously established protocol[19,23] as well

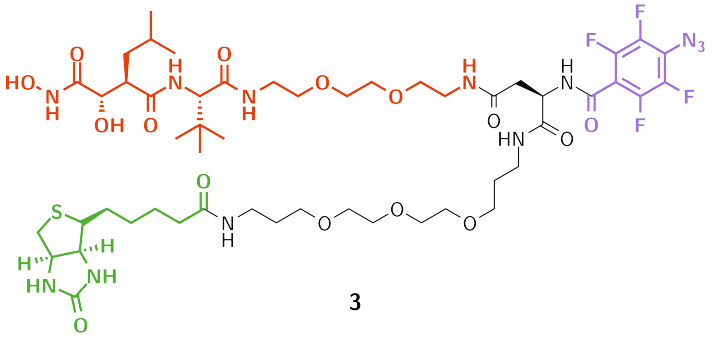

Figure 1.2: At-MMP targeting probe **3**. **Marimastat-based affinity probe**, **photoreactive group**, **biotin**.

as labeling of human MMP-9 before applying it to affinity-based labeling of At-MMPs. A specific and covalent interaction between the human MMP inhibitor marimastat and several At-MMPs as well as an endogenous MMP from *Nicotiana benthamiana* was demonstrated by LC-MS/MS analyses as well as streptavidin blotting.

2 Introduction to Activity- and Affinity-Based Proteomics

Proteomics comprises the analysis of the whole complement of proteins, and this includes the elucidation of various protein characteristics apart from abundance. Structure, interactions, post-translational modifications, localization and enzymatic activity are all decisive features for protein function. Assessing this information at once in a given proteome is out of reach even with the latest techniques at hand. Moreover, proteome states are time- and condition-dependent and neither accurately defined nor static.[25] Apart from conventional 2D-GE followed by fingerprint analysis for identification of the separated proteins, several high-throughput techniques for proteome characterization have been developed including LC-MS/MS strategies[26] and protein microarrays.[27] Yet, all of them still fail to assess *in vivo* activity of proteins which is arguably the most important protein feature since it is directly responsible for physiological or pathological conditions observed. There has been and still is a need for new tools to measure and detect specific activities within whole proteomes. One approach in chemical proteomics is to target enzymes with active site-directed activity- or affinity-based probes which is commonly referred to in the literature as activity-based proteomics (ABP).[28]

Why do we need ABP?

ABP displays the most powerful technique up to date for the selective analysis of active enzymes. Figure 2.1 schematically shows the two main workflows. Synthetic small molecule probes containing a **target-**

ing group and a **tag** connected by a **linker** are utilized to covalently label active sites of enzymes in a protein sample.

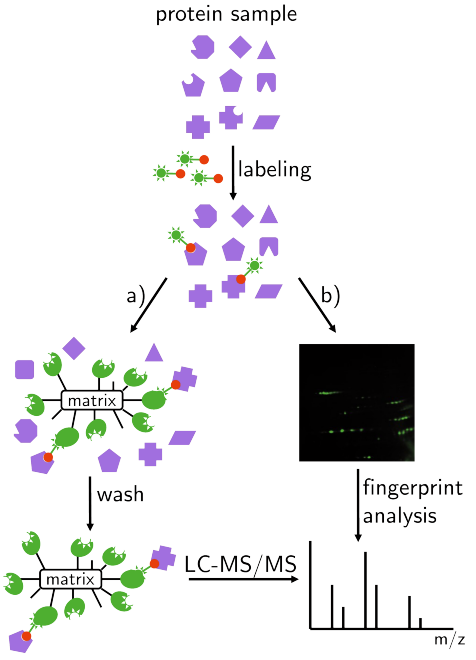

Figure 2.1: Schematic representation of the main ABP procedures. a) Biotinylated proteins are separated via streptavidin pull-down. After washing the bound proteins are trypsinated and identified by LC-MS/MS. b) Fluorescence dye-labeled proteins are visualized in-gel, trypsinated and identified in MS fingerprint analysis.

Biotinylated probes are used to first enrich labeled proteins on avidin or streptavidin beads and thereby separate them from the non-labeled background. Bound proteins are trypsinated directly on beads and identified in gel-free LC-MS/MS analysis. Fluorescent probes are used for gel-based approaches with protein separation via 1D- or 2D-GE. Labeling events are visualized in-gel with a fluorescence scanner allowing the subsequent fingerprint analysis of labeled proteins for identification purposes.

Most probes bind a wide variety of enzymes of the same family or with similar catalytic properties. Thereby, a whole group of proteins is rendered susceptible to downstream analysis in one experiment.[29] The majority of activity-based studies aim at the understanding of enzyme involvement in specific processes[2] thus improving the knowledge on the relationship between activity and function of many enzyme classes.[30] Another important application of ABP is inhibitor screening using a sophisticated probe in combination with inhibitors displaying uncharacterized inhibition profiles. A complex protein sample is pre-incubated with the inhibitor before labeling with the probe, and from the binding competition between them, new protein targets of unknown inhibitors can be assigned.[31] A multitude of reviews

ABP applications

has been published on ABP summarizing biochemical results and applications comprehensively.[32–36] This introduction gives a condensed summary of the growing field and exemplarily shows synthetic approaches and biochemical applications possible so far pointing at drawbacks and limitations.

2.1 Probe Design – the Crucial Step

Synthetic probes are the basis of each activity- or affinity-based study. They consist of a targeting group responsible for binding to the protein of interest, a linker and a reporter tag which is usually biotin or a fluorescence dye. Sensible probe design is the prerequisite for the success of subsequent biochemical applications. All probe moieties have to be adjusted to the scope of each individual study since shortcomings in design are costly if the synthetic strategy has to be altered and probe synthesis repeated.

2.1.1 Targeting Groups

The key feature of all probes is the targeting group since it is decisive for the proteins which are actually labeled. There are examples for irreversible as well as reversible inhibitors in ABP approaches. Irreversible inhibitors are incorporated into activity-based probes which necessitate probe conversion by the target enzyme for labeling.

Activity-based probes as displayed in Figure 2.2 are usually attacked by the enzyme to directly create a covalent adduct (mechanism-based inhibitors, **4**–**8**). Alternatively, a reactive derivative of the probe is created in the course of the enzyme reaction that should immediately bind and inactivate the enzyme (suicide inhibitors, **1**).

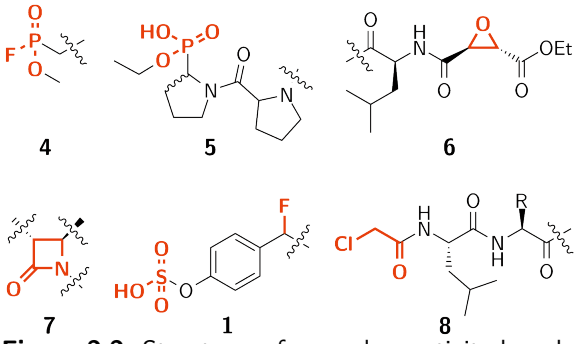

Figure 2.2: Structures of examplary activity-based probes: fluorophosphonate **4**,[28] alkylphosphonate **5**,[37] epoxysuccinyl derivative **6**,[38] β-lactam **7**,[39] monofluoromethylphenyl sulfate **1**,[8,40] α-chloroacetamide **8**.[41]

There are two main strategies for the design of activity-based probes: directed (**1**, **4**–**7**) and non-directed (**8**). Activity-based probes react with an enzyme class mostly based on active site nucleophilicity, thus fine-tuning of probe specificity often involves incorporation of amino acids or amino acid derivatives to mimic the enzyme substrates.

Directed

Fluorophosphonates **4** constitute one of the first probe classes extensively used for activity-based proteomics[28] and have yielded a lot of biological information so far. These probes display a high degree of promiscuity by generally phosphorylating active site serine residues of many serine hydrolases. This has led to the assignment of numerous previously uncharacterized proteins as serine hydrolases.[42] Fluorophosphonates **4** have also been applied in high-throughput screenings of compound libraries to identify potent specific inhibitors for single enzymes with unknown substrates. A broad-range binding probe for the whole class of serine hydrolases allowed the direct identification of off-target hits bound by the tested inhibitors.[43] Peptidic aryl- and alkylphosphonates like **5** have been developed to enable a more selective labeling of serine hydrolases. The incorporated amino acids imitate substrates; probe **5** is applied for postproline protease labeling.[37]

Epoxysuccinyl derivatives **6** are attacked by catalytic cysteine residues of the papain class of cysteine proteases thereby labeling a range of different enzymes.[38] The employment of more selective epoxysuccinyl probes has been described, e.g. the selective labeling of Cathepsin B which was

achieved by incorporation of a substrate-like dipeptide instead of the ethyl ester in **6**.[44]

Most ABP studies so far concentrate on enzymes which have previously been suggested as biomarkers for cancer. Recently, novel targets for ABP studies are emerging, among them bacterial enzymes involved in cell wall biosynthesis associated with antibiotics resistance. Various bacterial lysates were profiled successfully with β-lactams **7**,[39,45] and β-lactone libraries.[46] The probes and their bacterial targets will now be further evaluated e.g. by inhibitor screenings.

Suicide inhibitor **1** is turned over by a sulfatase. These compounds depend on the cleavage of their respective substrate moieties (sulfate in Figure 2.3), whereupon fluoride elimination generates the QM. The electrophilic carbon atom generated by sulfate cleavage should be attacked by a nucleophile of the sulfatase, supposedly, an active site residue. A diverse group of enzymes has been addressed by quinone or quinolimine methides but except for one example,[47] all studies still fail to prove the practicability of these compounds in complex samples, the target of all application-oriented ABP studies. Only purified enzymes were tested, and any unspecific labeling in more elaborate experiments was ignored.[8,48–57] Two of these studies hint towards the problem of unspecific binding. However, there are no follow-up publications affording details on these initial results.[53,54] Possibly, the generated quinone methide is stable enough to diffuse out of the sulfatase active site. As a result, it labels surrounding molecules leading to false positive hits which question the applicability of QM precursors for ABP approaches in general.

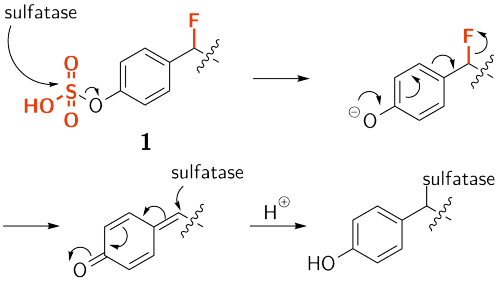

Figure 2.3: Binding mechanism of sulfatase probe **1**, a quinone methide precursor.

Non-directed

The lack of specific covalent inhibitors for many enzyme classes or protein families has led to the development of non-directed probe libraries containing general electrophiles like α-chloroacetamides or sulfonate esters to screen for novel targets which were not addressed by ABP before. One successful example for the application of a non-directed probe strategy is the α-chloroacetamide **8**. This probe was identified from a library of α-chloroacetamides to selectively target the nitrilase Upβ because of structural similarities to its natural substrate *N*-carbamoyl β-alanine.[41] Such examples prove the utility of non-directed probes for the assignment of substrates to novel enzymes.

Affinity-based targeting groups

Another important innovation for approaching a larger variety of enzymes using ABP workflows was made with the integration of photoreactive groups into probe design.[58] Many enzyme classes which were neither attacked by directed nor non-directed activity-based probes can be captured with affinity-based probes that contain a reversible inhibitor in combination with a photoreactive group (Figure 2.4).

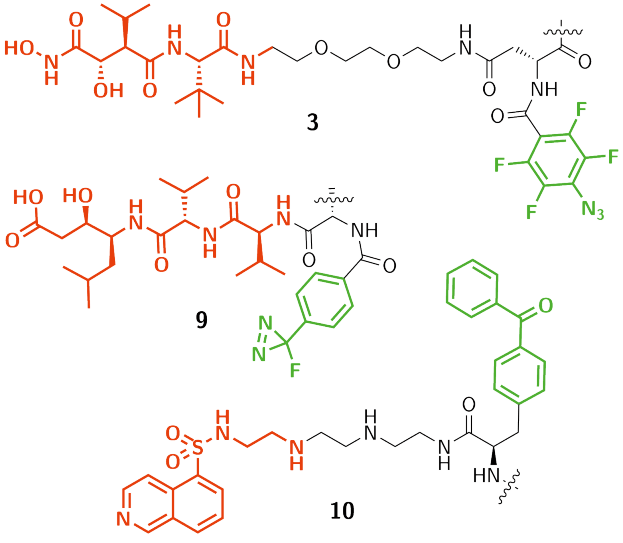

Figure 2.4: Structures of affinity-based probes: marimastat derivative **3**,[59] (3*S*,4*S*)-statine probe **9**,[60] H9-containing probe **10**.[61] **Affinity functions**, **photoreactive groups**.

Publications on affinity-based probes are mainly concerned with metalloprotease (MP) labeling since there are no mechanism-based inhibitors for this group of enzymes which do not possess active site nucleophilic residues. Instead, MP substrates are cleaved by an activated water molecule which is complexed through a zinc ion and an aspartate residue.[62] Probe **3** was developed as a commercial tool for the functional characteriza-

tion of MMPs in the course of this thesis.[59] It contains the well-known broad range MMP inhibitor **marimastat** and a **photoreactive group** to covalently label bound proteins upon UV-irradiation. Other hydroxamate probe libraries with benzophenone as the photoreactive group have been used for a case study about ranking human MMP-13 PubChem screening hits.[63]

Various enzyme classes were targeted by affinity-based probes with diverse photoreactive groups as shown exemplarily by probe **9** binding aspartic proteases[60] and probe **10** addressing kinases.[61] The advantages and drawbacks of the different photoreactive groups employed have been extensively discussed in literature.[64] This particular strategy renders affinity-based probes susceptible to activity-based methods by covalent bond formation and will eventually lead to an amplification of ABP results.

2.1.2 Tagging Strategies

Depending on the application of ABP probes, different tags[65] can be attached during synthesis. The smallest labels available for probe synthesis are radiolabels. Radioactive isotopes like ^{125}I can be introduced into phenyl rings without heavily altering probe structure. Even if an aromatic system has to be integrated into the probe for the purpose of radio-labeling, it creates a relatively small change compared to the addition of biotin or a fluorophore. Unfortunately, radio-isotopes are not robust enough for long-term storage, so the label has to be attached to the targeting group immediately prior to probe application.[66]

^{125}I

Another possibility for gel-free ABP experimental setups is the addition of stable isotopes, which have been used in quantitative proteomics for years.[67] Although there are only few studies with probes that incor-

Stable isotopes

porate stable isotopes, this is a powerful method for the relative quantitation of labeled enzymes originating from different proteomes.[68]

The reduction of sample complexity by ABP approaches is tightly connected to one of the most prominent tags applied in biochemical research: biotin. The strong binding to avidin and streptavidin allowed its application in affinity blotting and pull-down using avidin or streptavidin coated beads.[2,8,28,29,38–40,42–46,50,51,55,56,58,59,68] The captured proteins can subsequently be analyzed (Figure 2.1). Since endogenously biotinylated proteins cause a background of detected but non-labeled proteins, alternative unambiguous reporter tags were applied early on in ABP evolution.

Biotin

In comparison to biotin, fluorophores offer the advantage of immediate in-gel visualization (Figure 2.1) and the feasibility of fluorescence microscopy. No inherently fluorescent proteins (apart from e.g. GFP) interfere with the read-out which is the reason for the high sensitivity of this method. A multitude of fluorophores with different physico-chemical properties are commercially available as reactive esters which facilitates probe synthesis. The first fluorophores applied in ABP were rhodamine and fluorescein dyes.[28,69] Their disadvantage of photobleaching has led to the incorporation of dipyrromethene boron difluoride (BODIPY) and cyanine (Cy) dyes that display higher fluorescence quantum yields, an improved pH tolerance, excellent photostability and higher absorption coefficients which makes them more suitable for microscopy. They are able to penetrate cell membranes, and this allows for *in vivo* labeling.[70] Novel minimally invasive diagnostic imaging methods might be developed in the future as has been shown for near-infrared fluorescent *in vivo* labeling of tumors by application of activity-based probes in living mice.[71,72]

Fluorophores

2.1.3 Probe Assembly and Linker Design

A considerable amount of probes synthesized so far relies on peptide chemistry for the coupling of their three components targeting group, linker and tag. Additionally, many inhibitory groups are peptide derivatives which narrows the range of chemical reactions needed for probe assembly down and allows the application of established conditions and reagents. Some probes were even synthesized using solid phase peptide chemistry.[47]

CuAAC

A recent advance in linker and probe synthesis was made when CuAAC also known as one of the "click" reactions was first introduced to ABP.[73] This reaction does not only facilitate probe synthesis, moreover, it improves the practicability of many probes for *in vivo* labeling. Some tags (biotin, rhodamine, fluorescein) hinder membrane permeability which can be overcome by the synthesis of alkyne-modified targeting groups. The sample is labeled *in vivo*, homogenized or fixed on a slide for microscopy, and finally the reporter group is added via CuAAC (Figure 2.5).

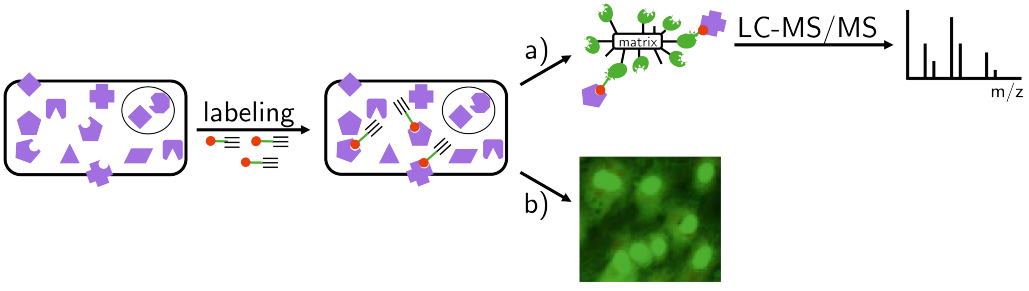

Figure 2.5: *In vivo* labeling using clickable probes. Tissue or cell samples are labeled with the alkyne-bearing targeting group. The sample is then either a) homogenized, biotin is added via CuAAC followed by pull-down and protein identification or b) fixed on a slide for fluorescence microscopy, and a fluorophore azide is attached to visualize localization of labeled proteins.

Linkers

Another disadvantage of the biotin tag is solved by incorporation of a cleavable site into the linker moiety. The biotin-avidin/streptavidin interaction is too strong to efficiently release captured proteins without ap-

plication of harsh conditions. Cleavable linkers offer the possibility to elute proteins via selective mechanisms like photo cleavage,[74,75] and tobacco etch virus protease cleavage.[76] A variant of the cleavable linkers are degrading linkers which decompose upon substrate-mimic cleavage. This offers the opportunity to include FRET-pairs into the probe enabling visualization only upon target protein binding.[57] Since this concept also relies on the generation of QMs its applicability remains to be proven for complex samples.

The recent years have seen a great methodological advance in activity-based proteomic research. This technique-oriented field has rather aspired to develop new methods to tackle increasingly complex problems than to actually apply the existing methods to biological systems. Most break-through studies published in ABP so far depend on the application of novel chemical strategies for probe synthesis which allow for the implementation of new biochemical procedures (e.g. CuAAC). It remains unclear whether ABP will be able to meet the challenge of focussing on the generation of biologically relevant information and not only on improving and developing techniques and methods. After all, many interesting enzyme classes are already addressable by probes but still lack sufficient functional characterization.

3 Targeting Sulfatases

Sulfatases catalyze the hydrolytic cleavage of sulfate esters and sulfamates with broad substrate specificities across the members of this enzyme class. They are structurally and mechanistically highly conserved and widely distributed among eukaryotes and prokaryotes.[7] During the past 20 years, great advance has been made in their exploration and characterization.

3.1 Introduction to Sulfatases

All sulfatases feature the same active site residue FGly that is post-translationally introduced by formylglycine generating enzymes (FGE for eukaryotes, AtsB, SUMF1 or similar proteins for prokaryotes) within the special signature sequence (C/S)TPSR(S/A)(A/S)LLTGR.[7,77,78] The human sulfatases are all processed for the secretory pathway and thus enter the endoplasmatic reticulum (ER) during their synthesis. In the course of this translocation, and before protein folding the FGly residue is generated by FGE.[79] It is generated via oxidation of a cysteine residue for all eukaryotic enzymes[80,81] and of either a serine[82] or a cysteine[83] residue for the prokaryotic sulfatases. Human sulfatases are glycosylated and display various localizations along the secretory way: within the ER, Golgi network, lysosomes and on the cell surface. Prokaryotic sulfatases are mostly localized in the cytosol or periplasma.

The FGly residue

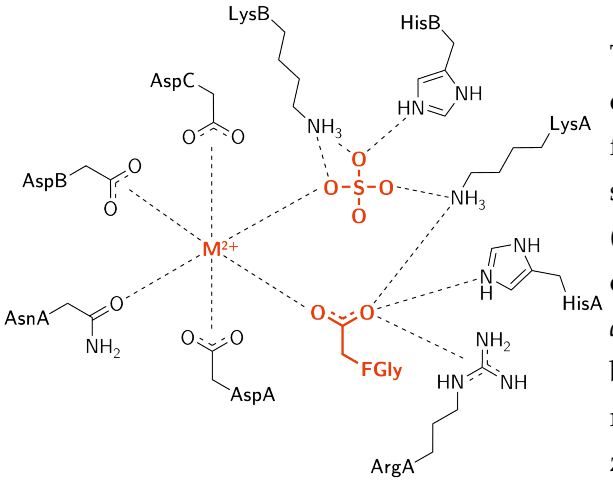

Figure 3.1: Structure of the highly conserved sulfatase active site.[7]

There are 17 human, at least eight other eukaryotic and more than five prokaryotic sulfatases described so far.[9,84] Three of the human (ARSA,[85] ARSB[86] and STS[87]) and one prokaryotic sulfatase from *Pseudomonas aeruginosa* (PARS[88]) have been structurally characterized by x-ray crystallography. All four enzymes display very similar globular shapes, except for the unique transmembrane domain of STS which consists of two hydrophobic helices protruding into the membrane. The catalytic site is formed by ten amino acids that are highly conserved and closely involved in a H-bond network which ties the side chains to an octahedrally coordinated M^{2+} ion and sulfate (Figure 3.1). Substrate recognition, and consequently, enzyme specificity is most likely due to protein surfaces other than the active site since most sulfatases readily accept small aryl sulfate esters as substrates. This hints towards a specific binding and correct orientation of large substrates by interactions with areas distant to the catalytic cleft.[7]

Mechanism of sulfate cleavage

Two mechanisms of sulfate cleavage have been discussed during the past 15 years. Structural similarities of the first human sulfatase that was crystallized (ARSB) to alkaline phosphatase inspired the addition-hydrolysis (AH) mechanism depicted in Figure 3.2a.[86] The structure of ARSA on the other hand suggested that FGly is only active in its hydrated form and thus a transesterification-elimination (TE) mechanism was proposed as can be seen in Figure 3.2b.[85]

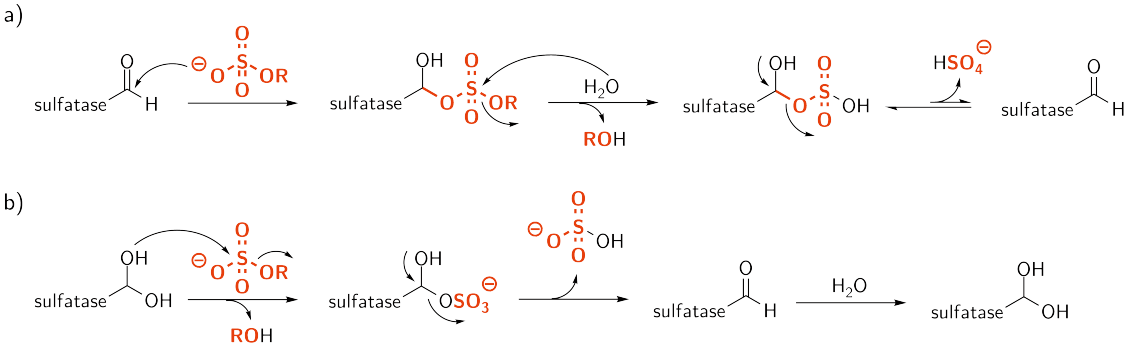

Figure 3.2: Proposed mechanisms for sulfate cleavage. a) AH mechanism: FGly is attacked by an oxygen atom of the sulfate group. First the alcohol is substituted by water, then sulfate is released to regenerate the aldehyde. b) TE mechanism: The geminal diol attacks sulfate, and the alcohol is eliminated to give a sulfate enzyme intermediate. Upon sulfate elimination the diol is regenerated by water.

In case of the TE mechanism, the FGly-hydrate nucleophilically attacks the sulfur atom of a sulfate, the alcohol is released, and an intermediate enzyme bound FGly-sulfate ester is formed. The second geminal hydroxy group is essential for sulfate release to regenerate the aldehyde. This mechanism is supported by ARSA and B mutants that feature a serine residue instead of FGly in the active site. The mutants are able to release the alcohol of a sulfate ester whereas the sulfate remains bound to the protein.[89] This study strongly argues for the TE mechanism and against the AH mechanism due to the relative unlikeliness of a nucleophilic attack of the serine residue by the sulfate oxygen atom. More proofs for a TE mechanism include inversion of configuration at the sulfur atom of a chiral substrate,[90] and the high-resolution (1.3 Å) x-ray crystallographic structure of PARS which clearly shows the FGly-hydrate in close proximity (2.96 Å) to a sulfate group.[88] Today it is generally accepted that the FGly aldehyde is hydrated to a geminal diol in its active form. However, it is still under discussion whether the TE mechanism rather follows a S_N2 or S_N1 pathway. In the majority of studies a dissociative S_N1 mechanism is considered most likely. For bacterial[91,92] as well as human[93] sulfa-

tases the pK_a, and therefore the leaving group properties of the alcohol play a decisive role for the enzymatic cleavage of sulfate esters.

Sulfatase inhibition

STS upregulation was found to be prominent in hormone-dependent breast cancer of post-menopausal women[94] as well as prostate tumors.[95] Several hormone precursors can be transformed to highly affine estrogenic or androgenic hormones by STS hence inducing cell proliferation and growth.[96]

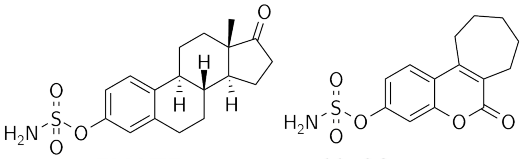

Figure 3.3: Potent sulfamate inhibitors EMATE and 667COUMATE.

Therefore, significant efforts have been put forward to develop potent inhibitors for human steroid sulfatase. The prototypic and potent inhibitor estrone-3-*O*-sulfamate (EMATE) was one of the first irreversible STS inhibitors described.[97] Even though it turned out to be highly estrogenic itself and therefore useless as a therapeutic,[98] it started the development of numerous sulfamate-type compounds including 667COUMATE which underwent a promising phase I clinical trial.[99] Other interesting applications for inhibitors arise from the importance of sulfatases in processes like bacterial pathogenesis,[100] and the evasion of plant defense mechanisms against insects.[101]

Small aryl sulfamates have been reported to inhibit sulfatases from various sources. However, their inhibitory mechanism has not been elucidated yet as the dead-end adduct of sulfatase inhibition has never been identified.[9,92,102] Irreversible inhibition of sulfatases was proven as activity is not regained even after extensive dialysis. Also, substrate protection has been observed which is consistent with an inactivation mechanism that involves covalent modification of the active site.[9] The scission of the arO-S bond during inhibition was proven by estradiol-3-*O*-sulfamate which was [^{3}H]-labeled at the 17-position of the steroid moi-

ety. Even though irreversible inhibition of the sulfatase was found, the enzyme was not ^{3}H-labeled.[96] The stoichiometry of inhibition was determined for several sulfamates including 667COUMATE to be between three and six inhibitor molecules per sulfatase before complete inhibition is attained.[92] Encompassing all this information various inhibitory mechanisms have been proposed as depicted in Figure 3.4.

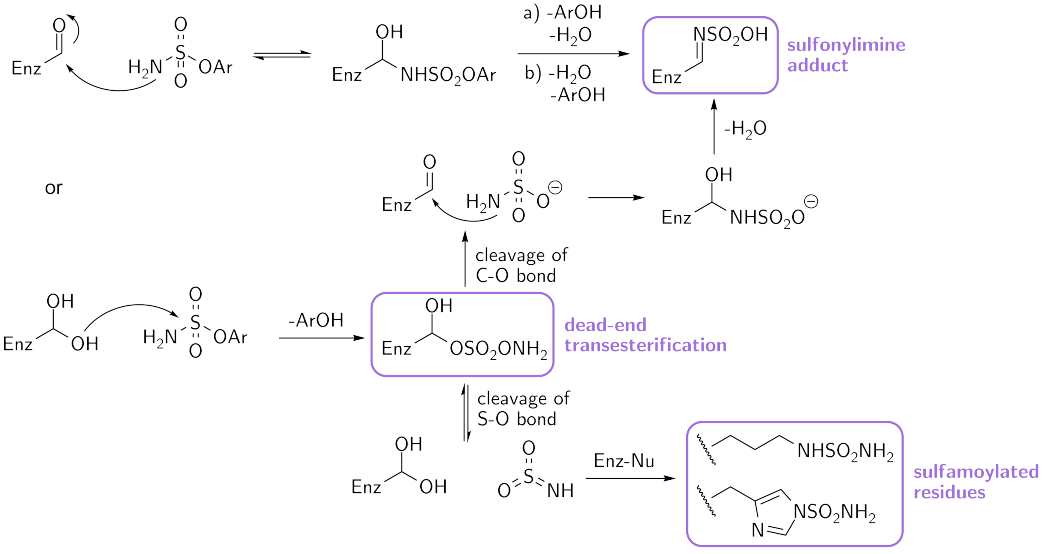

Figure 3.4: Proposed mechanisms for sulfatase inhibition by sulfamates.[9,92]

3.1.1 Activity-Based Studies of Sulfatases

Sulfatases are interesting targets for activity-based studies due to two facts: for some of them the substrates as well as functions are poorly understood, and lately their involvement in various diseases is unraveling. Additionally, as accounts for all enzymes, protein abundance does not reflect biological activity, and sulfatase activity has been found up- and down-regulated in cancer and inflammation.[7]

Quinone methide precursors have been extended to sulfatases[8,9,103] probably in light of precedent with other hydrolytic protein classes, including phosphatases,[50] β-glucosidase,[51] proteases,[53] neuramidase[56] and β-galactosidase.[57] The concept of QM traps is based on the generation of quinone methide intermediates which feature an electrophilic carbon atom that can be covalently captured via Michael-addition by a properly disposed nucleophile. Ideally, an active site residue of the target enzyme will capture the QM before it can diffuse out of the active site where it was generated. As shown schematically in Figure 2.3, the QM is masked as a fluoromethylphenol sulfate substrate surrogate prior to interaction with the enzyme. After cleavage of sulfate, fluoride is eliminated and the QM intermediate thereby generated.

In previous work, biochemical studies with PARS indicated that difluoromethylphenyl sulfate (DFPS) inhibitors were acting as competitive substrates or inhibitors, but not necessarily active-site directed inactivators as they do not exhibit time- and concentration-dependent inhibition of sulfatases,[9] a hallmark of mechanism-based inhibition.[104] In accordance to that, DFP substrates have demonstrated complicated kinetic behavior not following expected first-order kinetics and slow as well as loose binding in comparison to monofluoromethylphenyl substrates before.[105,106]

A biotinylated monofluoromethylphenyl sulfate (MFPS) QM precursor probe which was used for labeling STS did not display convincing results concerning labeling specificity and mechanism-based inhibition by MFP QMs.[8] The streptavidin-HRP western blot analysis of labeling clearly visualizes a number of proteins other than STS which were colabeled. No inhibition study was conducted, and the only evidence for an activity-dependent inhibition of STS shows a deviation of 40 % from the expected value. The most devastating result of this study was only pre-

sented in the supporting information. In a labeling study without streptavidin bead pull-down it becomes evident that nearly the whole proteome was labeled by this QM probe.[8] However, without further investigation, it cannot be excluded that the MFPS inhibitor moiety might be useful under optimized conditions or for other members of the sulfatase family.

A different approach was followed in a recently published study to increase specificity of a QM-based STS-inhibitor. An estrone-type QM was employed instead of the more general MFPS structure. Notably, the greater similarity to its natural substrate did not lead to a higher degree of binding specificity as was inferred from other inhibitors such as EMATE or 667COUMATE, since multiple QMs had to be generated before STS was inactivated. Only inhibition studies were presented in this publication, no labeling results were shown.[103] Therefore, a more specific binding in spite of multiple QM generation per enzyme unit is still possible.

An alternative motif for the development of activity-based sulfatase probes was presented in the first paper on sulfatase targeting QM precursors.[9] The authors examined the inhibitory characteristics of CySAs on PARS. They were able to prove it was a mechanism-based covalent inhibition which exhibited time- and concentration-dependent properties. Thus, CySAs are promising candidates for more specific sulfatase probes since most of the proposed binding mechanisms (depicted in Figure 3.4) lead to a specifically labeled sulfatase.

3.2 Objectives

ABP tools for the selective detection and isolation of sulfatases within complex mixtures should be developed in the course of this work. In this regard, two probe types with different traps were synthesized and biochemically evaluated: QM precursors based on MFPS, and CySA probes.

A diploma thesis[107] conducted in our laboratories provided the fluorescein-containing probe **1a** depicted in Figure 3.5. In continuation to the synthesis of **1a**, a novel route for the modular synthesis of QM probes but also ABP probes in general should be explored using CuAAC reactions for orthogonal probe assembly on solid support.

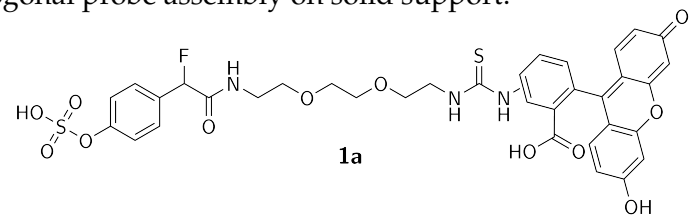

1a

Figure 3.5: Fluorescein-bearing QM probe **1a**.[107]

In cooperation with Dr. S.R. Hanson (TSRI, La Jolla) alkynylated cyclic sulfamates and azido-reporter groups were synthesized. These building blocks should help to extend the range of biochemical experiments feasible in our lab to *in situ* and *in vivo* labeling of proteomes by application of CuAAC reactions.

On the biochemical side of this project, the inhibition of different sulfatases by QM and CySA probes needed to be evaluated by dose-dependent sulfatase inhibition assays and various labeling studies to determine and compare probe properties like inhibition and specificity of QM versus CySA traps.

3.3 Synthesis of Sulfatase Probes

3.3.1 Quinone Methide Precursors

The synthesis of QM inhibitory fragments based on MFPS included key steps of installing a TCE protected sulfate before introducing the benzylic fluoride with DAST. Fluorescent probe **1a** was synthesized by a solution-phase route via a key coupling of the masked inhibitory QM amine with

fluorescein isothiocyanate.[107] In contrast to that, the biotinylated probe **1b** was prepared using a modular approach based on peptide coupling and CuAAC. The inhibitory moieties and the reporter groups can be orthogonally attached without protection group modifications.
The synthesis of inhibitor moiety **15** proceeded smoothly except for deprotection of the hydroxyl groups (step c) in Figure 3.6). Product **13** could not be extracted from the aqueous phase which then had to be lyophilized prior to adsorption on celite for chromatographic purification. This led to a high loss of product in this step.

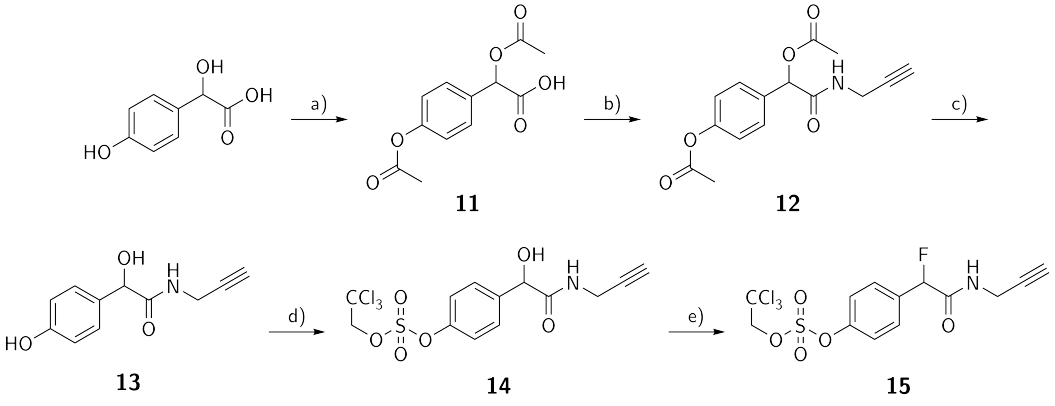

Figure 3.6: Synthesis of probe precursor **15**. a) Ac_2O, pyridine, 0 °C, 30 min, 86 %; b) 0.8 eq. propargylamine, 1.9 eq. EDC·HCl, 2.9 eq. TEA, DCM, rt, on, 90 %; c) NaOH, MeOH, 0 °C–rt, 3 h, 17 %; d) 3.6 eq. 2,2,2-trichloroethyl chlorosulfate, 1.2 eq. DMAP, 1.4 eq. TEA, DCM, rt, 19 h, 91 %; e) 1.9 eq. DAST, DCM, -20 °C–rt, 15 h, 99 %.

To increase QM electrophilicity and reactivity at the position of enzyme nucleophilic attack, we synthesized a second MFPS **20** according to the reaction scheme in Figure 3.7. Key step was the deprotection of the sulfate ester which only proceeded very slowly and needed a large amount of activated zinc compared to previous reactions (step d) in Figure 3.9). After purification by preparative HPLC only 16 % (10 mg) of pure product **20** were obtained. In the course of its NMR-spectroscopic characterization,

it became evident that **20** is not stable since it decomposed completely during overnight measurements.

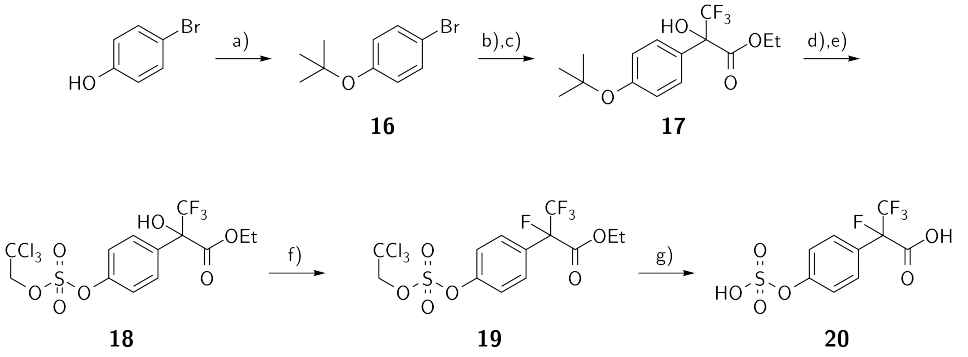

Figure 3.7: Synthesis of probe precursor **20**. a) 2.4 eq. Boc_2O, $Mg(ClO_4)_2$, DCM, reflux, on, 73 %; b) 1.1 eq. Mg, THF, reflux, 4 h; c) 0.8 eq. ethyl-3,3,3-trifluoropyruvate, THF, -78 °C–rt, on, 66 %; d) TFA, rt, 20 min, quant.; e) 3.3 eq. 2,2,2-trichloroethyl chlorosulfate, 1.1 eq. DMAP, 1.3 eq. TEA, DCM, rt, on, 62 %; f) 3.3 eq. DAST, DCM, -20 °C, 1 h, then rt, on, 89 %; g) 1.5 g activated Zn dust, MeOH/PBS pH 7.2 = 1:1, rt, 2 d, 16 %.

All attempts to incorporate a trichloroethyl-protected derivative of **20** into a probe failed since coupling of propargylamine to the carboxylic acid using EDC/HOBt, PyBOP[108] or *N,N'*-carbonyldiimidazole[109] did not lead to amide formation even though these conditions had been reported for very similar molecules.

As a reporter group, we wanted to be able to employ biotin as well as a fluorophor for the orthogonal probe assembly on resin. To extend the panel of biochemical applications, we wanted to synthesize a BODIPY dye derivatized as a carboxylic acid. Compared to fluorescein-functionalized probes, BODIPY-bearing probes are suitable for fluorescence microscopy. This specific BODIPY dye was selected due to its similar spectroscopic characteristics with respect to fluorescein.

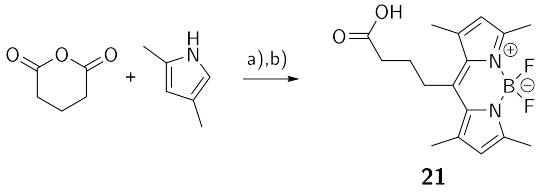

Figure 3.8: Synthesis of BODIPY dye **21**. a) 1.3 eq. $BF_3{\cdot}OEt_2$, DCM, reflux, 5 h; b) 6.7 eq. $BF_3{\cdot}OEt_2$, 5 eq. TEA, rt, on.

Despite following a published procedure[110] that was used several times in the literature, problems that occured during the purification process of the product could not be solved. TLC analysis showed the formation of a fluorescent product, but it could not be purified by application of the described chromatographic procedures and was too sensitive for HPLC. Adjusting the eluent polarity for chromatography did not result in improved separation.

Very similar reaction conditions were used to synthesize an alkyne functionalized BODIPY dye using 5-hexinoyl acid chloride and 2,4-dimethylpyrrole (Figure 3.9).[111] This time the difficulties in separation could be solved successfully by crystallization from toluene and petrol ether.[112] The alkyne was then clicked to an azido carboxylic acid to yield the desired BODIPY dye.

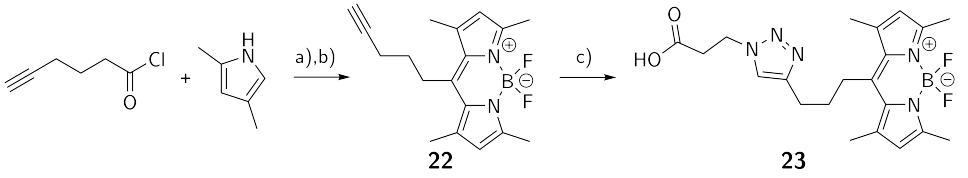

Figure 3.9: Synthesis of BODIPY dye **23**. a) DCM, reflux, 2 h; b) 5 eq. $BF_3{\cdot}OEt_2$, 4 eq. DIPEA, rt, on, 15 %; c) 1 eq. 3-azidopropionic acid, 1 eq. Cu powder, ACN, H_2O, rt, 4 d, 73 %.

To test the generality of our orthogonal probe assembly approach, molecule **1b** was synthesized. Notably, this novel route affords the design of application-tailored parallel synthesis of other ABPs since resin **24** can be stored in the fridge for several months without quality loss. It features two orthogonal attachment sites for the inhibitory moiety and the reporter group. This allows for parallel synthesis of desired conjugates

upon the design of a biochemical experiment with its individual requirements. Probe **1a** was prepared in solution with inevitable purification after each step.[107] This could be reduced to preparative HPLC at the end of the synthesis of **1b** which drastically reduced synthesis time. The biotinylated probe was deliberately prepared to widen the range of possible applications of sulfatase QM probes. Using the on-resin synthetic route different inhibitors and reporter groups like fluorophores or isotopic labels can be easily combined to synthesize probe libraries. In this context probe **1b** was synthesized as a model probe for future derivatives; biotin was added via peptide coupling, and the alkynyl inhibitory QM fragment was coupled by CuAAC (Figure 3.10).

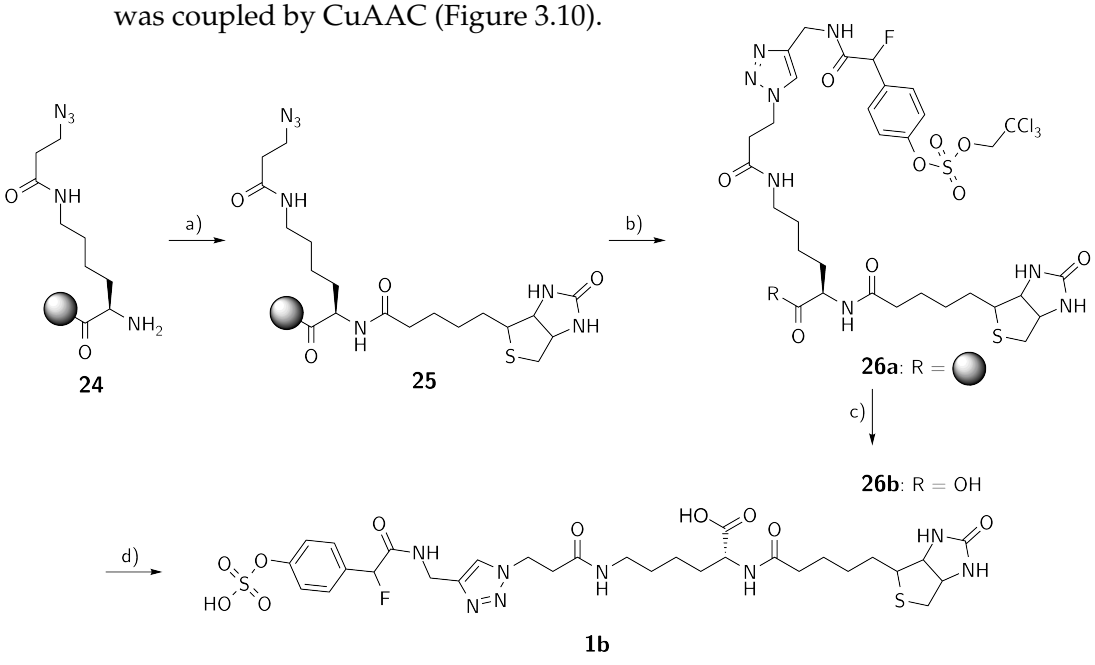

Figure 3.10: Synthetic pathway for the solid phase synthesis of QM type probe **1b**. a) 3 eq. biotin, 3 eq. TBTU, 6 eq. DIPEA, DMF, rt, 2 h; b) 1 eq. alkyne **15**, 12 eq. sodium ascorbate, 24 eq. CuI, DMF, rt, on; c) 20 % (*v*/*v*) HFIP, DCM, rt, 60 min, 29 %; d) activated Zn dust, MeOH, PBS pH 7.2, rt, 5 d, 39 %.

3.3.2 Cyclic Sulfamate Probes

Following the initial plan to compare two different ABPPs for sulfatases, the cyclic sulfamate **2b** was synthesized with an additional alkyne group following a literature procedure for the sulfamate moiety.[9] There are two key steps in this synthetic sequence. First, the introduction of the tosyl protection needs to be monitored closely by TLC to maximize product yield. The reaction has to be worked up immediately after completion to circumvent severe product losses. The base also plays an important role, as triethylamine leads to tosylation of the phenolic oxygen atom which can be hardly distinguished from the desired amine protection by NMR-spectroscopy.[113]

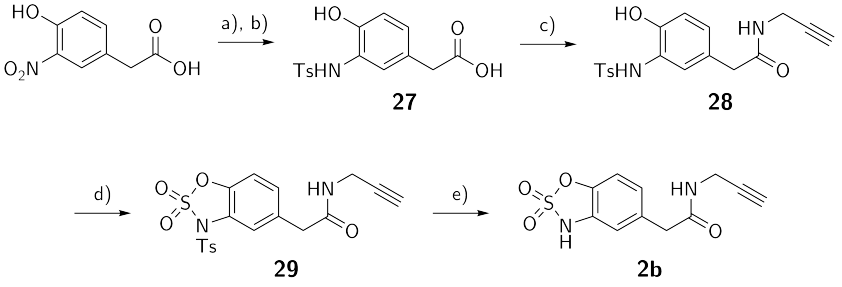

Figure 3.11: Synthesis of alkyne **2b**. a) Pd/C, H_2, MeOH, rt, 4 h, 99 %; b) 1.2 eq. TsCl, DCM/Pyridin = 1:1, 4 °C, 1 h, 96 %; c) 2 eq. propargylamine, 2.8 eq. EDC·HCl, 2.8 eq. HOBt·H_2O, 3.8 eq. NMM, DCM, rt, 50 h, 32 %; d) 3 eq. SO_2Cl_2, 4 eq. TEA, DCM, -78 °C, 2 h, 30 %; e) NaN_3, ACN:MPW = 1/1, rt, 3.5 h, quant.

Second, generation of the cyclic sulfamate only proceeds well under dry conditions and at constantly low temperatures. A prominent side reaction that occurs at slightly elevated temperatures when applying sulfuryl chloride to aryl compounds is the chlorination of the ring.[114]

CySA alkyne **2c** which features a slightly different linker was also synthesized. The incorporated amine alkyne linker **32** was prepared following standard procedures as depicted in Figure 3.12. Its coupling to acid **27** proceeded with a yield of 28 % which is very similar to the coupling yield

of amide **28**. Formation of the cyclic sulfamate **34** could be improved by 23 % compared to the synthesis of **29** by elongation of the reaction time. Removal of the tosyl group gives probe precursor **2c**.

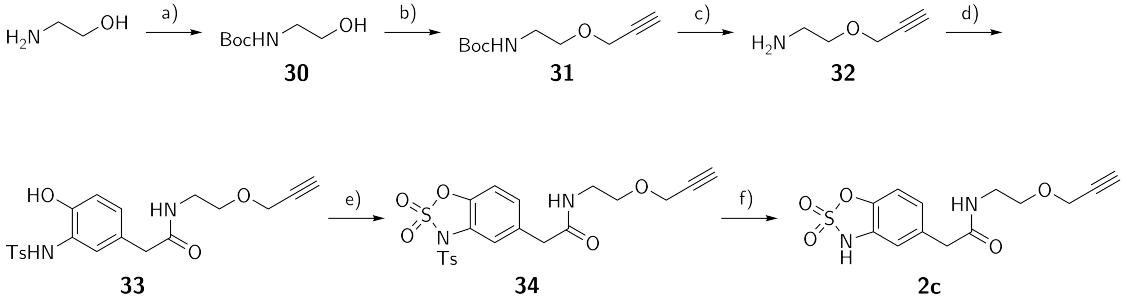

Figure 3.12: Synthesis of amine alkyne linker **32** and *para*-alkyne **2c**. a) 0.8 eq. Boc_2O, 2.5 eq. NaOH, ACN/H_2O = 1:1, 4 °C–rt, 24 h, 85 %; b) 1.1 eq. NaH, 1.1 eq. propargylbormide, THF, 4 °C–reflux–rt, 48 h, 60 %; c) DCM/TFA = 4:1, rt, 1 h, quant.; d) 0.5 eq. acid **27**, 1.0 eq. EDC·HCl, 1.0 eq. HOBt·H_2O, 2.5 eq. pyridine, DCM, rt, 50 h, 28 %; e) 3 eq. SO_2Cl_2, 4 eq. TEA, DCM, -78 °C, 4 h, 53 %; f) NaN_3, ACN:MPW = 1/1, rt, 3.5 h, quant.

For inhibition studies and as a negative control for labeling experiments the original inhibitor CySA **2a** without a linker or reporter group was also synthesized according to literature.[9]

3.3.3 Azido Reporter Groups and *in situ* CuAAC

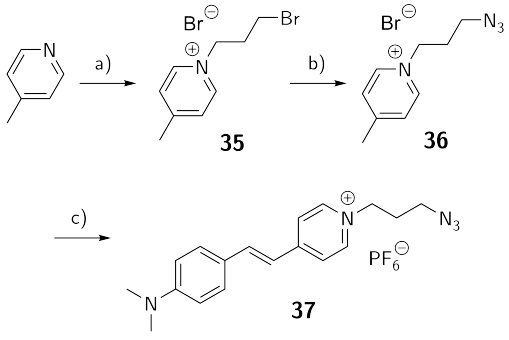

Figure 3.13: Synthesis of clickable cyanine dye **37**. a) 4 eq. 1,3-dibromopropane, ACN, reflux, 4 h, 80 %; b) 2.5 eq. NaN_3, ACN, reflux, 17 h, quant.; c) 1 eq. 4-(dimethylamino)benzaldehyde, cat. piperidine, EtOH, 60 °C, 16 h, 83 %.

For clickable inhibitors **2b** and **c** two different reporter groups were synthesized: a cyanine dye and biotin both derivatized as azides. The cyanine dye **37** was chosen due to its facile synthesis according to literature[115,116] as well as its interesting spectroscopical properties. The reaction route as depicted schematically in Figure 3.13 was straight-forward and featured no unexpected challenges. Purification of

the intermediates **35** and **36** was not necessary, and the final product **37** could be purified by two consecutive flash chromatographies. Yields were similar to the literature even though we used dibromo- instead of diiodopropane in the first step.

Compared to other labels like fluorescein or a BODIPY-dye which were both previously synthesized and applied for activity-based probes in our hands, the isolated overall yield and the ease of purification represented a great improvement. Cyanine dye **37** features some special properties that are particularly useful for biochemical applications. Its absorption maximum at 480 nm and emission maximum at 600 nm with a high extinction coefficient of 47,000 $M^{-1} \cdot cm^{-1}$ [115] account for the extremely large Stokes shift which makes **37** a perfect fluorophore for FRET approaches. Additionally, the high quantum yield and stability against photobleaching are advantageous for fluorescence microscopy.

For sulfatase pull-down, the biotin derivative **39** was synthesized according to literature.[117] The azidoethylamine **38** was prepared from the chloro- instead of the bromoethylamine which might account for the 15 % lower yield. It has to be handled very carefully since azide derivatives with such low ratios of carbon to nitrogen are potent explosives.[118] The second step is carried out slightly different compared to literature[117] regarding equivalents of azide **38** and TEA which improved the yield of azide **39** by 25 %.

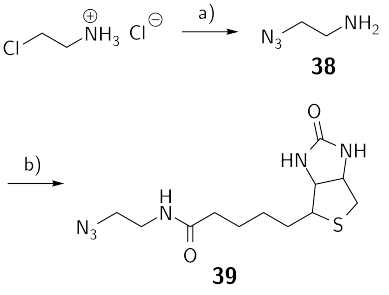

Figure 3.14: Synthesis of clickable biotin **39**. a) 3 eq. NaN_3, H_2O, 75 °C, 21 h, 67 %; b) 0.83 eq. NHS-biotin, 2 eq. TEA, DMF, rt, 16 h, quant.

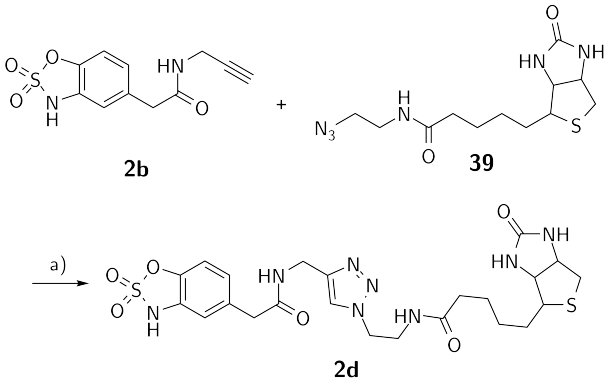

Figure 3.15: CuAAC reaction of biotin azide **39** and CySA alkyne **2b**. a) 1 mM alkyne **2b**, 1 mM azide **39**, 1 mM sodium ascorbate, 1 mM TBTA, 1 mM $CuSO_4$, PBS/MeOH/DMSO = 1:2.8:1.4, rt, 1 h, 47 %.

The CuAAC reaction was carried out following a protocol especially optimized for *in situ* activity-based proteomics applications in water.[119] This procedure makes use of the TBTA ligand that has been described to enhance the yield of Cu(I) catalyzed click reactions in water.[120] The purpose of this small-scale reaction was to establish a click protocol in our lab which can be transferred to the *in situ* labeling of sulfatases. In this respect the reaction was successfully expanded to our system. Analytical HPLC comparison of **2b**, **39** and the crude reaction mixture clearly show that no starting material remained after one hour. Preparative HPLC yields 47 % of pure product **2d**.

3.3.4 Conclusion of Sulfatase Probe Synthesis

In conclusion we generated two sets of probe building blocks which were combined to form new sulfatase probes. For QMs a novel approach was developed; alkynylated monofluoromethylphenyl inhibitor **15** and reporter groups that were functionalized as carboxylic acids (biotin and BODIPY dye **23**) could be joined orthogonally by solid phase assembly. As a proof of concept we successfully synthesized the biotinylated probe **1b**. For CySA probes we decided to delay attachment of the inhibitor to the reporter group until the biochemical labeling process had transpired. Therefore, alkynylated CySAs **2b** and **2c** as well as azido-bearing reporter groups **37** and **39** were synthesized. CuAAC reaction conditions from the literature[119] were successfully adapted to our building blocks for the

synthesis of probe **1d**. Therefore, *in situ* labeling should now be feasible with CySA probes.

3.4 Biochemical Evaluation of Quinone Methide Type Probes

Broad-range inhibitory function toward the members of a targeted enzyme class can be an important property of activity-based probes. With the synthesized sulfatase probes, different activity states of known human and bacterial sulfatases should be investigated. Moreover, unknown sulfatases from plants might be detected and identified by future experiments if probes with a wide-range binding motif are available.

To test the generality of our quinone methide precursors, we tested a panel of sulfatases: recombinantly expressed and purified cysteine- and serine-type aryl sulfatases from bacteria (PARS[9] and KARS[121]), human aryl sulfatase G (ARSG[122]) and steroid sulfatase (STS[123]). Each has distinct features: the bacterial sulfatases are active against a broad range of aryl sulfate substrates under basic (pH of 8.9 for PARS) and neutral (pH 7.5 for KARS) conditions; STS is a membrane-bound sulfatase of the endoplasmic reticulum or resident in the Golgi lumen with neutral pH optimum and a high specificity for steroid sulfates; and ARSG is a newly discovered lysosomal enzyme, with acidic pH optimum and unknown biological substrate and function.[7]

To evaluate the applicability of QM probes it is important to consider sulfatase inhibition versus QM formation and inactivation. These criteria for characterizing QM precursor probes were addressed by ^{19}F-NMR measurements (Figure 3.17) which have previously been used to definitively investigate the elimination of fluoride and thereby the generation of QMs.[50,51] Sulfatase inhibition was investigated by dose-dependent

(Figure 3.18a-c) and time-dependent (Figure 3.18d and 3.19) activity assays. Sulfatase labeling performance of QM precursor probes was tested by means of 2D-GEs and subsequent fluorescence scans (Figure 3.20, 3.21 and 3.23) as well as mass spectrometry of labeled proteins (Figure 3.24 and 3.25).

3.4.1 ^{19}F-NMR Experiments

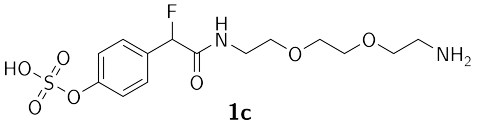

1c

Figure 3.16: QM probe precursor **1c**

The cleavage of the sulfate ester of probe precursor **1c** by KARS, PARS, ARSG and STS was monitored in real-time using ^{19}F-NMR spectroscopy. Upon hydrolysis of the sulfate ester by the enzyme, fluoride is eliminated and appears as a new signal at δ = -120 ppm. After a reaction time of about twelve hours the conversion ceased for KARS which implies complete enzyme inhibition at this point (Figure 3.17). Controls verified that KARS remained active under the applied conditions without addition of inhibitor.

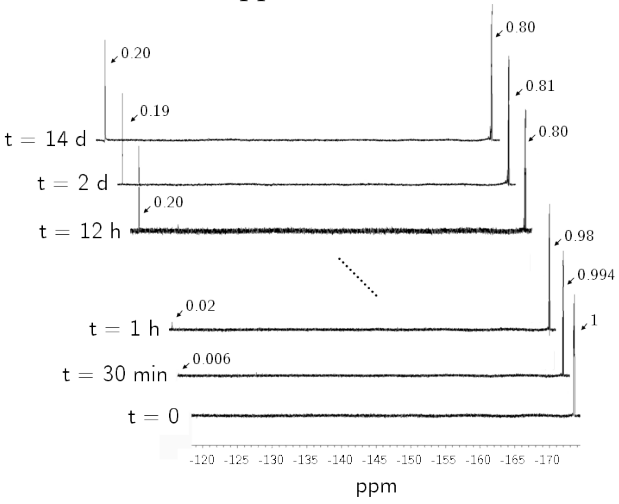

Figure 3.17: Time-dependent ^{19}F-NMR spectrum of fluoride generation triggered by KARS-mediated sulfate cleavage of QM precursor **1c**. The new signal at a shift of -120 ppm is assigned to the released fluoride.

The ratio of integrals of probe-bound fluorine and liberated fluoride indicated that about 20 % of the probe were converted before KARS was finally inactivated. Considering the 2000-fold excess of QM precursor **1c** over KARS it is obvious that the inhibition is inefficient. Approximately 400 molecules of probe were converted by one KARS enzyme before it was deactivated.

Various reasons for this lack of efficiency can be put forward. Either the

QM is deactivated before it binds active site residues of KARS or it binds in a way that enzyme activity is preserved. In the latter case, more than one QM would react per protein, as has been reluctantly discussed earlier.[48,51,124] Alternatively, diffusion of QM out of the active site before covalent bond formation might occur, and the probe could then be inactivated by any nucleophile on the protein surface or of the surrounding medium. This process would lead to a high degree of undesired background protein labeling.

While KARS and PARS cleaved the sulfate ester readily, as can be seen exemplarily for KARS in Figure 3.17, the human enzymes ARSG and STS did not. The respective integrals of the ^{19}F-NMR signals of the intact probe did not change, and no new fluoride signals arose in either of the two spectra. One reason why the human enzymes did not cleave **1c** might be a drastically reduced turnover due to structural differences in comparison to the natural substrates of these enzymes. From pseudo-substrates for assaying sulfatase activities it is known that ARSG prefers substrates with an additional hydroxyl group in ortho position to the sulfate ester.[122] STS, however, has been shown to turn over small aryl sulfates like **1c**. Another possibility that could not be excluded is enzyme inactivation due to unfavorable conditions (i.e. too low protein concentration, too low buffer concentration, adhesion of the enzyme to the glass walls of the NMR tube). The final concentrations and activities of the human enzymes in the NMR-samples were too low to assess their activity by sulfatase activity assay.

Substrate cleavage from QM precursor probes has been previously investigated by ^{19}F-NMR-spectroscopy.[50,51] Those probes contained a phosphate ester or a β-glycoside which were cleaved by the enzymes tyrosine phosphatase PTP-1B and β-glycosidase, respectively. Although probe to protein ratios exceeded 10,000:1 a complete turnover of the pro-

bes was observed in both cases. Probes with such a low inhibitory efficiency should rather be considered as pseudo-substrates not inhibitors. Compared to these results it is obvious that the sulfatase QMs presented in this work are at least capable of completely inhibiting the bacterial enzymes under the tested conditions.

3.4.2 Inhibition Studies

For QM probes it is important to distinguish between sulfate cleavage of the ester moiety and actual binding to and inhibition of the investigated enzyme. The results of QM formation obtained from ^{19}F-NMR experiments were supported by sulfatase activity assays. Complete inhibition of KARS could be achieved after 30 minutes preincubation with 10 mM probe **1c** which corresponds to a ratio of KARS to probe of approximately 1:4000 (Figure 3.18a). PARS was only partially inactivated at the applied QM precursor concentrations (Figure 3.18b). However, it is very likely that it is completely inactivated at higher concentrations.

In contrast to that, the activity of ARSG remained nearly unaffected at all tested conditions even upon overnight incubation (Figure 3.18c). The human enzyme STS was also only partially inhibited. The time-dependence of inhibition was pronounced for STS as can be seen in Figure 3.18d. It is striking that STS was inhibited by QM precursors but did not generate QMs in ^{19}F-NMR experiments. Apparently, the experimental conditions of the NMR measurements led to enzyme inactivation independent of inhibitor addition.

STS and ARSG inactivations were measured after preincubation at 37 °C to mimic native conditions. However, STS inhibition was not temperature-dependent when comparing residual activities after incubation for four hours at room temperature and at 37 °C. For all enzymes, residual actives are reported as a percentage of the uninhibited control, and all measure-

ments were done in triplicate. Error bars are standard deviations between individual measurements

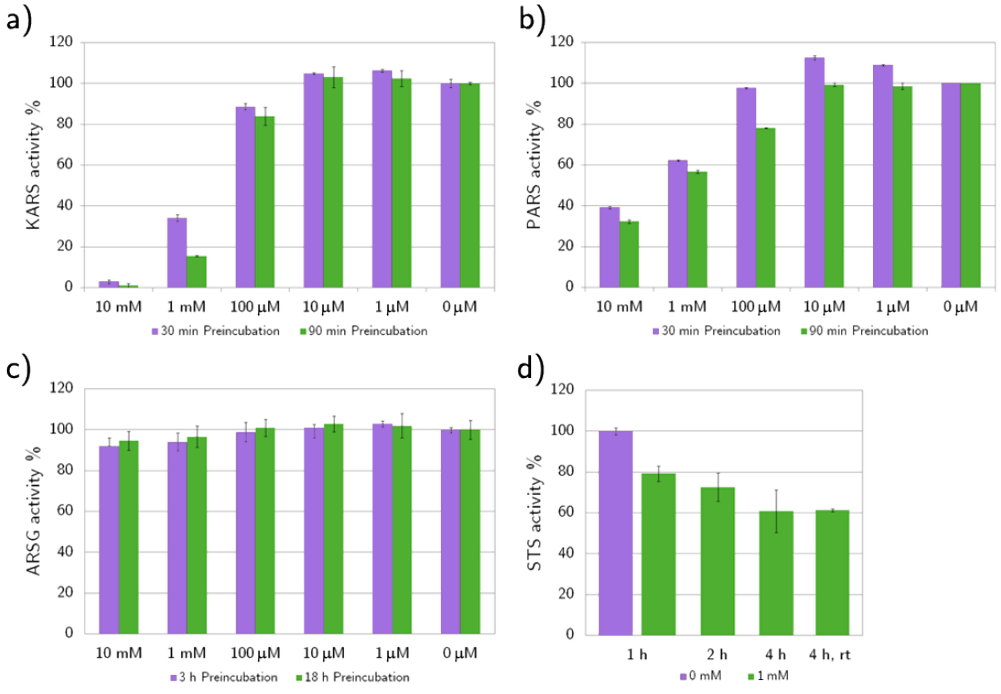

Figure 3.18: Inhibition of a) KARS, b) PARS and c) ARSG by probe precursor **1c** at different concentrations. d) Time-dependent inhibition of STS by 1 mM **1c**.

Time-dependent inactivation of enzymes can be seen if active site residues are involved in QM capture.[104] This was exemplarily assessed by time- and concentration-dependent inhibition of KARS by QM precursor **1c**. A dependency of both time and concentration can clearly be seen in Figure 3.19. However, a determination of the kinetic parameters k_{inact} and K_i using the Kitz-Wilson method[104] usu-

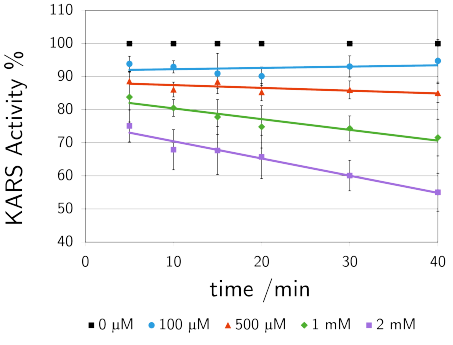

Figure 3.19: Time- and concentration-dependent inhibition of KARS by **1c**.

ally applied for mechanism-based inhibition is not possible. Kitz-Wilson methodology requires time-dependent measurement of initial substrate conversion rates at different inhibitor concentrations. Using *p*NCS as the pseudo-substrate of sulfatase activity determination, residual activity needs to be monitored at pH 10 which terminates sulfatase activity and leads to end point activity measurement.

3.4.3 Labeling Results

The next step was to extend the application of QM probes to their designated purpose i.e. the selective labeling of sulfatases in complex mixtures. To directly assess probe activation and selectivity, we opted for three model proteomes containing an active sulfatase, an inactive sulfatase and no sulfatase. These proteomic samples consisted of crude lysates from *E. coli* DH5α cells which expressed

1. recombinant KARS together with its post-translational activating enzyme AtsB[121] (Figure 3.20a),
2. recombinant KARS alone, which will remain inactive without AtsB (Figure 3.20b), and
3. no sulfatase (null vector control, Figure 3.20c).

E. coli lysate provides a non-sulfatase protein background, as it does not have any known endogenous sulfatases whereas human lysates natively contain active sulfatases.[121] KARS was chosen as the model sulfatase to be labeled since it shows QM substrate activity in the low mM range, which is representative of the biological K_m of most human sulfatases. The lysates were labeled with 1 mM probe **1a** for 60 min. Respective sulfatase activity and inactivities were confirmed via *p*NCS assays before labeling. The labeled samples were then separated by 2D-GEs. The fluorescence scans (left panel) show light spots for each labeled protein

with several horizontal spots due to modifications that influence protein pI. Coomassie stains of the gels containing active (Figure 3.20a), inactive (3.20b) and no sulfatase (3.20c) are also depicted and show about the same amount of protein (50 μg as determined by Bradford assay) were loaded on the gels.

This experiment clearly proves the necessity of active sulfatase for QM labeling. The fluorescence scans of *E.coli* lysate containing inactive KARS and wildtype *E. coli* lysate (Figure 3.20b and c, left panel) both lack fluorescent proteins. All three scans were developed for ten minutes, and the tone value was narrowed digitally beyond the usual range for the scans containing no active sulfatase to definitely visualize all labeled proteins. The bright cloud in the lower left corner of 3.20c is caused by excess of probe. Initial labeling experiments with inactive sulfatase expressing *E. coli* cells failed due to the low expression rates so that the inactive sulfatase was not visible in the coomassie stains of these gels. Low expression of inactive KARS has been previously observed[125] and might be attributed to formation of inclusion bodies. This problem was evaded by purification of inactive KARS and spiking of the lysate to approximately the same level as for the active sulfatase in Figure 3.20a. The fact that nearly no labeling was observed in the control samples even when scanning for 20 minutes and covering the area containing excessive probe proves that active sulfatase is crucial for labeling.

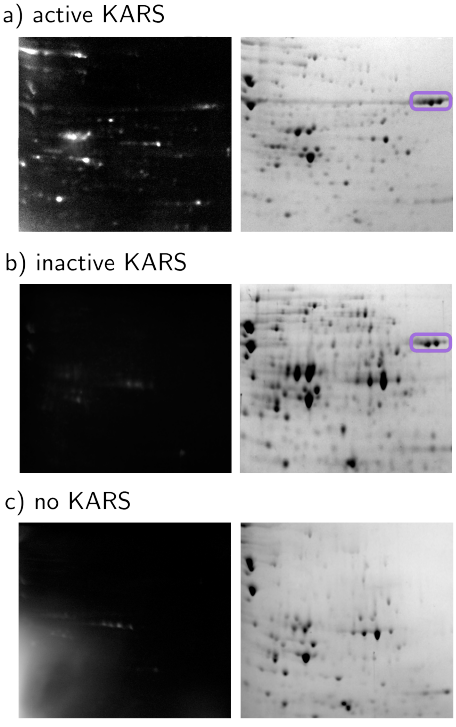

Figure 3.20: Fluorescence (left panel) and corresponding coomassie-stained (right panel) images of the 2D-GEs of probe **1a**-labeled *E. coli* lysates. The purple box indicates KARS.

A lack of specificity for QM probe **1a** was demonstrated by this experiment as most of the background proteins also show up in the fluorescence scan of active sulfatase lysate. One obvious conclusion to be drawn from these findings is that the QM precursor probe **1a** which is cleaved and activated by the sulfatase subsequently dissociates out of the active site, while still in its reactive form. Consequently, the QM-fluorescein conjugate binds to other proteins in the solution.

To verify that this is not a unique characteristic of KARS, cell lysate of STS-overexpressing cells was investigated. STS was expressed as previously described [40,123] by Eva Ennemann (BCI, Bielefeld University) and then labeled with 1 mM of probe **1a** for 60 min at 37 °C. The sample was separated by 2D-GE, and labeled proteins were detected by fluorescence scanning (Figure 3.21a).

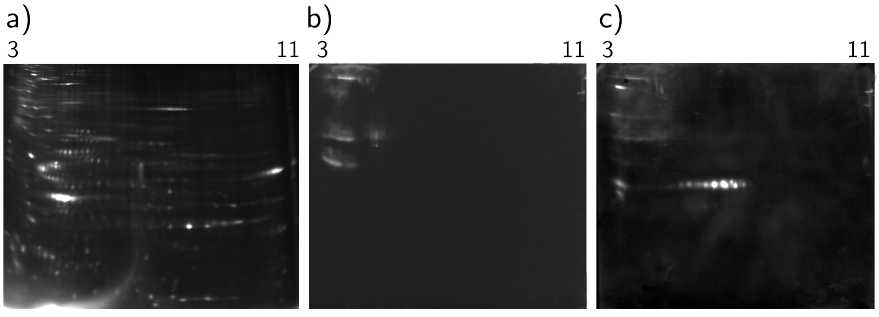

Figure 3.21: Labeling of STS-expressing cell lysate with probe **1a**. The sample was separated by 2D-GE a) fluorescence scan of the gel, b) α-STS western blot c) α-FGE western blot.

It becomes evident that just as for KARS-lysate many proteins were labeled and therefore fluorescent. STS and FGE were visualized by western blotting (WB) with an intermediate stripping step (Figure 3.20b and c; blotting was done by Eva Ennemann, BCI, Bielefeld University). STS was not transferred to the IPG strip as it is a membrane-associated protein, and therefore it could not be detected by WB (Figure 3.20b). The presence of the soluble luminal ER protein FGE was detected by WB which serves

as an indicator for successful blotting. This experiment verifies the unspecific nature of QM-labeling: the sulfatase mainly responsible for QM generation was not transferred into the gel, hence, all visible spots are due to diffused QMs.

To further investigate the nature of background protein labeling, a KARS-enriched *E. coli* lysate was used to determine whether higher abundance of sulfatase influences specificity of labeling. Incubation with probe **1a** was done exactly as described for the other *E. coli* lysates. A number of the background proteins were identified by LC-MS/MS analysis of tryptic digests as indicated by the purple frames in Figure 3.22. The results support unspecificity of background labeling since these proteins do not share common properties concerning structure, function or active site composition. By comparing labeling as detected in the fluorescence scan (left panel, Figure 3.22) with abundance as visualized by coomassie staining (right panel, Figure 3.22) of spots 8 and 9, it becomes clear that labeling does not merely correlate with abundance. Even the content of cysteine residues which are the preferred labeling sites of QM probes[55] cannot be directly correlated to the amount of labeling (compare Figure 3.22 and Table 3.1). Most probably, a mixture of factors like accessibility of cysteine side chains or other less reactive nucleophiles and abundance determines protein labeling efficiency.

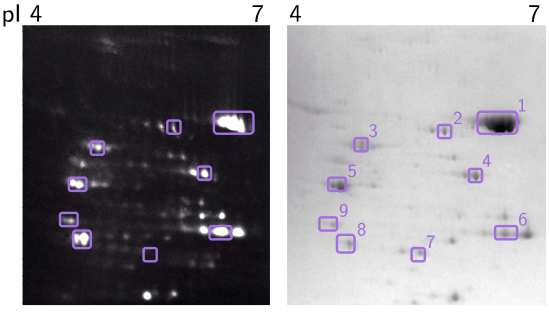

Figure 3.22: Fluorescence and corresponding coomassie-stained images of the 2D-GE of probe **1a**-labeled KARS-enriched *E. coli* lysate. The purple frames mark the identified protein spots.

Table 3.1: Proteins identified via tryptic digestion and LC-MS/MS analysis.

Spot	Protein	Sequence Coverage	Cysteine Residues
1	KARS	46 %	0
2	Pyruvate kinase I	41 %	6
3	Glutamate decarboxylase α	30 %	9
4	Serine hydroxymethyltransferase	42 %	3
5	Phosphoglycerate kinase	50 %	3
6	Glyceraldehyde-3-phosphate dehydrogenase A	53 %	3
7	Chaperone protein hchA	34 %	2
8	Elongation factor Ts	40 %	2
9	Transaldolase B	30 %	3

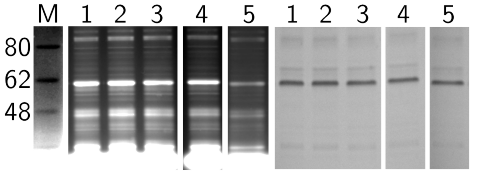

Figure 3.23: Fluorescence and respective coomassie-stained gel images of KARS-labeling with probe **1a** at increasing concentrations of ethanolamine.

Attempts were made to reduce the amount of unspecific labeling by addition of small-molecule nucleophiles (i.e. ethanolamine) to trap any diffused activated species. Prepurified KARS was used which features a high ratio of sulfatase to background protein. Labeling was conducted as described for 2D-GE experiments. Unfortunately, the addition of ethanolamine also resulted in decreased labeling of KARS, again supporting that labeling is of a non-specific origin (Figure 3.23).

Even more evidence for the non-specific nature of QM-labeling was gathered by MS studies of probe **1c**-labeled PARS and KARS. Whole protein was submitted to MALDI-ToF/ToF analysis and a clear shift of protein weight by at least around 550 Da was detected for PARS (Figure 3.24). This corresponds to about two modifications for each protein with a single modification resulting in a mass increase of 280 Da.

Only little unmodified PARS was detected as the whole protein peak shifted and this finding provides another strong clue for unspecific labeling. It is impossible that the whole population of enzyme in the sample was in its active state before labeling. The peak also broadens considerably indicating a wide mass distribution with up to ten modifications per protein accounting for an average mass shift of about 2 kDa.

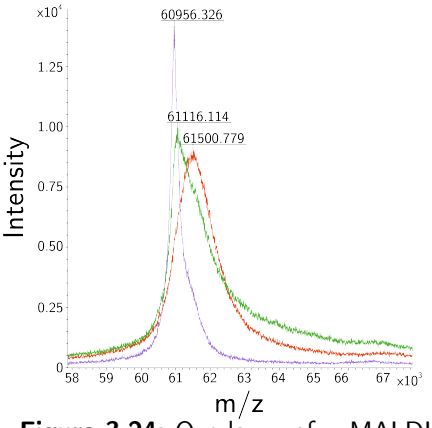

Figure 3.24: Overlay of MALDI-ToF/ToF spectra of PARS, labeled PARS and a 1:1 mixture of both samples.

The same effect was observed when labeling KARS with probe **1c**. KARS is expressed with a cleavable N-terminal propeptide which leads to three main masses even without addition of QM precursor. Therefore, the spectrum is more complicated to analyze and not as conclusive as for PARS.

These MS results prompted us to try and map exact QM targeting sites to the three-dimensional protein structure of PARS. QM **1c**-labeled and tryptically digested PARS peptides were identified using LC-MS/MS analysis. The data was scanned by Mascot MS/MS search and annotated using the in-house software QuPE.[126] The QM modification was searched as a variable mass addition to possibly all amino acid residues.

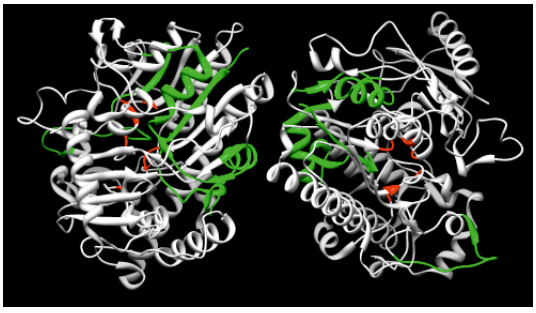

Figure 3.25: QM labeling sites of PARS (1HDH, RCSB protein data base) incubated with probe **1a**. Active site residues, labeled peptides.

The sample was unambiguously identified as PARS with a Mascot score above 2000 and about 70 % sequence coverage. Three labeled peptides were identified (Figure 3.25), although, there are most likely more which

are too low abundant and hence not detected. Importantly, these three peptides were not identified in control samples of non-labeled PARS.

The position of labeling within the peptide sequences could not be assigned since their MS/MS fragmentation patterns were not complete. The location of labeled peptides within the protein clearly supports our hypothesis of QM diffusion after sulfate ester cleavage since these peptides are too far from the active site for labeling to have occurred without prior diffusion. In our opinion labeling results in a heterogenous distribution of peptides with differing masses. The discrete peptides form low abundant populations and are therefore hard to detect via LC-MS/MS studies of crude tryptic digests.

By labeling KARS with the biotinylated probe **1b**, the biotinylated peptides should be enriched using streptavidin beads. This could lead to a more precise mapping of QM binding sites within the 3D-structure of the protein. The labeled sample and a non-labeled control were both separated by 2D-GE. Spots in the region of KARS were cut out and the peptides obtained after trypsination were applied to streptavidin beads. No protocol was available to elute peptides from the beads which is compatible with LC-MS/MS analysis. Therefore, TFA was applied to denature streptavidin and elute all bound peptides. Even though the success of biotinylation was monitored by streptavidin blotting of a 2D-GE of **1b**-labeled KARS, no peptides were detected in LC-MS/MS analysis. Either they were not eluted from the beads using TFA, other substances were coeluted and evaded detection of labeled fragments, or the distribution of labeled peptides is too heterogenous for single molecules to stick out.

3.4.4 Conclusion of QM-Type Probe Experiments

In conclusion, our results support the assumption that sulfatase-generated QMs are most likely stable enough to diffuse from the active site. Under these circumstances the electrophilic position of the QM is attacked by any other nucleophile different form an active side chain of the actual target enzyme. Sulfatase QM probes were only useful to detect sulfatase activities but there are cheaper commercially available pseudo-substrates for this purpose.

Several other studies about QM probes only examine and prove labeling of purified proteins[51,53,55,56] or unspecific labeling was ignored.[8,48] Both practices are misleading. The successful application of QM precursor probes for the selective labeling of enzymes in complex mixtures still remains to be proven. The only successful example of a specific QM-based probe was recently published for protein tyrosine phosphatase.[47] The authors added a peptide sequence to the probe to increase binding specificity to their target enzyme. It must be stated however, that this probe only targets one enzyme within the class of protein tyrosine phosphatases. Therefore, it is not useful for general ABP problems like monitoring up- and down-regulation of a whole enzyme family or identification of new enzymes.

3.5 Cyclic Sulfamates as Sulfatase Targeting Groups

Cyclic sulfamates were biochemically investigated for their dose-dependent inhibitory action on various sulfatases. Their inhibitory mechanism was partially elucidated via PARS active site labeling and LC-MS/MS analysis of labeled and tryptically digested samples. First experiments of labeling purified PARS as well as KARS and STS in a more complex mix-

tures were followed by *in situ* labeling of STS with subsequent CuAAC reaction to couple the reporter group.

3.5.1 Inhibition Experiments

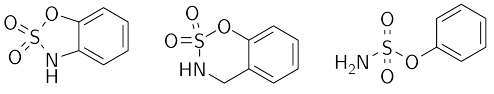

Figure 3.26: Structures of cyclic sulfamates **2a** and **40** as well as linear sulfamate **41**.

In comparison to the panel of sulfatases used to evaluate QM precursor probe **1c**, inhibition by CySA **2a**, CySA **40** and linear sulfamate (LiSA) **41** was assessed with two additional human sulfatases. Thereby, wide applicability at comparable inhibitor concentrations should be demonstrated.

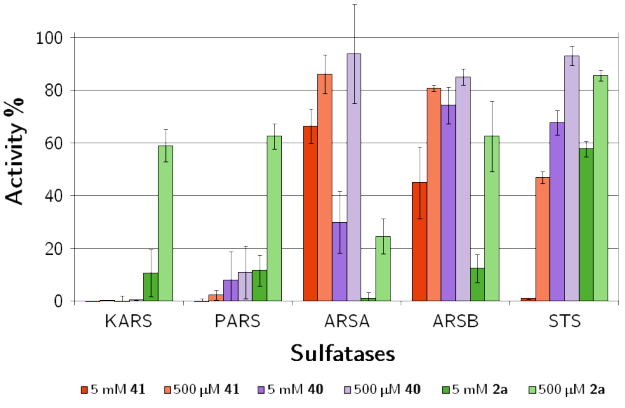

Figure 3.27: Inhibition of five different sulfatases by CySA **2a** and **40** as well as LiSA **41**.

As can be seen in Figure 3.27, the two bacterial sulfatases PARS and KARS are better inhibited by all tested molecules than the human enzymes which seem to be more specific and less tolerable towards non-native substrates. The only exception was inhibition of ARSA by CySA **2a**. For the bacterial sulfatases inhibitor **2a** displays weaker inhibitory properties requiring mM concentrations in contrast to **40** and **41** which show satisfying results at high μM concentrations.

The three human sulfatases tested respond differently to the panel of inhibitors used in this study. The linear phenyl sulfamate **41** is at the same time the most effective inhibitor and the least sterically demanding. However, due to the postulated inhibitory mechanism (Figure 3.4) this molecule is not believed to be useful for activity-based proteomics applications since it most certainly would eliminate its label. Comparing the

two cyclic sulfamates **2a** and **40**, it becomes evident that **2a** is the more potent inhibitor for ARSA, ARSB and STS.

In summary, cyclic sulfamate **2a** was chosen for incorporation into our probes. It was active against all tested sulfatases at low mM concentrations which is what we opted for. Unfortunately, time- and concentration-dependent inhibition studies to determine kinetic parameters of binding could not be recorded since the inhibition process was too fast to be accurately monitored.

3.5.2 Investigation of the Inhibitiory Mechanism

To further understand the mechanism of CySA inhibition several experiments were conducted. First, it was investigated whether the FGly residue was covalently modified by inhibiting PARS with CySA **2a** before labeling with an aldehyde addressing fluorophore. Additionally, cyanogen-bromide digestion of CySA **2a**-labeled PARS was used to detect any new peptides. These new conjugates could be generated by substitution of the enzyme-inhibitor intermediate by an internal Schiff-base formed with a lysine residue. Lastly, **2a**-labeled tryptic digests of PARS were analyzed via LC-MS/MS to identify labeling sites and dead-end adducts.

The irreversible inactivation of active sites is an important property of activity-based probes. The question of whether cyclic sulfamates were able to modify sulfatase FGly residues covalently and quantitatively was addressed by application of aldehyde and ketone directed fluorescent probes as depicted in Figure 3.28. The infrequent occurrence of aldehydes and ketones in biomolecules has stimulated the development

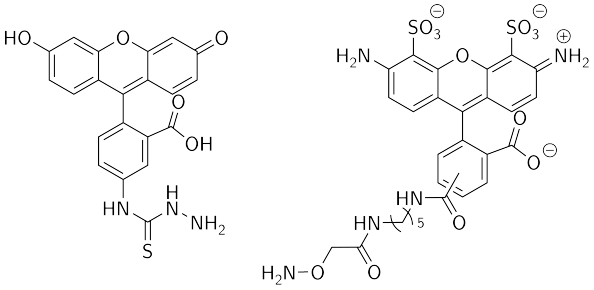

Figure 3.28: Structures of fluorescein-5-thiosemicarbazide and Alexa Fluor® 488 hydroxylamine.

of these probes to selectively introduce fluorescent labels. Various methods have been developed to first insert a carbonyl function into proteins, thus providing unique sites for chemical modification and greatly extending the possibilities of these probes.[127] For our application we used the dyes depicted in Figure 3.28: fluorescein-5-thiosemicarbazide and Alexa Fluor® 488 hydroxylamine.

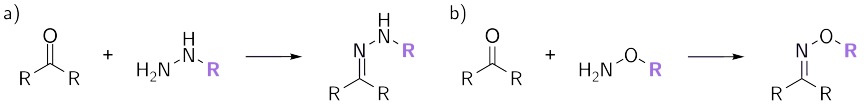

Figure 3.29: Reaction of a fluorescent hydrazine derivative as shown above with an aldehyde or ketone to form a) a hydrazone derivative or b) an oxime.

The semicarbazone formed with the semicarbazide (as seen in Figure 3.29a) as well as the O-substituted oxime formed with the hydroxylamine (Figure 3.29b) during the labeling reactions can be stabilized by reduction with $NaCNBH_3$ to avoid elimination of the label. Notably, $NaCNBH_3$ does not reduce aldehyde functions.

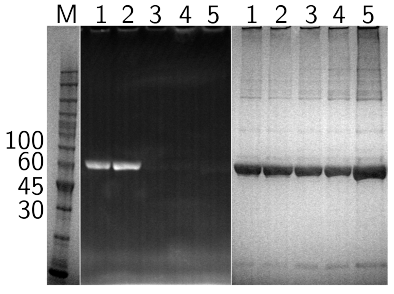

Figure 3.30: Fluorescence scan (left panel) and coomassie stain (right panel) of Alexa Fluor® 488 hydroxylamine-labeled PARS. 1) PARS; 2) reduced PARS; 3) PARS with 20 mM CySA **2a**; 4) reduced PARS with 20 mM CySA; 5) 20 μg PARS with 20 mM CySA **2a**.

The result of PARS active site modification by CySA **2a** can be seen in Figure 3.30. For this particular experiment, 5 μg PARS were incubated with 20 mM CySA **2a** to investigate whether the active site is irreversibly modified by this inhibitor class. Inactivity of preinhibited samples was verified with 4-MUS activity assays. To prove that oxime stabilization by treatment with $NaCNBH_3$ after labeling does not alter the outcome we also treated PARS with $NaCNBH_3$ before labeling with the Alexa dye overnight. We also applied a bigger amount of labeled PARS (20 μg) to detect any residual fluorescence. The samples were separated on a 1D-GE and fluorescence was measured. Lanes 1 and 2 show the labeling of FGly by the Alexa dye. Inhibi-

tion with cyclic sulfamate **2a** suppresses this labeling completely as seen in lanes 3–5. It is evident that CySA modifies FGly residues quantitatively and irreversibly. The coomassie stain clearly indicates equal amounts of protein were loaded for all samples.

To investigate the nature of active site modification, we labeled PARS with CySA **2a** until complete inhibition and then digested the sample with cyanogenbromide (CNBr). This yields relatively large peptide fragments which can be separated by 1D-GE, as CNBr only cleaves after methionine residues. One hypothetical dead-end product of CySA inhibition is a Schiff-base formed by substitution of the enzyme-CySA intermediate with the N_ϵ of a conserved lysine residue situated within the active site of sulfatases. To stabilize this potential Schiff-base, the inhibited sample was treated with $NaCNBH_3$ before the digest was initiated by addition of CNBr. After resolution by electrophoresis, no new peptide bands were detected. We therefore concluded that the FGly modification that evades labeling with the Alexa dye in Figure 3.30 was due to a covalently bound inhibitor and not a newly created intramolecular bond.

The samples used for the Alexa-labeling were also trypsinated in solution and analyzed via LC-MS/MS by Dr. S.R. Hanson (TSRI, La Jolla). The results strongly indicate a covalent modification of the tryptic peptide containing the active site FGly residue. Spectral counts of all other peptides remained unaffected by CySA inhibition, only the number of the detected FGly-containing peptide species went down to about 0–10 % of the non-labeled control. However, no dead-end adducts were detected in these experiments, probably, due to the sensitive nature of the CySA-enzyme bond.

3.5.3 Preliminary Sulfatase Labeling Results

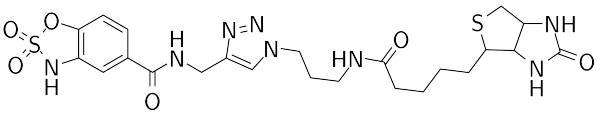

2e

Figure 3.31: CySA-biotin conjugate **2e**.

For first visualization and labeling studies biotinylated CySA **2e** as depicted in figure 3.31 was used (provided by Dr. S.R. Hanson, TSRI, La Jolla). This probe allows for enrichment of labeled proteins by interaction of the biotin moiety with streptavidin-coated sepharose beads. 5 μg of PARS were labeled with 20 mM probe **2e**. As negative controls the protein was preincubated with CySA **2a** and LiSA **41**. The results of this experiment are shown in Figure 3.32. Beads enrichment, SDS-GE and western blotting were conducted by Dr. S.R. Hanson (TSRI, La Jolla).

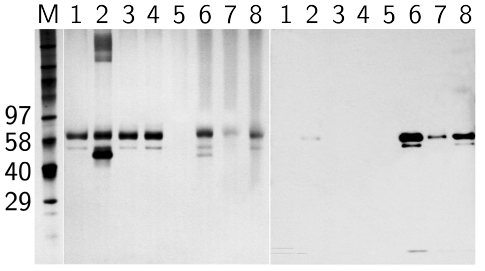

Figure 3.32: Coomassie stain (left) and α-biotin blot (right) of CySA **2e** labeled PARS. 1-4) flow-through; 5-8) beads elutions. 1, 5) 0 mM probe **2e**; 2, 6) 20 mM probe **2e**; 3, 7) preincubation with 20 mM CySA **2a** before 20 mM **2e**; 4, 8) preincubation with 20 mM SA **41** then 20 mM **2e**.

The first four lanes of both gel and blot correspond to the supernatant of streptavidin beads. Lanes 5–8 depict the respective proteins eluted from the beads by boiling. The sample without probe (lanes one and five) does not bind to the beads and is not visualized on the blot. PARS treated with the biotinylated probe binds to the beads as can be seen both in the coomassie stain as well as in the blot. PARS seen in lane two of the coomassie stain is only slightly visible in the streptavidin blot. This might be inactive protein possibly lacking the post-translational modification of the FGly residue which was therefore not labeled by **2e**. Samples applied to lanes three and four were preincubated with inhibitors and displayed about 15 % and 0 % residual activity, respectively. This might explain the slight amount of labeling seen in the blot. However, much less protein is labeled, bound and eluted in these preinhibited samples. It is striking that

the inhibitory potency of CySA **2a** and LiSA **41** towards PARS (compare Figure 3.27) does not correlate with residual labeling. The better inhibitor **41** allows for more binding of probe **2e**. This could be due to a different binding mode of the linear versus the cyclic inhibitor **2d**, the latter seems to form a more stable covalent adduct than LiSA **41**.

Since the labeling results of purified PARS were promising, we extended the same protocol to HT1080 cells expressing STS. Crude cell lysate was first incubated with the same set of inhibitors before addition of probe **2e**. Subsequently, the biotinylated proteins were enriched via streptavidin beads, the samples were split for separation on two SDS-GEs for silver staining and for western blotting.

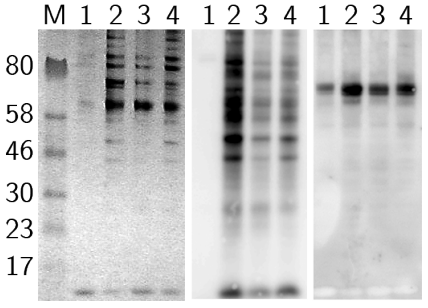

Figure 3.33: Silver stained gel (left), streptavidin (middle) and α-His blot (right) of a streptavidin pull-down experiment of STS-expressing HT1080 cell lysate labeled after incubation with probe **2e**. 1) no probe; 2) 20 mM **2e**; 3) preincubation with 20 mM CySA **2a**; 4) preincubation with 20 mM LiSA **41**.

The silver stain shows nearly no protein bound unspecifically to the streptavidin beads as can be seen in lane 1 in the left panel. The highest amount of protein bound to the sample without preincubation with other inhibitors (lane 2, left panel). However, considerable amounts of protein bound to the probe after treatment with both CySA **2a** and LiSA **41** (lanes 3 and 4, left panel). From the inhibition tests we already knew that treatment with 20 mM CySA **2a** prior to probe **2e** incubation might not completely suppress STS activity (Figure 3.27) and LiSA **41** inhibition already proved not to prevent probe **2e** binding in PARS labeling experiments (Figure 3.32). Therefore, it is not surprising that protein shows up in these lanes.

The streptavidin blot clearly confirms these results, as it shows the amount of protein biotinylation is highest in lane 2 of the middle panel. The α-His blot shows the amount of STS in all four samples. So even few

protein can be detected in the sample that was not treated with probe **2e** in the silver stain and streptavidin blot (lane 1, middle), it does contain some STS. The membrane-associated sulfatase is expressed at very low levels in human cell culture and is well detected in the selective α-His blot. In comparison, it becomes evident that probe **2e** is able to enrich STS (lane 2, right panel) and just as for PARS, preincubation with CySA **2a** and LiSA **41** does not completely reduce labeling. Even though these results look promising, further experiments are necessary to reduce the amount of unspecifically labeled proteins and investigate the nature of residual binding. Several mechanisms could account for the residual labeling as observed in lanes three and four (right panel, Figure 3.32). The activated species might diffuse out of the active site as was proven for QM-type probes, the inhibitor used for preincubation does not inhibit covalently or preinhibition was not complete. Most probes exhibit some amount of unspecific binding and require optimization of their labeling protocol.

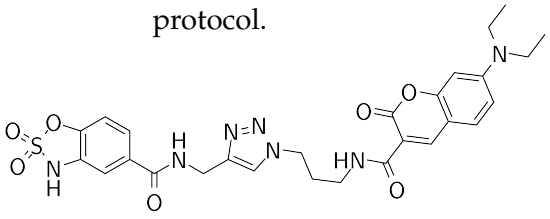

2f

Figure 3.34: CySA-coumarin conjugate **2f**.

For a better comparison of the specificity of QM and CySA labeling, we used CySA-coumarin **2f** (provided by Dr. S.R. Hanson, TSRI, La Jolla) to label KARS-enriched *E. coli* lysate (Figure 3.35). The same protocol was used as for the fluorescein derivative **1a**. Compared to Figure 3.22, fluorescence is weaker due to technical limitations of the CCD camera used for detection. The coumarin dye of probe **2f** requires different excitation and emission wavelengths which the camera does not feature.

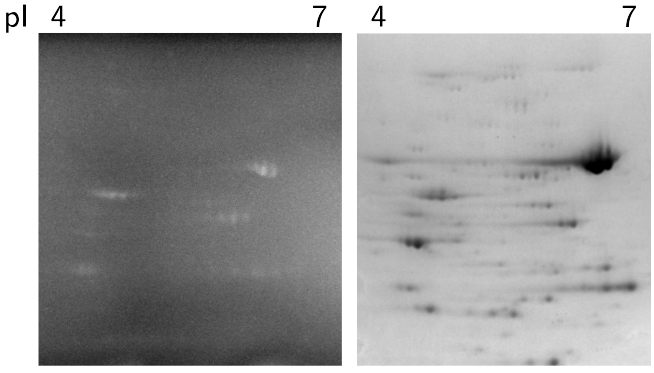

Figure 3.35: Fluorescence scan and coomassie stain of CySA **2f**-labeled KARS-enriched *E. coli* lysate.

Under these conditions CySA-labeling seems to be more specific than the QM-labeling but no definite conclusion should be drawn from these preliminary results at this point. Further experiments might be visualized using a Typhoon scanner with a wider variety of excitation and emission wavelengths. However, since only a limited amount of the probe **2f** was supplied (from Dr. S.R. Hanson, TSRI, La Jolla), the experiment could only be conducted twice.

More and more activity-based proteomic studies make use of *in situ* CuAAC reactions of inhibitor moieties and reporter groups. There are many advantages if the fluorescent dye is attached after the labeling event has occurred. The inhibitor alone is not sensitive to photobleaching so that the labeling process is less critical for the later detection. Another advantage is that the alkynylated probe precursors are much smaller and therefore more likely to diffuse through membranes. It is important which component bears the alkyne and which the azide function. Studies have shown that the alkyne is not completely bioorthogonal so that the label should bear the azide to avoid elevated levels of background binding.[119] For our first experiments with *in situ* CuAAC we used a previously published protocol which makes use of the TBTA ligand to improve the yield of this reaction in buffer systems.[73]

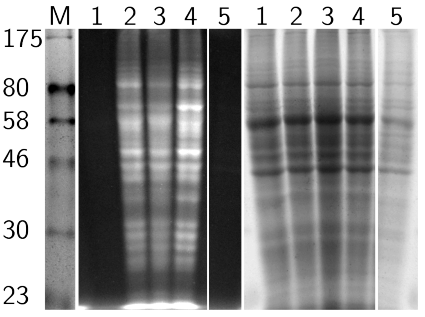

Figure 3.36: Fluorescence scan (left panel) and corresponding coomassie stain (right panel) of **2b**-labeled STS-expressing HT1080 cell lysate reacted with the reporter group **37**. 1) 0 mM **2b**; 2) 0.1 mM **2b**; 3) 0.5 mM **2b**; 4) 1 mM **2b**; 5) preincubation with 10 mM CySA **2a** before addition of 5 mM **2b**.

STS-expressing HT1080 cells were lysed and then labeled with different concentrations of alkynylated CySA **2b**. No probe **2b** and preincubation with CySA **2a** served as the negative controls. Similar to Figure 3.33 there is a band at about 70 kDa that is clearly labeled in a dose-dependent manner. Unfortunately, the identity of the other proteins visible in the fluorescence scan could not be investigated by tryptic digest and LC-MS/MS. They were either endogenously expressed sulfatases or other proteins that were unspecifically labeled. As for the other labeling experiments these results need further optimization and verification.

3.5.4 Conclusion of Cyclic Sulfamate Probe Investigations

In conclusion, CySA **2** probes are promising tools for the activity-based analysis of sulfatases. They are general inhibitors in mM concentrations of a wide range of sulfatases (Figure 3.27). The mechanism of inhibition was not fully elucidated. However, we were able to prove that CySAs are covalent inhibitors that target the active site FGly residue (Figure 3.30). First labeling studies were promising for future applications like fluorescence microscopy and the investigation of samples with unknown sulfatases.

3.6 Experimental

3.6.1 Synthesis of Quinone Methide Precursor Probe 1b

2-Acetoxy-2-(4-acetoxyphenyl)acetic acid (11)

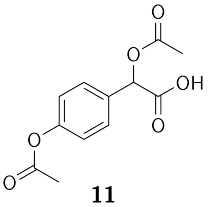

11

4-Hydroxymandelic acid (1.11 g, 6.57 mmol) was dissolved in 6 mL pyridine and cooled to 0 °C. 2 mL of Ac_2O were added and the reaction mixture was stirred for 30 min at 0 °C. The solvent was removed in vacuum and the residue was dissolved in 20 mL DCM. The product was acidified with 10 mL of 2 M HCl and the phases were separated. The organic layer was dried over Na_2SO_4 and after evaporation of DCM in vacuum, product **11** was obtained as a colorless solid (1.42 g, 5.61 mmol, 86 %).
^{1}H-NMR (500 MHz, $CDCl_3$, TMS): δ [ppm] = 2.20 (s, 3H, C**H**$_3$), 2.32 (s, 3H, C**H**$_3$), 5.95 (s, 1H, C**H**OC), 7.12 (m, 2H, **H**$_{ar}$), 7.50 (m, 2H, **H**$_{ar}$), 9.99 (s br, 1H, COO**H**).
^{13}C-NMR (126 MHz, $CDCl_3$, TMS): δ [ppm] = 20.6 (**C**H$_3$), 21.1 (**C**H$_3$), 73.4 (**C**HOC), 122.1 (**C**$_{ar}$), 128.9 (**C**$_{ar}$), 130.7 (**C**$_{ar}$), 151.4 (**C**$_{ar}$O), 169.3 (**C**=O), 170.3 (**C**=O), 173.8 (**C**OOH).

2-Acetoxy-2-(4-acetoxyphenyl)-*N*-(2-propynyl)acetamide (12)

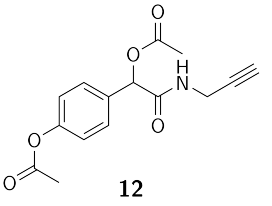

12

Carboxylic acid **11** (1.42 g, 5.61 mmol) was dissolved in 60 mL DCM and 282 μL (4.40 mmol) propargylamine, 2.01 g (10.5 mmol) EDC·HCl and 2.23 mL (16.1 mmol) TEA were added. After stirring overnight at rt, the mixture was washed with 2 M HCl (1 $\times$ 30 mL) and brine (1 $\times$ 30 mL) before drying over Na_2SO_4. Evaporation in vacuum yielded **12** as a colorless solid (1.47 g, 5.07 mmol, 90 %).
^{1}H-NMR (500 MHz, $CDCl_3$, TMS): δ [ppm] = 2.19 (s, 3H, C**H**$_3$), 2.26 (t, 1H, ^4J = 2.5 Hz, C≡C**H**), 2.30 (s, 3H, C**H**$_3$), 4.05-4.19 (m, 2H, C**H**$_2$), 6.11 (s, 1H, C**H**OC), 6.49 (s br, 1H, N**H**), 7.10 (m, 2H, **H**$_{ar}$), 7.45 (m, 2H, **H**$_{ar}$).
^{13}C-NMR (126 MHz, $CDCl_3$, TMS): δ [ppm] = 21.0 (**C**H$_3$), 21.1 (**C**H$_3$), 29.2 (**C**H$_2$), 72.2 (C≡**C**H), 74.3 (**C**HOC), 78.9 (**C**≡CH), 122.0 (**C**$_{ar}$), 128.8 (**C**$_{ar}$), 132.8 (**C**$_{ar}$), 151.2 (**C**$_{ar}$O), 167.8 (**C**=O), 169.0 (**C**=O), 169.3 (**C**=O).

2-Hydroxy-2-(4-hydroxyphenyl)-*N*-(2-propynyl)acetamide (13)

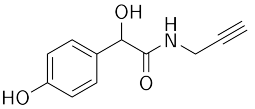

13

1.44 g (4.90 mmol) of amide **12** were dissolved in 50 mL MeOH. The solution was cooled to 0 °C before slowly adding 80 mL 2 M NaOH and stirring for 3 h. The reaction was acidified to a pH of 1-2 with 2 M HCl. The mixture was washed with DCM (4 $\times$ 50 mL) and the aqueous phase was lyophilized. The residue was adsorbed to Celite for flash chromatographic separation (EA/*n*-hexanes = 2:1). The product **13** was obtained as a colorless oil (164 mg, 0.08 mmol, 17 %).
^{1}H-NMR (500 MHz, $CDCl_3$, D_4-MeOH, TMS): δ [ppm] = 2.38 (m, 1H, C≡C**H**), 4.03 (m, 2H, C**H**$_2$), 4.96 (s, 1H, C**H**OH), 6.79 (m, 2H, **H**$_{ar}$), 7.23 (m, 2H, **H**$_{ar}$).

^{13}C-NMR (126 MHz, $CDCl_3$, D_4-MeOH, TMS): δ [ppm] = 28.9 (**C**H_2), 71.7 (C≡**C**H), 73.9 (**C**HOH), 79.2 (**C**≡CH), 115.6 (**C**$_{ar}$), 128.3 (**C**$_{ar}$), 130.8 (**C**$_{ar}$), 157.2 (**C**$_{ar}$OH), 173.8 (**C**ONH).
MS (ESI): m/z = 204.0 (calcd. 204.1 for [M-H]$^-$), 240.0 (calcd. 240.0 for [M+Cl]$^-$).

4-(1-Hydroxy-2-oxo-2-(2-propynylamino)ethyl)phenyl 2,2,2-trichloroethyl sulfate (14)

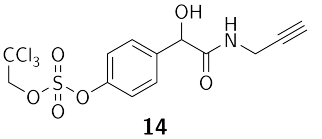

14

Alcohol **13** (60 mg, 0.27 mmol) was dissolved in 60 mL DCM, and 39 mg (0.32 mmol) DMAP as well as 54 μL (0.39 mmol) TEA were added. 239 mg (0.97 mmol) 2,2,2-trichloroethyl chlorosulfate were dissolved in 10 mL DCM and added dropwise over 10 h to the reaction mixture. The solution was stirred for further 9 h at rt before it was washed with water (1 × 30 mL), 5 % (w/v) $KHSO_4$ (3 × 30 mL), 10 % $NaHCO_3$ (w/v) (2 × 30 mL) and brine (2 × 30 mL). The organic layer was dried over Na_2SO_4 and the crude product was adsorbed to Celite for flash chromatographic purification (EA/PE = 1:1) to give **14** as a colorless oil (102 mg, 0.24 mmol, 91 %).
^{1}H-NMR (500 MHz, $CDCl_3$, TMS): δ [ppm] = 2.26 (m, 1H, C≡C**H**), 3.64 (s, 1H, O**H**), 3.98-4.17 (m, 2H, NHC$\mathbf{H}_2$), 4.85 (s, 2H, $CCl_3C\mathbf{H}_2$), 5.07 (s, 1H, C**H**OH), 6.71 (s br, 1H, N**H**), 7.36 (m, 2H, **H**$_{ar}$), 7.51 (m, 2H, **H**$_{ar}$).
^{13}C-NMR (126 MHz, $CDCl_3$, TMS): δ [ppm] = 29.2 (NHC$\mathbf{H}_2$), 72.1 (C≡**C**H), 73.2 (**C**HOH), 78.7 (**C**≡CH), 80.4 ($CCl_3\mathbf{C}H_2$), 92.3 (**C**Cl_3), 121.4 (**C**$_{ar}$), 128.5 (**C**$_{ar}$), 138.8 (**C**$_{ar}$), 150.0 (**C**$_{ar}$OS), 171.0 (**C**ONH).
MS (ESI): m/z = 413.9 (calcd. 413.9 for [M-H]$^-$), 451.8 (calcd. 451.9 for [M+Cl-H]$^-$).

4-(1-Fluoro-2-oxo-2-(2-propynylamino)ethyl)phenyl 2,2,2-trichloroethyl sulfate (15)

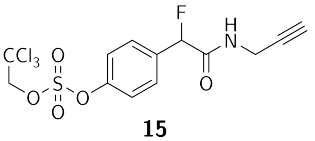

15

80 mg (0.19 mmol) of compound **14** were dissolved in 5 mL DCM and cooled to -20 °C. 49 μL (0.37 mmol) DAST were added and the mixture was stirred for 1 h at -20 °C followed by 14 h at rt. 1 mL MeOH was added and stirred for 10 min before removal of the solvent in vacuum. The crude product was purified by flash chromatography (DCM/MeOH = 35:1) to yield **15** as a colorless oil (56 mg, 0.13 mmol, 70 %).
^{1}H-NMR (500 MHz, $CDCl_3$, TMS): δ [ppm] = 2.30 (t, 1H, ^{4}J = 2.5 Hz, C≡C**H**), 4.03-4.21 (m, 2H, NHC$\mathbf{H}_2$), 4.72-4.90 (s, 2H, $CCl_3C\mathbf{H}_2$), 5.83 (d, 1H, ^{2}J = 47.7 Hz, C**H**F), 6.71 (s br, 1H, N**H**), 7.40 (m, 2H, $\mathbf{H}_{ar}$), 7.57 (m, 2H, $\mathbf{H}_{ar}$).
^{13}C-NMR (126 MHz, $CDCl_3$, TMS): δ [ppm] = 29.1 (NH**C**H_2), 72.4 (C≡**C**H), 78.4 (**C**≡CH), 80.5 ($CCl_3\mathbf{C}H_2$), 90.6 (d, ^{1}J= 190.8 Hz, **C**HF), 92.3 (**C**Cl_3), 121.4 ($\mathbf{C}_{ar}$), 128.3 (d, ^{3}J = 6.9 Hz, C_{ar}CHF), 134.2 (d, ^{2}J = 19.4 Hz, C_{ar}), 150.6 ($\mathbf{C}_{ar}$OS), 167.5 (d, ^{2}J = 20.7 Hz, **C**ONH).
^{19}F-NMR (471 MHz, $CDCl_3$, $CFCl_3$ external): δ [ppm] = -181.5 (d, ^{2}J = 48.2 Hz, CH**F**).

Probe 1b Assembly

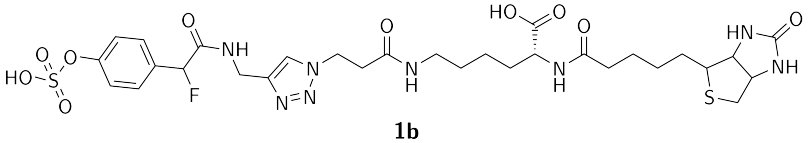

1b

Preloaded resin **24** was synthesized under standard peptide chemistry conditions. Briefly, 1 g of 2-chlorotrityl resin (loading capacity 1 mmol/g)

was loaded by reacting 1.5 mmol Fmoc-Lys(Alloc)-OH and 6 mmol DIPEA in DCM to give a total loading of 0.90 mmol/g resin. Side-chain Alloc-deprotection was achieved using 6 eq. phenylsilane and 0.1 eq. $Pd(PPh_3)_4$ in DCM under argon atmosphere. Coupling of 3-azidopropionic acid was done with 3 eq. each of the acid and TBTU and 6 eq. of DIPEA in DCM. Fmoc-cleavage was accomplished using 4 % (v/v) piperidine and 4 % (v/v) DBU in DMF. To couple biotin, 3 eq. of the acid, 3 eq. TBTU and 6 eq. DIPEA were dissolved in DMF and added to the resin with occasional stirring for 2 h at rt. The CuAAC proceeded with 1 eq. alkyne **15**, 12 eq. sodium ascorbate and 24 eq. CuI in DMF under argon atmosphere over night. All steps were monitored by MALDI-ToF-MS analysis. The resin was treated with 20 % (v/v) HFIP in DCM, and the product was purified by preparative HPLC to give **26b** as a colorless solid (25.7 mg, 0.029 mmol, 29 %).

^{1}H-NMR (500 MHz, $CDCl_3$, TMS): δ [ppm] = 1.21-1.91 (m, 12H, C**H**$_2$), 2.30 (m, 2H, C**H**$_2$CO), 2.72 (m, 1H, SC**H**$_{\mathbf{2a}}$), 2.81 (m, 2H, C**H**$_2$CO), 2.93 (m, 1H, SC**H**$_{\mathbf{2b}}$), 3.09-3.22 (m, 3H, SC**H**, C**H**$_2$), 4.31 (m, 1H, C**H**$_{biotin}$), 4.44 (m, 1H, C**H**$_{biotin}$), 4.47-4.58 (m, 3H, C**H**$_2$, C**H**COOH), 4.63 (t, 2H, ^3J = 6.6 Hz, NCH$_2$C**H**$_2$CO), 4.91 (s, 2H, C**H**$_2$CCl$_3$), 5.82 (s, 1H, ^2J = 47.7 Hz, C**H**F), 7.42 (m, 2H, **H**$_{ar}$), 7.58 (m, 2H, **H**$_{ar}$), 7.68 (s, 1H, C**H**N).

^{13}C-NMR (126 MHz, $CDCl_3$, TMS): δ [ppm] = 22.9 (**C**H$_2$), 25.8 (**C**H$_2$), 28.1 (**C**H$_2$), 28.7 (**C**H$_2$), 31.2 (**C**H$_2$), 34.5 (**C**H$_2$), 35.5 (**C**H$_2$), 36.0 (**C**H$_2$), 39.2 (**C**H$_2$), 40.6 (**C**H$_2$S), 41.6 (**C**H$_2$NH), 46.7 (**C**H$_2$NN), 52.2 (**C**HCOOH), 55.9 (**C**HS), 60.4 (**C**H$_{biotin}$), 61.9 (**C**H$_{biotin}$), 80.7 (CCl$_3$**C**H$_2$), 90.6 (d, ^1J = 189.7 Hz, **C**HF), 92.6 (**C**Cl$_3$), 121.6 (**C**$_{ar}$), 123.9 (**C**$_{triazole}$), 128.8 (d, ^3J = 6.9 Hz, **C**$_{ar}$), 135.1 (d, ^2J = 19.5 Hz, **C**$_{ar}$), 144.2 (**C**$_{triazole}$), 150.8 (**C**$_{ar}$OS), 164.7 (NH**C**ONH) 169.0 (d, ^2J = 23.0 Hz, **C**ONH), 170.2 (**C**ONH), 174.9 (**C**ONH), 175.0 (**C**OOH).

^{19}F-NMR (471 MHz, $CDCl_3$, $CFCl_3$ external): δ [ppm] = -180.5 (d, ^2J = 47.6 Hz, CH**F**).

For the final deprotection of the sulfate ester 22 mg (0.025 mmol) of the probe **26b** were dissolved in MeOH/PBS pH 7.28 = 1:1 and 1 g HCl-activated zinc dust was added. The reaction proceeded very slowly over five days until reaction monitoring via MALDI-ToF showed no further starting material. Zinc powder was removed by filtration over Celite and the crude product was purified by preparative HPLC to give probe **1b** as a colorless solid (7 mg, 0.010 mmol, 40 %).
MS (ESI-FT-ICR): m/z = 377.11125 (calcd. 377.10936 monoisotopic mass for $[M\text{-}H]^{2-}$).

3.6.2 Synthesis of Cyclic Sulfamate Probe Components

Pyridinium-2-(4-hydroxy-3-(*N*-tosyl)phenyl)acetic acid 27

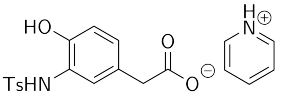

27

2-(3-Nitro-4-hydroxyphenyl)acetic acid (4.99 g, 25.31 mmol) was dissolved in 150 mL MeOH, a pinch of Pd/C was added, and Ar was bubbled through the suspension for 15 min. Then the atmosphere was exchanged by H_2 and the reduction was allowed to proceed under stirring for 4 h at rt until no starting material was detected by TLC (DCM/MeOH = 9:1). The precipitated product was dissolved by addition of 150 mL acetic acid, Pd/C was removed by filtration over Celite, and removal of the solvents in vacuum yielded the amine as a light brown solid (4.23 g, 25.29 mmol, 99 %)

587 mg (3.51 mmol) of the amine were dissolved in 20 mL of DCM/pyridine = 1:1 and the mixture was cooled to 4 °C. 1.2 eq. of tosylchloride

(794 mg, 4.24 mmol) were added and the reaction was stirred for 60 min at rt. The solvent was removed by coevaporating twice with toluene. The pyridinium salt **27** was obtained as a colorless solid (1.35 g, 3.37 mmol, 96 %) after flash chromatography (DCM/MeOH = 9:1).
TLC (DCM/MeOH = 9:1): R_f = 0.26.
^{1}H-NMR (500 MHz, $CDCl_3$, TMS): δ [ppm] = 2.34 (s, 3H, C$\mathbf{H}_3$), 3.46 (s, 2H, C$\mathbf{H}_2$), 6.68 (m, 1H, $\mathbf{H}_{ar}$), 6.85 (m, 1H, $\mathbf{H}_{ar}$), 7.18 (m, 2H, $\mathbf{H}_{ar}$), 7.24 (m, 1H, $\mathbf{H}_{ar}$), 7.35 (m, 2H, $\mathbf{H}_{pyridinium}$), 7.64 (m, 2H, $\mathbf{H}_{ar}$), 7.76 (m, 1H, $\mathbf{H}_{pyridinium}$), 8.55 (m, 2H, $\mathbf{H}_{pyridinium}$).
^{13}C-NMR (126 MHz, $CDCl_3$, TMS): δ [ppm] = 21.5 (**C**H_3), 40.5 (**C**H_2), 115.5 (**C**$_{ar}$), 123.5 (**C**$_{ar}$), 124.3 (**C**$_{ar}$), 124.4 (**C**$_{ar}$), 126.0 (**C**$_{ar}$), 126.9 (**C**$_{ar}$), 127.4 (**C**$_{ar}$), 129.5 (**C**$_{ar}$), 136.0 (**C**$_{ar}$), 137.1 (**C**$_{ar}$), 143.8 (**C**$_{ar}$), 147.6 (**C**$_{ar}$), 149.0 (**C**$_{ar}$), 174.7 (**C**OOH).
MS (ESI): m/z = 319.9 (calcd. 320.3 for [M-H-pyridinium]$^-$).

N-(2-Propynyl)-2-(4-hydroxy-3-(*N*-tosyl)phenyl)acetamide 28

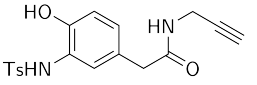

28

The pyridinium salt **27** (1.35 g, 3.37 mmol) was dissolved in 23 mL DCM. To this solution 1.1 eq. HOBt·H_2O (502 mg, 3.72 mmol), 3.2 eq. NMM (1.15 mL, 10.29 mmol), 1.1 eq. EDC·HCl (711 mg, 3.71 mmol) and 1.6 eq. propargylamine (344 μL, 5.43 mmol) were added, and it was stirred at rt for 36 h. The mixture was washed with 0.1 M HCl (3 $\times$ 10 mL), and the product precipitated as a colorless solid in the organic layer. This was filtered, taken up in EA and crystallized from DCM to give **28** as a colorless solid (333 mg, 0.93 mmol, 29 %).
TLC (DCM/EA = 9:1): R_f = 0.4.

^{1}H-NMR (500 MHz, D_4-MeOH): δ [ppm] = 2.35 (s, 3H, C**H**$_3$), 2.60 (t, 1H, ^{4}J = 2.6 Hz, C≡C**H**), 3.35 (s, 2H, C**H**$_2$), 3.94 (d, 2H, ^{3}J = 2.5 Hz, NHC**H**$_2$), 6.62 (m, 1H, **H**$_{ar}$), 6.85 (m, 1H, **H**$_{ar}$), 7.25 (m, 3H, **H**$_{ar}$), 7.63 (m, 2H, **H**$_{ar}$).
^{13}C-NMR (126 MHz, D_4-MeOH): δ [ppm] = 21.5 (**C**H$_3$), 29.7 (NH**C**H$_2$), 42.8 (**C**H$_2$), 72.4 (C≡**C**H), 80.6 (**C**≡CH), 116.2 (**C**$_{ar}$), 125.3 (**C**$_{ar}$), 125.8 (**C**$_{ar}$), 127.7 (**C**$_{ar}$), 127.9 (**C**$_{ar}$), 128.5 (**C**$_{ar}$), 130.4 (**C**$_{ar}$), 138.1 (**C**$_{ar}$), 144.9 (**C**$_{ar}$), 149.8 (**C**$_{ar}$), 173.9 (**C**OOH).

2-(1-Tosyl-2,2-dioxo-benzo[*d*]-1,2,3-oxathiazole-5-yl)-*N*-(2-propynyl) acetamide 29

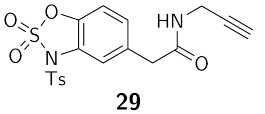

29

The alkyne **28** (333 mg, 0.93 mmol) was dissolved in 20 mL DCM/DMF = 3:1, and 4 eq. TEA (541 μL, 3.88 mmol) were added at rt. The solution was cooled to -78 °C then 3 eq. sulfurylchloride (213 μL, 2.63 mmol) in 4 mL DMF were added over 2 h. The suspension was warmed to 0 °C, and washed with water. The aqueous phase was extracted with 50 mL DCM, and the combined organic phases were washed with brine and dried over Na_2SO_4. After removal of the solvent the brown oil was subjected to flash-chromatography (DCM/EA = 9:1) to yield **29** as a colorless solid (117 mg, 0.28 mmol, 30 %).
TLC (DCM/EA = 9:1): R_f = 0.3.
^{1}H-NMR (500 MHz, $CDCl_3$, TMS): δ [ppm] = 2.30 (t, 1H, ^{4}J = 2.4 Hz, CH_2C≡C**H**), 2.42 (s, 3H, C**H**$_3$), 3.57 (s, 2H, C**H**$_2$), 4.03 (s, 2H, NHC**H**$_2$), 7.03 (m, 1H, **H**$_{ar}$), 7.15 (m, 1H, **H**$_{ar}$), 7.35 (m, 2H, **H**$_{ar}$), 7.64 (m, 1H, **H**$_{ar}$), 7.88 (m, 2H, **H**$_{ar}$).
^{13}C-NMR (126 MHz, $CDCl_3$, TMS): δ [ppm] = 21.8 (**C**H$_3$), 29.4 (NH**C**H$_2$), 42.5 (**C**H$_2$), 71.6 (C≡**C**H), 79.4 (**C**≡CH), 112.0 (**C**$_{ar}$), 116.4 (**C**$_{ar}$), 126.2

($\mathbf{C}_{ar}$), 127.4 ($\mathbf{C}_{ar}$), 129.0 ($\mathbf{C}_{ar}$), 130.3 ($\mathbf{C}_{ar}$), 132.4 ($\mathbf{C}_{ar}$), 133.2 ($\mathbf{C}_{ar}$), 140.2 ($\mathbf{C}_{ar}$), 147.3 ($\mathbf{C}_{ar}$), 170.6 (**C**=O).
MS (ESI): m/z = 443.0 (calcd. 443.5 for $[M+Na]^+$).

N-(2-Propynyl)-2-(2,2-dioxo-benzo[*d*]-1,2,3-oxathiazole-5-yl)acetamide 2b

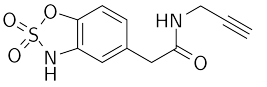

2b

The cyclic sulfamate **29** (117 mg, 0.28 mmol) was suspended in 7.5 mL ACN/H_2O = 4:1. After addition of 1.5 eq. NaN_3 (28 mg, 0.43 mmol), the starting material dissolved completely, and the reaction was stirred for 2.5 h at rt until TLC (EA/*n*-hexanes/AcOH = 7:3:0.1) showed nearly complete turnover. Additional 12 mg (0.19 mmol) of NaN_3 were added to the mixture, and it was stirred for another hour at rt. The solvents were removed in vacuum and the residue was taken up in 10 mL water. The pH was adjusted to 2 using 0.1 M HCl, and the aqueous phase was extracted with EA (3 × 10 mL). The combined organic phases were dried over Na_2SO_4. The solvent was removed and the residue was purified by flash chromatography (EA/*n*-hexanes/AcOH = 7:3:0.1). The product **2b** (85 mg, 0.28 mmol, quant.) was obtained after coevaporating twice with toluene.
TLC (EA/*n*-hexanes/AcOH = 7:3:0.1): R_f = 0.3.
^{1}H-NMR (500 MHz, D_6-acetone): δ [ppm] = 2.64 (t, 1H, ^4J = 2.5 Hz, C≡C**H**), 3.54 (s, 2H, CH_2), 3.98 (m, 2H, NHC$\mathbf{H}_2$), 7.03 (m, 1H, $\mathbf{H}_{ar}$), 7.09 (m, 1H, $\mathbf{H}_{ar}$), 7.15 (m, 1H, $\mathbf{H}_{ar}$).
^{13}C-NMR (126 MHz, D_6-acetone): δ [ppm] = 30.1 (NH**C**H_2), 43.8 (**C**H_2), 73.1 (C≡**C**H), 82.2 (**C**≡CH), 112.4 ($\mathbf{C}_{ar}$), 115.3 ($\mathbf{C}_{ar}$), 125.6 ($\mathbf{C}_{ar}$), 132.1 ($\mathbf{C}_{ar}$), 134.8 ($\mathbf{C}_{ar}$), 143.8 ($\mathbf{C}_{ar}$), 171.5 (**C**=O).

MS (ESI): m/z = 266.9 (calcd. 267.3 for $[M+H]^+$), 288.9 (calcd. 289.3 for $[M+Na]^+$).
MS (ESI-FT-ICR): m/z = 289.02522 (monoisotopic mass calcd. 289.02535 for $[M+Na]^+$ deviation 0.45 ppm).

O-tert-Butyl-*N*-(2-hydroxyethyl)carbamate 30

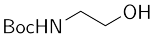

30

2-Aminoethanol (5.09 g, 52.13 mmol) was dissolved in 100 mL ACN/H_2O = 1:1 cooled to 4 °C, and 2.5 eq. NaOH (5.20 g, 130 mmol) were added. Then 0.8 eq. Boc_2O (9.45 g, 43.30 mmol) were added. The reaction was stirred at 4 °C for 30 min and then at rt overnight. The pH was adjusted to 7 using 5 % (w/v) $KHSO_4$, and the product was extracted with EA (4 × 30 mL). The combined organic phases were washed with 5 % (w/v) $KHSO_4$ (2 × 30 mL) dried over Na_2SO_4, and the solvent was removed in vacuum to yield **30** as a yellow oil (5.9 g, 36.8 mmol, 85 %).
^{1}H-NMR (500 MHz, $CDCl_3$, TMS): δ [ppm] = 1.45 (s, 9H, C**H**$_3$), 2.56 (s, 1H, OH), 3.28 (m, 2H, C**H**$_2$), 3.69 (t, 2H, ^3J = 5.0 Hz, C**H**$_2$), 5.04 (s, 1H, N**H**).
^{13}C-NMR (126 MHz, $CDCl_3$, TMS): δ [ppm] = 14.1 (**C**H_3), 40.7 (N**C**H_2), 61.0 (O**C**H_2), 115.5 (**C**$(CH_3)_3$), 143.4 (**C**=O).
MS (ESI): m/z = 184.00 (calcd. 184.20 for $[M+Na]^+$).

O-tert-Butyl-*N*-(2-propynyloxy)ethylcarbamate 31

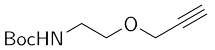

31

1.1 eq. NaH (1.60 g, 40 mmol) were suspended in 100 mL THF and cooled to 4 °C. Carbamate **30** (5.90 g, 36.7 mmol) in 100 mL THF and 1.1 eq. propargylbromide (6.0 g, 40 mmol) in 50 mL THF were added.

The reaction was refluxed for 10 min and then stirred at rt for 48 h. The mixture was then diluted with water, and THF was removed in vacuum. The aqueous phase was extracted with EA (4 × 30 mL), and the combined organic phases were washed with brine (1 × 30 mL), dried over Na_2SO_4, and the solvent was removed in vacuum. The product **31** (5.80 g, 29.2 mmol, 60 %) was obtained as a yellow oil after flash chromatography (DCM/EtOH = 30:1).
TLC (DCM/EtOH = 10:1): R_f = 0.8.
^{1}H-NMR (500 MHz, $CDCl_3$, TMS): δ [ppm] = 1.45 (s, 9H, C**H**$_3$), 2.45 (m, 1H, C**H**), 3.35 (d, 2H, ^3J = 5.0 Hz, C**H**$_2$), 3.59 (t, 2H, ^3J = 5.0 Hz, C**H**$_2$), 4.16 (d, 2H, ^4J = 1.8 Hz, C**H**$_2$C≡CH), 4.92 (s, 1H, N**H**).
^{13}C-NMR (126 MHz, $CDCl_3$, TMS): δ [ppm] = 28.4 (**C**H$_3$), 40.3 (N**C**H$_2$), 58.2 (O**C**H$_2$), 69.1 (O**C**H$_2$), 74.6 (≡**C**H), 79.3 (**C**(CH$_3$)$_3$), 79.4 (**C**≡CH), 155.9 (**C**=O).

2-(2-Propynyloxy)ethylammonium trifluoroacetate 32

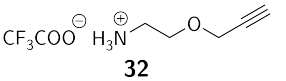

32

Carbamate **31** (4.30 g, 21.6 mmol) was dissolved in 200 mL DCM/TFA = 4:1 and stirred at rt for 1 h. The product was coevaporated twice with toluene and then lyophilized to give **32** (5.00 g, 23.3 mmol, quant.) as a yellow oil after flash chromatography (DCM/EtOH = 30:1).
TLC (DCM/EtOH = 10:1): R_f = 0.1.
^{1}H-NMR (500 MHz, $CDCl_3$, TMS): δ [ppm] = 2.51 (t, 1H, ^4J = 2.5 Hz, CH$_2$C≡C**H**), 3.21 (s, 2H, C**H**$_2$), 3.77 (t, 2H, ^3J = 5.0 Hz, C**H**$_2$), 4.20 (m, 2H, C**H**$_2$), 8.00 (s, 3H, N**H**$_3$).
^{13}C-NMR (126 MHz, $CDCl_3$, TMS): δ [ppm] = 39.4 (N**C**H$_2$), 58.3 (O**C**H$_2$), 65.0 (O**C**H$_2$), 75.6 (≡**C**H), 78.5 (**C**≡CH).

N-(2-(2-Propynyloxy)ethyl)-2-(4-hydroxy-3-(*N*-tosyl)phenyl)acetamide 33

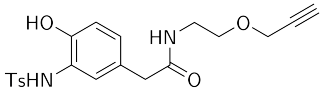

33

Amine **32** (271 mg, 2.00 mmol) was dissolved in 5 mL DMF. 0.5 eq. HOBt·H_2O (135 mg, 1.00 mmol), 2.5 eq. pyridine (400 μL, 5.00 mmol), 0.5 eq. EDC·HCl (192 mg, 1.00 mmol) and 1.7 eq. carboxylic acid **27** (389 mg, 1.21 mmol) were dissolved in 2 mL of DMF and added to the reaction mixture before stirring at rt overnight. DMF was removed under vacuum, and the residue was taken up in DCM, washed with 0.5 M HCl (3 × 10 mL), 10 % (*w*/*v*) $NaHCO_3$ (3 × 10 mL), and brine (1 × 10 mL). The organic phase was dried over Na_2SO_4, and the solvent was removed in vacuum. Column chromatography (*n*-hexanes/iPrOH = 6:1) yielded **33** as a colorless solid (114 mg, 0.28 mmol, 28 %).

^{1}H-NMR (500 MHz, $CDCl_3$, TMS): δ [ppm] = 2.32 (s, 3H, C**H**$_3$), 2.48 (t, 1H, ^4J = 2.3 Hz, C≡C**H**), 3.33 (s, 2H, C**H**$_2$CO), 3.46 (m, 2H, C**H**$_2$NH), 3.61 (t, 2H, ^3J = 5.1 Hz, OC**H**$_2$), 4.14 (d, 2H, ^4J = 2.4 Hz, C**H**$_2$C≡CH), 7.03 (m, 1H, **H**$_{ar}$), 7.16 (m, 2H, **H**$_{ar}$), 7.18 (m, 1H, **H**$_{ar}$), 7.61 (m, 2H, **H**$_{ar}$), 8.05 (m, 1H, **H**$_{ar}$).

^{13}C-NMR (126 MHz, $CDCl_3$, TMS): δ [ppm] = 21.7 (**C**H$_3$), (N**C**H$_2$), 58.5 (O**C**H$_2$), 64.5 (O**C**H$_2$), 68.3 (C≡**C**H), 75.2 (**C**≡CH), 123.7 (**C**$_{ar}$), 124.5 (**C**$_{ar}$), 126.0 (**C**$_{ar}$), 127.4 (**C**$_{ar}$), 127.5 (**C**$_{ar}$), 129.6 (**C**$_{ar}$), 129.7 (**C**$_{ar}$), 136.0 (**C**$_{ar}$), 144.0 (**C**$_{ar}$), 148.1 (**C**$_{ar}$), 172.7 (**C**=O).

2-(1-Tosyl-2,2-dioxo-benzo[*d*]-1,2,3-oxathiazole-5-yl)-*N*-(2-(propargyloxy)ethyl)acetamide 34

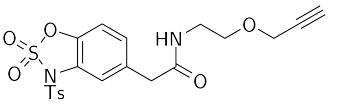

34

The alkyne **33** (114 mg, 0.28 mmol) was dissolved in 6 mL DCM, and 4 eq. TEA (157 μL, 1.13 mmol) were added at rt. The solution was cooled to -78 °C and 3 eq. sulfurylchloride (69 μL, 0.85 mmol) in 2 mL DCM were added over 2 h. The reaction mixture was stirred at -78 °C for further 90 min, then it was diluted with 10 mL DCM/H_2O = 1:1. The phases were separated, and the aqueous phase was extracted with DCM (2 $\times$ 20 mL). The combined organic phases were dried over Na_2SO_4. After removal of the solvent the product was subjected to flash-chromatography (DCM/EA = 3:1) to yield **4** as a colorless solid (70 mg, 0.15 mmol, 53 %).
TLC (DCM/EA = 9:1): R_f = 0.3.

N-(2-(Propargyloxy)ethyl)-2-(2,2-dioxo-benzo[*d*]-1,2,3-oxathiazole-5-yl)acetamide 2c

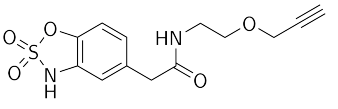

2c

The cyclic sulfamate **34** (50 mg, 0.11 mmol) was suspended in 6.5 mL ACN/H_2O = 4:1. After addition of 1.2 eq. NaN_3 (9 mg, 0.13 mmol), the starting material dissolved completely, and the reaction was stirred for 16 h at rt. ACN was removed, the pH of the solution was adjusted to 2 with 1 M HCl, and the aqueous phase was extracted with EA (3 $\times$ 10 mL). The combined organic phases were dried over Na_2SO_4. The solvent was removed, and the residue was purified by vacuum filtration over silica

gel (eluent: EA). The product **2c** (35 mg, 0.11 mmol, quant.) was obtained as a colorless solid after coevaporating twice with toluene.
^{1}H-NMR (500 MHz, D_4-MeOH): δ [ppm] = 2.83 (t, ^4J = 2.4 Hz, 1H, C≡C**H**), 3.37 (t, ^3J = 5.3 Hz, 2H, NHC$\mathbf{H}_2$), 3.49 (s, 2H, C$\mathbf{H}_2$CO) 3.57 (t, ^3J = 5.5 Hz, 2H, **C**$\mathbf{H}_2$O), 4.15 (d, ^4J = 2.5 Hz, 2H, C$\mathbf{H}_2$C≡CH), 6.94-6.97 (m, 2H, $\mathbf{H}_{ar}$), 7.04-7.10 (m, 1H, $\mathbf{H}_{ar}$).
^{13}C-NMR (126 MHz, D_4-MeOH): δ [ppm] = 40.4 (**C**H_2CO), 43.2 (NH**C**H_2), 58.8 (O**C**H_2), 69.1 (**C**H_2O), 76.0 (C≡**C**H), 80.5 (**C**≡CH), 111.6 ($\mathbf{C}_{ar}$H), 114.0 ($\mathbf{C}_{ar}$H), 124.4 ($\mathbf{C}_{ar}$H), 132.0 ($\mathbf{C}_{ar}$), 133.9 (C_{ar}NH), 143.5 ($\mathbf{C}_{ar}$O), 173.7 (**C**=O).

N-(2-(4-(((2,2-Dioxo-benzo[*d*]-1,2,3-oxathiazol-5-yl)acetamido)methyl)-1H-1,2,3-triazole-1-yl)ethyl)biotinamide 2d

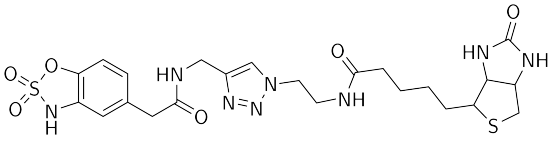

2d

3.11 mL of a 5 mM solution of alkyne **2b** in MeOH, 3.11 mL of a 5 mM solution of biotin azide **39** in MeOH, and 3.11 mL 5 mM TBTA in DMSO were combined. To this solution 0.6 mL 54 mM ascorbate and 0.6 mL 47 mM $CuSO_4$ both in water were added. The pH of the resulting suspension was adjusted with 1 mL PBS pH 7.2, and the reaction was allowed to proceed for 1 h at rt before lyophilization. The resulting colorless residue was taken up in ACN/H_2O = 1:1 and purified by preparative HPLC to give **2d** as a colorless solid (4.2 mg, 0.007 mmol, 47 %).
^{1}H-NMR (600 MHz, D_4-MeOH): δ [ppm] = 1.36 (m, 4H, C=OCH$_2$CH_2-CH_2CH_2), 1.64 (m, 4H, C=OCH$_2$CH_2CH_2CH_2), 2.14 (m, 2H, C=OCH$_2$-CH_2CH_2CH_2), 2.70 (m, 1H, SC$\mathbf{H}_{2a}$), 2.93 (dd, 1H, ^2J = 5.0 Hz, ^3J = 12.7 Hz, SC$\mathbf{H}_{2b}$), 3.19 (m, 1H, SC**H**), 3.50 (s, 2H, C=OC$\mathbf{H}_{2,ar}$), 3.62 (t, 2H, ^3J = 5.8 Hz, NCH$_2$C$\mathbf{H}_2$NHC=O), 4.30 (dd, 1H, ^2J = 4.4 Hz, ^3J = 7.8 Hz, SCHC**H**),

4.43 (s, 2H, NHC$\mathbf{H}_{2,triazole}$), 4.48 (m, 3H, $SCH_2C\mathbf{H}$, $NC\mathbf{H}_2CH_2NHC{=}O$), 6.97 (m, 2H, $\mathbf{H}_{ar}$), 7.09 (m, 1H, $\mathbf{H}_{ar}$), 7.79 (s, 1H, $C\mathbf{H}_{triazole}$).
MS (ESI-FT-ICR): m/z = 579.18193 (monoisotopic mass calcd. 579.18025 for $[M+H]^+$ deviation 2.91 ppm.

3.6.3 Biochemical Evaluation of QM Precursors

^{19}F-NMR Measurements

^{19}F-NMR real-time investigations of QM sulfate cleavage were conducted with KARS containing *E. coli* lysate, PARS, STS containing HT1080 cell lysate and ARSG. All experiments were performed in regular NMR tubes at 37 °C on a Bruker Avance 600. After an initial ^{19}F-NMR spectrum of probe **1c** was recorded, the respective enzymes were added, and fluoride liberation was followed by continuous NMR measurements for up to 14 d.

Table 3.2: Sample compositions for ^{19}F-NMR measurements of 1c turnover by various sulfatases.

Enzyme	Concentration or Lysate Volume	Inhibitor 1c Concentration	Buffer in D_2O
KARS	10 μL; 70 nM	140 μM	500 μL 10 mM Tris pH 7.5
PARS	70 μM	5 mM	600 μL 100 mM Tris pH 8.0
STS	20 μL	5 mM	500 μL 10 mM Tris pH 7.2
ARSG	3 nM	5 mM	500 μL 0.5 M NaAcOH pH 5.6

Inhibition Assays of Arylsulfatases

Turnover of *p*NCS by sulfatases to *p*-nitrocatechol (*p*NC) was measured by absorbance at 515 nm after stopping the enzyme reactions with 0.33 M NaOH. All measurements were performed in triplicate and repeated twice.

KARS (1 μM, in 50 mM Tris, pH 7.5, 250 mM NaCl) or PARS (1 μM, in 50 mM Tris, pH 8.5) were incubated for various times with different concentrations of inhibitor **1c** in 10 μL assay volume at room temperature. After preincubation, the sulfatase activity assay was initiated by adding *p*NCS to a final volume of 310 μL with a final assay composition of 35 nM sulfatase, 8 mM *p*NCS and 8 mM Tris (at pH 7.5 or pH 8.5, for KARS and PARS, respectively). The enzyme reaction was allowed to proceed for 10 min at room temperature before quenching by addition of 600 μL 1 M NaOH. For ARSG the assay was conducted as follows: ARSG (20 nM, in 0.5 M NaOAc, pH 5.6) was incubated with **1c** for 3 h and for 18 h at 37 °C. Sulfatase activity assay was then initiated by adding *p*NCS to a final concentration of 8 mM in 0.5 M NaOAc, pH 5.6, with a total volume of 150 μL, and the enzyme was allowed to react for 60 min at 37 °C. The reaction was stopped by addition of 150 μL 1 M NaOH.

Steroidsulfatase Activity Assay as Conducted by E. Ennemann

STS lystate (5 μL) was preincubated with inhibitor **1c** for 0, 1, 2 and 4 h at 37 °C with different concentrations of **1c** in 50 mM Tris, pH 7.4 (final volume of 47.5 μL). STS activity was determined using ^{3}H-Dehydroepiandrosterone-3-sulfate (^{3}DHEAS) as substrate.[123,128] The reaction was started by adding DHEAS to a final concentration of 5 μM containing 25,000 cpm ^{3}H-DHEAS (kindly supplied by Bernhard Schmidt, Institut für Biochemie II, Universität Göttingen) in a final volume of 50 μL. After 10 min of incubation at 37 °C the reaction was stopped by addition of 25 μL 1 M NaOH. Radioactivity of the product ^{3}H-DHEA was detected by liquid scintillation counting as previously described.[123] All measurements were done in triplicate and repeated twice.

Time- and Concentration-Dependent Inhibition Studies

KARS was incubated with different concentrations of QM precursor **1c** from 10–60 min time intervals at rt before measuring residual activity with *p*NCS as described above. The measurements were conducted as triplicates and repeated twice.

Fluorescence-Labeling Studies

50 μg prepurified KARS was incubated with 1 mM probe **1a** in 35 mM Tris pH 7.2, 140 mM NaCl, 3.5 mM $CaCl_2$ for 60 min in the dark at rt in a total volume of 20 μL. The sample was diluted and submitted to 2D-GE as described in section 5.3.1. Visualization of the fluorescence signal was achieved using in-gel fluorescence detection with a CCD-camera (excitation at λ = 460 nm, detection at λ = 515 nm). Selected spots were cut out from the gel and tryptic digestion was carried out as described in section 5.3.2. The samples were lyophilized, and stored at -20 °C until LC-MS/MS measurement. Labeling and LC-MS/MS runs were repeated twice to prove reproducibility of results.

Labeling with QM precursor **1a** in the presence of competitive nucleophile was conducted with enriched KARS lysate. 5 μg of protein were labeled with 1 mM of probe **1a** for 60 min in the presence of different concentrations of ethanolamine. Protein was separated on a 1D-SDS-GE and visualized as described in section 5.3.1.

MS Analysis of labeled PARS and KARS as Conducted in Cooperation with B. Müller

MALDI-ToF MS measurements of labeled PARS and KARS were performed on an ultrafleXtreme mass spectrometer (Bruker Daltonik). The spectra were acquired in the linear mode. 5000 single spectra were sum-

marized with a 1 kHz smartbeam-II laser for each sample. Spectral processing (smoothing and baseline subtraction) was done in flexAnalaysis (Bruker Daltonik). 10 μg purified KARS and PARS were labeled at rt with 5 mM **1c** in a total volume of 20 μL for 1 and 12 h, respectively. For MALDI-ToF MS analysis: 2 μL of the labeling mixture were mixed with 2 μL of 2 % (v/v) TFA and 2 μL of matrix solution (7.6 mg 2,5-dihydroxyacetophenone dissolved in 375 μL EtOH and 125 μL of a solution containing 18 mg/mL aqueous diammonium hydrogen citrate solution). The protein-matrix mixture (0.5 μL) was spotted onto a ground steel target for MALDI-Tof MS analysis.

LC-MS/MS analysis was done with protein spots from gels depicted in Figure 3.22. The samples were digested and analyzed as described in section 5.3.2. Protein identification was performed with MASCOT MS/MS ion search (Matrixscience) against the SwissProt-database (search parameters: taxonomy: proteobacteria, instrument: ESI-TRAP, 2 missed cleavage sites, variable modifications: oxidation (M), carbamidomethyl (C), peptide tolerance: 1000 ppm, MS/MS tolerance: 500 mmu, peptide charge: +1,+2,+3 monoisotopic, significance threshold (p<): 0.05, automatic scoring) and annotated with the in-house program QuPE[126] (FDR threshold: 0.05, minimal number of hits: 2).

50 μg PARS were labeled with 10 mM QM-precursor **1c** overnight at rt. The protein was precipitated by TCA precipitation as described in section 5.3.2. The pellet was taken up in 50 μL 6 M urea in PBS and incubated with 6 μL of 100 mM DTT for 10 min. Then 6 μL of iodoacetamide (7.4 mg in 200 μL PBS) wre added for 10 min. The sample was diluted with 90 μL of PBS and digested overnight with 15 μL trypsin at 37 °C. The sample was stored at -20 °C until LC-MS/MS measurements which were conducted as described in section 5.3.2. Protein identification was performed with MASCOT MS/MS ion search (Matrixscience) against the

SwissProt-database. Search parameters: taxonomy: proteobacteria, instrument: ESI-TRAP, 2 missed cleavage sites, variable modifications: oxidation (M), carbamidomethyl (C), labeling with probe **1c**, peptide tolerance: 1000 ppm, MS/MS tolerance: 800 mmu, peptide charge: +1,+2,+3 monoisotopic, significance threshold (p<): 0.05, automatic scoring. Proteins were annotated with the in-house program QuPE[126] (FDR threshold: 0.05, minimal number of hits: 2).

3.6.4 Biochemical Evaluation of Cyclic Sulfamates

IC_{50} Inhibition Studies

KARS, PARS, ARSA, ARSB and STS were inhibited by 500 μM and 5 mM concentrations of CySAs **2a** and **40** as well as LiSA **41**. Residual activities of KARS, PARS, ARSA and ARSB were assessed using the pseudosubstrate 4-MUS at their respective optimum pH values and buffer conditions (KARS: 0.1 M Tris pH 7.0, PARS: 0.1 M Tris pH 8.5, ARSA, ARSB: 0.5 M NaAcOH pH 5.5). It was safeguarded before that 4-MU fluorescence behaved linear to its concentration under these conditions.

4-MUS was tested for substrate inhibition and consequently all four enzymes were assayed with a pseudosubstrate concentration of 5 mM to avoid any interference with sulfatase activity. The preincubations of inhibitors and sulfatases were done in a volume of 20 μL for 60 min and the inhibitions were stopped by addition of 80 μL of 6.25 mM 4-MUS. Initial rates of 4-MUS conversion were monitored immediately at an excitation wavelength of 335 nm and an emission wavelength of 460 nm. The slopes were converted to activity percent in comparison to uninhibited sulfatase control.

STS inhibition was measured by E. Ennemann (BCI, Bielefeld University) following the protocol described above for QM precursor probes.

PARS Active Site Labeling

100 μg purified PARS were inhibited with 20 mM LiSA **41** or 20 mM CySA **2a** in a total volume of 50 μL for 60 min at rt with or without the addition of 20 mM $NaCNBH_3$. For the four inhibited samples no residual activity was detected when comparing to the uninhibited controls. All three samples were then treated with 20 mM $NaCNBH_3$ in a total volume of 62 μL for 2 h at 37 °C. The samples were precipitated using TCA precipitation as described in section 5.3.2. The protein pellets were taken up in 50 μL 50 mM NaAcOH, 150 mM NaCl, 1 % (w/v) SDS, pH 4.0. Protein concentrations of the samples were evaluated via absorption at 280 nm using a nanodrop and about 5 μg of protein was used for aldehyde labeling of all samples. 0.2 mM fluorescein-5-thiosemicarbazide or 30 eq. of Alexa Fluor® 488 hydroxylamine were added to the protein samples and incubated overnight at rt in the dark.

LC-MS/MS analysis was conducted with approximately 10 μg of the samples. They were digested with 5 μL of trypsin overnight at 37 °C and stored at -20 °C until LC-MS/MS measurement as conducted by Dr. S.R. Hanson (TSRI, La Jolla).

Biotin-Labeling

10 μg PARS were labeled for 60 min with 20 mM of the biotinylated probe **2d** with and without preinhibition by 20 mM CySA **2a** or 5 mM LiSA **41** in a total volume of 15 μL. Residual activities were checked before preinhibited samples were biotin-labeled. The protein was precipitated with TCA as described in section 5.3.2, and the pellets were taken up in 10 μL 1 % (w/v) SDS at 60 °C for 5 min. The resuspended protein was diluted by a factor of 5 in PBS buffer pH 7.2 and allowed to bind to 25 μL streptavidin beads for 2 h. The beads were washed 20 μL 3 $\times$ with 500 μL

of 0.2 % (w/v) SDS in PBS buffer pH 7.2 and 20 μL 3 $\times$ with 500 μL PBS pH 7.2. The samples were submitted to 1D-SDS-GE and western blot analysis by Dr. S.R. Hanson (TSRI, La Jolla).

70 μL STS-overexpressing HT1080 cell lysate as supplied by E. Ennemann (BCI, Bielefeld University) were labeled with CySA-biotin **2d** using the same protocol. Labeled samples were enriched using 20 μL magnetic streptavidin beads. The samples were washed 3 $\times$ with MMP buffer, divided in two and each was separated on a 15 % SDS-GE. One gel was silver stained, the other gel was used for western blotting with streptavidin-HRP conjugate as described in section 5.3.1. The gel was stripped and developed again with an αHis antibody as the primary antibody and αmouse-HRP conjugate as the second antibody by E. Ennemann (BCI, Bielefeld University).

Fluorescence-Labeling

50 μg of KARS-enriched *E. coli* lysate were incubated with 1.5 mM probe **2e** for 60 min at rt in the dark. The sample was then submitted to 2D-GE as described in section 5.3.1.

20 μL STS-overexpressing cell lysate (34 μg total protein) as supplied by E. Ennemann (BCI, Bielefeld University) were labeled with 0, 0.1, 0.5 and 1 mM CySA-alkyne **2b**. Another 20 μL of cell lysate were preincubated with 10 mM CySA **2a** before labeling with 5 mM **2b** as the negative control. All incubations were conducted for 60 min at 37 °C. Subsequently, 1 mM TBTA in DMSO, 1 mM sodium ascorbate and 1 mM **37** were added to the samples and they were mixed. After addition of 1 mM $CuSO_4$ the reaction was mixed again and then allowed to proceed for 60 min in the dark. The protein was precipitated by acetone precipitation as described in section 5.3.2 and the protein pellets were taken up in 10 μL of water and 5 μL of 3 $\times$ SDS sample buffer and submitted to 1D-SDS-GE.

4 Expression and Affinity-Based Labeling of *Arabidopsis thaliana* MMPs

Matrix metalloproteases are zinc-containing endopeptidases that reside in the extracellular matrix either as soluble, transmembrane or membrane-associated proteins.[10] Their activity is tightly regulated and misregulations have been linked to various pathological conditions from periodontal inflammation[129] over rheumatoid arthritis[130] to metastasis, angiogenesis and other cancer-related processes.[131]

4.1 Introduction to Matrix Metalloproteases

The Merops database classifies all MMPs in clan MA, family M10. They are found in bacteria, archaea, fungi, plants, animals and viruses.[132] There are 23 genes encoding for human matrix metalloproteases, and all hMMPs are expressed with a signal peptide for extracellular localization (**pre-domain**, Figure 4.1). Most hMMPs are secreted as soluble enzymes into the ECM[133] but there are also five transmembrane (**TM**) metalloproteases referred to as membrane-type hMMPs[133,134] as well as two glycosylphosphoinositol (**GPI**) anchored hMMPs.[135]

Figure 4.1: Domain structures of MMPs.

All hMMPs contain a **pro-domain** that comprises the cysteine switch, a conserved sequence important for enzyme latency through exclusion of the catalytically active

water molecule from the active site.[136] The **catalytic domain** with the conserved HEXGHXXGXXH-sequence is responsible for zinc ion coordination. In addition, all except for two hMMPs contain various **C-terminal domains** whose functions are not yet fully understood but most probably involve interaction with their substrates.[133]

MMP activitiy

Human MMPs have important functions in tissue remodeling and their activity is tightly regulated at multiple levels including transcription, activation through propeptide cleavage, inactivation by extracellular inhibitors and location inside and outside of the cell.[133] MMP activation is post-translationally regulated by inter- and intra-proteolytical removal of the pro-domain. Thereby, the conserved cysteine residue that coordinates the active site zinc ion is displaced and a water molecule can enter instead.[137] Once activated, MMPs are controlled by four classes of inhibitors found in the ECM: tissue inhibitors of metalloproteases (TIMPs), a peptide generated by proteolytic cleavage of the procollagen C-proteinase enhancer, the membrane-anchored reversion-inducing cysteine-rich protein with Kazal motifs (RECK) and α2-macroglobulin.[133] An imbalance of this post-translational regulation is connected to various pathological conditions.[129–131,138]

MMP functions

Classically, hMMPs are described as tissue remodeling enzymes with a role in protein homeostasis of the extracellular space. They are the only enzymes that can degrade triple-helical collagen as well as many other proteinaceous ECM components (e.g. aggrecan, casein, elastin, fibronectin, gelatin, laminin, nidogen, perlecan, proteoglycan link protein, serpins, tenascin, versican and vitronectin). However, more and more non-matrix constituting substrates have been identified. Some of them trigger the release of growth factors (e.g. tumor necrosis factor α, fibroblast growth factor 1, insulin-like growth factor 1 and transforming growth factor β) by either cleavage of growth-factor binding proteins or

matrix proteins to which the growth-factor binding proteins attach.[133] MMPs are also responsible for shedding of membrane-bound proteins (L-selectin,[139] soluble Fas ligand[140]) for growth-factor release. In addition to the activation, MMPs also proteolytically inactivate growth factors and cytokines both directly (e.g. chemokine connective tissue activating peptide III, monocyte chemoattractant protein, stromal cell-derived factor 1[141]) and indirectly through shedding of receptors (fibroblast growth factor receptor[142]). MMPs are also important for the immune system since they activate part of the innate immune response (defensins, by cleavage of their prodomain[143]) and cleave immunoglobulin G[144] to prevent the complement cascade.

Apart from vertebrates, MMPs have been found in various organisms: *Caenorhabditis elegans*,[145] *Drosophila*,[146] sea urchin,[147] hydra,[148] *Volvox carteri*,[149] and *Chlamydomonas reinhardtii*.[150] In these cases, MMPs were found to play diverse roles in development and tissue remodeling as was expected from their homology to hMMPs.

plant MMPs

Plant MMPs have been described for soybean,[151,152] *Arabidopsis thaliana*,[21] Cucumis sativus,[153] *Medicago trancatula*,[154] pine,[155] *Nicotiana tabacum*,[156] and *N. benthamiana*.[157] Plant MMPs are encoded by intronless genes and, like most of their human homologs, consist of a signal peptide, a pro-domain, a catalytic protease domain carrying the zinc-binding motif and often a C-terminal transmembrane domain. They play versatile biological roles in growth and development[153–155,158] as well as in pathogen and symbiont infections.[156,157,159] Transcript levels of MMP-encoding genes in soybean, tobacco and *N. benthamiana* are strongly induced during infection with pathogenic bacteria,[156,157,159] and silencing NMMP1 in *N. benthamiana* enhances susceptibility to infections by *Pseudomonas syringae* pv. *tabaci*.[157] Furthermore, MtMMPL1 from *M. trun-*

catula is induced early during nodulation with symbiotic bacteria, and silencing of this gene disturbs the nodulation process.[154]

The *Arabidopsis thaliana* genome encodes for At1–5-MMPs[21] which all display a high homology to hMMP-7. At1-, At2-, At3-, and At5-MMPs carry a C-terminal transmembrane domain and At3-MMP carries an additional putative GPI anchor motif.[21] Similar to the activation of human MMPs,[137] incubation with an organomercury compound like *para*-aminophenylmercuric acetate with At1-MMP leads to the formation of an active truncated protein of 25 kDa.[21] It can be assumed that At2–5-MMPs also require processing before they gain activity. Once activated, animal MMPs are regulated by endogenous proteinaceous inhibitors,[137] but no functional inhibitor homologs have been identified in plants yet. Plant MMPs are interesting research subjects involved in diverse biological processes. However, their post-translational regulation hampers a prediction of their activity based on transcript or protein levels. A direct readout of At-MMP activity in complex proteomes by affinity-based protein labeling would therefore represent a valuable tool to provide functional information.

At-MMPs

4.1.1 Affinity-Based Studies of Matrix Metalloproteases

There are only very few mechanism-based inhibitors described for MMPs. The derivatization of such an electrophile- and mechanism-based covalent inhibitor of MMPs[160] into ABPP probes is compromised by either weak potency[161] or restricted target selectivity.[162] Because the catalytic mechanism of metalloproteases does not involve a covalent intermediate with its substrate,[10] metalloprotease probes are based on reversible inhibitors, equipped with a photoreactive group.[12–17] Photoaffinity probes that target the active site of an enzyme display the availability of the active site, which is a hallmark for enzyme activity. Proteins that have af-

finity to the reversible inhibitor are subsequently covalently attached via photo-activation by irradiation with light.

The principle of using a photoreactive probe in combination with streptavidin-based pull-down and subsequent LC-MS/MS-based identification of the extracted proteins is called capture compound mass spectrometry (CCMS).[163] In contrast to classical activity-based proteomics, CCMS potentially addresses all proteins interacting reversibly with a small molecule including inhibitors, substrates or substrate analogs and drugs.

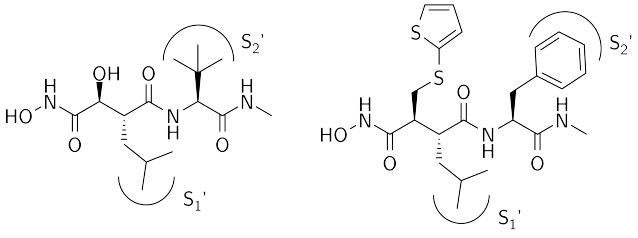

42 43

Figure 4.2: Marimastat **42** and batimastat **43** are examples for hydroxamate inhibitors of a broad range of hMMPs.

Hydroxamates are a well-studied group of reversible inhibitors suitable for metalloprotease probes. They are bidendate chelators that bind the zinc ion in the active site and are potent broad-spectrum inhibitors of MMPs. Marimastat **42** and batimastat **43** (Figure 4.2) are two important examples of this compound class.[164] Most hydroxamate metalloprotease probes exhibit structural similarities to these two inhibitors.[12–16] All previously published probes can be further divided into three groups.

The first group contains marimastat-like probes which all carry a hydroxyl group adjacent to the hydroxamate functionality as well as an *iso*-propyl side chain next to it. In comparison to marimastat **42**, other residues addressing the metalloproteases' S_2' pocket are introduced as a panel of amino acids to generate probe libraries. The methyl group of the C-terminal amide is substituted by a linker conjugated to the reporter group or a bioorthogonal attachment site (i.e. an alkyne functionality). The photoreactive group can either be part of this linker-reporter sub-

stituent or address the S_2' pocket instead of the *tert*-leucin of marimastat **42**.[12,13]

The second group comprising most metalloprotease probes are hydroxamate derivatives of succinic acid. The hydroxyl group of marimastat **42** is substituted by a hydrogen atom. The S_1' pocket of the target enzyme is addressed by various amino acid side chains[13,14] or the photoreactive group[15] similar to the P_2' site (photoreactive group[13,14] or amino acid side chain[13]). The C-terminal methyl group of marimastat **42** is substituted by a linker bearing the reporter group.[13–15]

The third and smallest group of hydroxamate probes are peptides with a hydroxamate functionality at their C-terminus. The reporter group and different photocrosslinkers are attached via linker moieties to the N-terminus of the peptide.[16]

Another very different set of hMMP probes are phosphinic peptides exhibiting K_i values in the picomolar range.[17] Interestingly, these molecules are most potent when used without irradiation as pure affinity purification tools.[166] There are also other non-covalent approaches targeting metalloproteases with hydroxamates. These probes lack the photoreactive group and are attached to a solid support for inhibitor affinity chromatography.[19,20,23,165] However, so far only one study succeeded in the detection of native hMMPs from synovial fluid[20] and no attempts have been made to extend this approach to the investigation of MMPs outside of human samples.

4.2 Objectives

To investigate MMPs in plants, a photoaffinity probe based on the MMP inhibitor marimastat **42** should be applied in this study. Such an approach seemed reasonable since plant MMPs are sensitive towards hydroxamate inhibitors: At1-MMP[21] and Cs1-MMP from cucumber[153] are efficiently inhibited by batimastat which shares a similar inhibition profile with marimastat.[164] Since first experiments to characterize endogenous proteins using an affinity-based approach with *A. thaliana* leaf extracts were not effective, At1–5-MMPs should be overexpressed *in planta*. Also, previous efforts to express these extracellular plant proteins in *E. coli* did not succeed due to the formation of inclusion bodies.[167] At-MMP overexpressing leaf lysates should be investigated by covalent labeling with a marimastat-bearing probe. The subsequent analysis of the captured proteins could be done by biotin-based enrichment and LC-MS/MS analysis.

4.3 Development of Covalently-Binding Marimastat Probes

For probe synthesis, a previously described marimastat-linker conjugate[18] was coupled to a biotinylated linker construct containing an azidotetrafluorobenzoyl group as the photoreactive moiety to yield probe **3**. Another marimastat-benzophenone conjugate[24] was biotinylated to give probe **44**. These coupling steps were conducted by Dr. C. Dalhoff (caprotec bioanalytics GmbH, Berlin).

These probes differ from previously described hydroxamate-based probes[12–16] as the majority of published probes are peptidomimetics of succinyl hydroxamate.[13–15] The hydroxyl group adjacent to the hydroxa-

mate is missing and various amino acids to target the S_2' pocket of the enzyme are employed (compare to Figure 4.3). Some of the hydroxylated hydroxamate-based probes contain their photoreactive group or different amino acid side chain residues to target the S_2' pocket. Even though these probes are similar to our probes **3** and **44**, the original marimastat moiety with the *tert*-butyl group in the S_2' position has never been used to covalently label MMPs before.

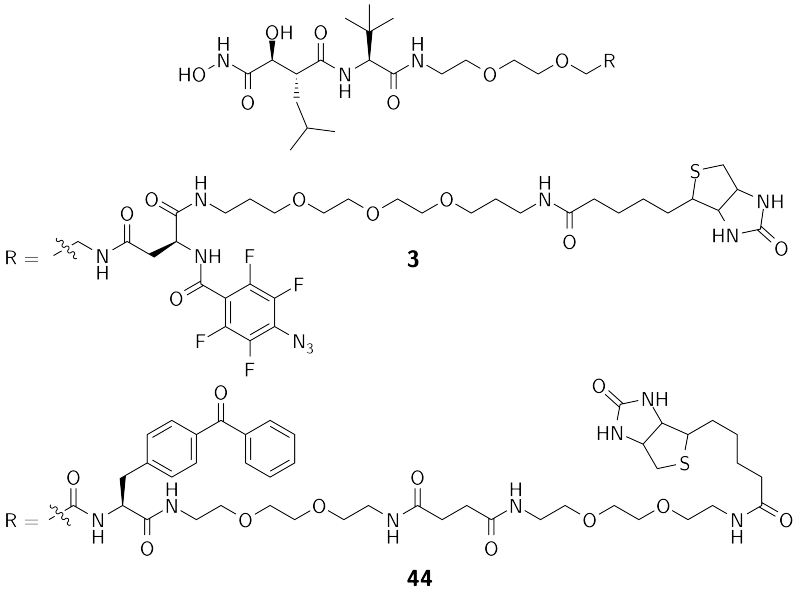

Figure 4.3: Structure of the Marimastat-based probes **3** and **44** which were used for labeling of *Arabidopsis thaliana* MMPs.

The position[15] and nature[16] of the photoreactive group of MMP targeting probes seem to be more important for labeling efficiency of photoactivatable probes than their inhibitory moiety. We therefore incorporated an azidotetrafluorobenzoyl moiety into probe **3** and benzophenone into probe **44** (Figure 4.3) in comparison to the previously used benzophenone[12,13,16] and trifluoromethyldiazirin groups.[14–16]

The IC_{50}-value for the inhibition of recombinant hMMP-2 by probe **3** was determined to be 4.7± 0.9 nM. If the sample was irradiated during inhibition, the value slightly increased to 11.1±0.6. An IC_{50}-value can still be determined with covalent photoinduced crosslinking since this bond probably still allows for diffusion of the marimastat moiety out of the active site. The photoreactive group cannot bind to the catalytic site as this is blocked by marimastat. Such an inhibition mode is comparable to pro-MMP where the Cystein-switch is covalently attached to the protein and closes the active site via a non-covalent interaction.[136] The measured values are comparable to marimastat **42** itself with an experimental IC_{50}-value of 3.2±1.0 nM[23] and a reported value of 6 nM for MMP-2.[164] The affinity of probe **3** is relatively high, since other previously reported metalloprotease probes had IC_{50}-values in the range of low nM to high μM.[12–16]

In addition to inhibition, the labeling properties of probe **3** were evaluated with recombinant hMMP-9. The labeled protein was pulled down with streptavidin beads and subsequently trypsinated. LC-MS/MS analysis of the captured protein yields a sequence coverage for hMMP-9 of 17 % with 13 unique peptides, 16 unique spectra and 17 total spectra (green peptides in Figure 4.4). The specificity of labeling was monitored by preincubation with marimastat prior to addition of probe **3**. Only one peptide was identified in this sample (green and underlined peptide in Figure 4.4). The general applicability of probe **3** for affinity-based investigation of MMPs was thereby successfully demonstrated and the probe was used for the labeling of overexpressed *Arabidopsis thaliana* MMPs.

MSLWQPLVLV LLVLGCCFAA PRQRQSTLVL FPGDLRTNLT DRQLAEEYLY RYGYTRVAEM RGESKSLGPA
LLLLQKQLSL PETGELDSAT LKAMRTPRCG VPDLGRFQTF EGDLKWHHHN ITYWIQNYSE DLPRAVIDDA
FARAFALWSA VTPLTFTRVY SRDADIVIQF GVAEHGDGYP FDGKDGLLAH AFPPGPGIQG DAHFDDDELW
SLGKGVVVPT RFGNADGAAC HFPFIFEGRS YSACTTDGRS DGLPWCSTTA NYDTDDRFGF CPSERLYTQD
GNADGKPCQF PFIFQGQSYS ACTTDGRSDG YRWCATTANY DRDKLFGFCP TRADSTVMGG NSAGELCVFP
FTFLGKEYST CTSEGRGDGR LWCATTSNFD SDKKWGFCPD QGYSLFLVAA HEFGHALGLD HSSVPEALMY
PMYRFTEGPP LHKDDVNGIR HLYGPRPEPE PRPPTTTTPQ PTAPPTVCPT GPPTVHPSER PTAGPTGPPS
AGPTGPPTAG PSTATTVPLS PVDDACNVNI FDAIAEIGNQ LYLFKDGKYW RFSEGRGSRP QGPFLIADKW
PALPRKLDSV FEERLSKKLF FFSGRQVWVY TGASVLGPRR LDKLGLGADV AQVTGALRSG RGKMLLFSGR
RLWRFDVKAQ MVDPRSASEV DRMFPGVPLD THDVFQYREK AYFCQDRFYW RVSSRSELNQ VDQVGYVTYD
ILQCPED

Figure 4.4: Sequence coverage of probe **3** labeling of human recombinant MMP-9 is 17 % as indicated by the **labeled peptide fragments**. **Propeptide**, **cysteine switch**, **HEXGHXXGXXH domain**, the signal peptide is underlined. The peptide identified in the control sample is green and underlined.

4.4 Transient At-MMP Expression

Full-length At1–5-MMPs were supposed to be expressed by cloning the respective genes into a binary vector behind the CaMV 35S promoter and transformation into *Agrobacterium tumefaciens*. Transient overexpression can then be achieved by *Agrobacterium* infiltration of *Nicotiana benthamiana* leaves which results in nearly native At-MMPs with a plant protein background: a well-suited model to optimize labeling with probe **3**. The workflow of At-MMP overexpression was amplification of *Arabidopsis thaliana* cDNA by PCR (4.4.1); cloning into the replication plasmid pFK26[168] for simple and fast amplification of the DNA by *E. coli* and cloning into the binary vector pTP5[168] which is pertinent for replication as well as protein expression. Another amplification step of the plasmid in *E. coli* is followed by the transformation of *Agrobacterium tumefaciens* (4.4.2) which enables the bacteria to induce protein expression in plants via agroinfiltration[168] (4.4.3).

Polymerase Chain Reaction

For expression of all five predicted At-MMPs, primers were designed by Dr. Kaschani (MPI for Plant Breeding Research, Cologne). PCR was done using cDNA of *Arabidopsis thaliana* col-0 which was prepared by Dr. Sommer (MPI for Plant Breeding Research, Cologne). The HA-tag which later allows a selective detection of the expressed At-MMPs via western blotting was C-terminally added by add-on-primers.

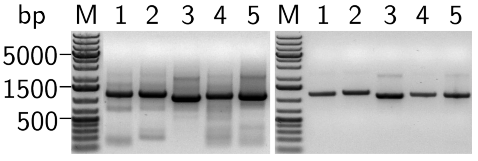

Figure 4.5: Agarose gel of crude PCR products (left) and the subsequent purification (right). 1: At2-; 2: At3-; 3: At4-; 4: At1-; 5: At5-MMP.

As depicted in Figure 4.5 it appears as if all five genes were successfully amplified from cDNA. The biproducts which are clearly visible in the agarose gel of the crude PCR products (left panel, Figure 4.5) could be removed by purification using a DNA purification kit (right panel, Figure 4.5). No optimization of PCR was needed at this point since all constructs were amplified to yield products of the expected respective DNA lengths. PCR was not anticipated to work without optimization in light of precedent experiments on the expression of At-MMPs in *E. coli* which required extensive adjustment of PCR parameters.[167]

Transformation

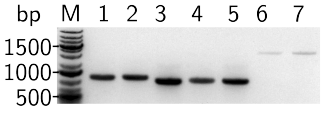

Figure 4.6: Agarose gel of purified digests. 1: At2-; 2: At3-; 3: At4-; 4: At1-; 5: At5-MMP; 6 and 7: pFK26.

To incorporate these amplified DNA fragments into the replication plasmid pFK26,[168] the plasmid and the At-MMP-encoding DNA needed to be cut by restriction enzymes that produce sticky ends. The enzymes NCoI/PstI or XhoI/PstI (see section 4.6.2) were used for DNA restriction, and the agarose gel in Figure 4.6 shows the purified

digests. Ligation of plasmid and inserts was done using the T4-DNA ligase to yield the five plasmids ready for amplification in *E. coli*.

Transformation of *E. coli* was achieved by electroporation[170] and subsequent plating of the bacteria on ampicillin LB-plates for selection. Successful incorporation of the At-MMP DNA fragments was verified by colony PCR of 16 clones for each construct (Figure 4.7). Except for At3-MMP, enough positive clones were selected and the framed ones were purified and submitted to nucleotide sequencing. For At3-MMP, further 64 clones were picked which resulted in four positive clones. All of them were purified and submitted to sequencing.

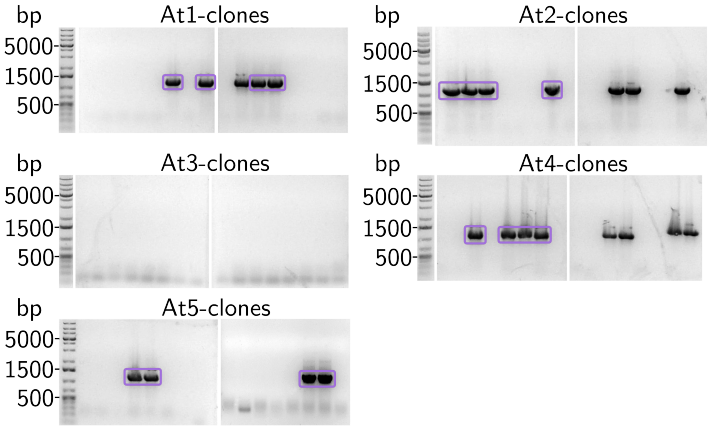

Figure 4.7: Agarose gels of colony PCR. Purple frames indicate the clones selected for nucleotide sequencing.

The sequencing results were satisfying for At1-, At2-, At4- and At5-MMPs (see Figure 4.8). All sequenced clones contained several mutations on the gene level which were only partially silent and therefore cause mutations within the protein sequences. The clones with the least amount of protein mutations were used for further studies.

At1a-MMP:
MARNLIYRRNRALCFVLILFCFPYRFGARDTPEAEQSTAKATQIIHVSNSTWHDFSRLVDVQIGSHVS
GVSELKRYLHRFGYVNDGSEIFSDVFDGPLESAISLYQENLGLPITGRLDTSTVTLMSLPRCGVSDTH
MTINNDFLHTTAHYTYFNGKPKWNRDTLTYAISKTHKLDYLTSEDVKTVFRRAFSQWSSVIPVSFEEV
DDFTTADLKIGFYAGDHGDGLPFDGVLGTLAHAFAPENGRLHLDAAETWIVDDDLKGSSEVAVDLESV
ATHEIGHLLGLGHSSQESAVMYPSLRPRTKKVDLTVDDVAGVLKLYGPNPKLRLDSLTQSEDSIKNGT
VSHRFLSGNFIGYVLLVVGLILFLYPYYDVPDYA

At1b-MMP:
MARNLIYRRNRALCLVLILFCFPYRFGARNTPEAEQSTAKATQIIHVSNSTWHDFSRLVDVQIGSHVS
GVSELKRYLHRFGYVNDGSEIFSDVFDGPLESAISLYQENLGLPITGRLDTSTVTLMSLPRCGVSDTH
MTINNDFLHTTAHYTYFNGKPKWNRDTLTYAISKTHKLDYLTSEDVKTVFRRAFSQWSSVIPVSFEEV
DDFTTADLKIGFYAGDHGDGLPFDGVLGTLAHAFAPENGRLHLDAAETWIVDDDLKGSSEVAADLESV
ATHEIGHLLGLGHSSQESAVMYPSLRPRTKKVDLTVDDVAGVLKLYGPNPKLRLDSLTQSEDSIKNGT
VSHRFLSGNFIGYVLLVVGLILFLYPYYDVPDYA

At2-MMP:
MVSSVVFGFLSLFLVVSPASAWFFPNSTAVPPSLRNTTRVFWDAFSNFTGCHHGQNVDGLYRIKKYFQ
RFGYIPETFSGNFTDDFDDILKAAVELYQTNFNLNVTGELDALTIQHIVIPRCGNPDVVNGTSLMHGG
RRKTFEVNFSRAHLHAVKRYTLFPGEPRWPRNRRDLTYAFDPKNPLTEEVKSVFSRAFGRWSDVTALN
FTLSESFSTSDITIGFYTGDHGDGEPFDGVLGTLAHAFSPPSGKFHLDADENWVVSGDLDSFLSVTAA
VDLESVAVHEIGHLLGLGHSSVEESIMYPTITTGKRKVDLTNDDVEGIQYLYGANPNFNGTTSPPSTT
KHQRDTGGFSAAWRIDGSSRSTIVSLLLSTVGLVLWFLFYPYDVPDYA

At4-MMP:
MGHHHHPCNRKPFTTIFSFFLFYLNLHNQQIIEARNPSQFTTNPSPDVSIPEIKRHLQQYGYLPQNKE
SDDVSFEQALVRYQKNLGLPITGKPDSDTLSQILLPRCGFPDDVEPKTAPFHTGKKYVYFPGRPRWTR
DVPLKLTYAFSQENLTPYLAPTDIRRVFRRAFGKWASVIPVSFIETEDYVIADIKIGFFNGDHGDGEP
FDGVLGVLAHTFSPENGRLHLDKAETWAVDFDEEKSSVAVDLESVAVHEIGHVLGLGHSSVKDAAMYP
TLKPRSKKVNLNMDDVVGVQSLYGTNPNFTLNSLLASETSTNLADGSRIRSQGMIYSTLSTVIALCFL
NWYPYDVPDYA

At5-MMP:
MGTLLLTILIFFFTVNPISAKFYTNVSSIPPLQFLNATQNAWETFSKLAGCHIGKNINGLSKLKQYFR
RFGYITTTGNCTDDFDDVLQSAINTYQKNFNLKVTGKLDSSTLRQIVKPRCGNPDLIDGVSEMNGGKI
LRTTEKYSFFPGKPRWPKRKRDLTYAFAPQNNLTDEVKRVFSRAFTRWAEVTPLNFTRSESILRADIV
IGFFSGEHGDGEPFDGATGTLAHASSPPTGMLHLDGDEDWLISNGEISRRILPVTTVVDLESVAVHEI
GHLLGLGHPSVEDAIMFPAISGGDRKVELAKDDIEGIQHLYGGNPNGDGGGSKPSRESQSTGGDSVRR
WRGWMISLSSIATCIFLISVYPYDVPDYA

Figure 4.8: Protein sequences of the four At-MMPs which were selected for further experiments. The predicted[21] signal peptide is underlined, **mutated amino acid residues**, **cysteine switch**, **plant specific conserved motif**, **HEXXH domain**, **transmembrane domain** followed by the HA-tag (YPYDVPDYA).

Two At1-clones were used for all further experiments since both contained mutations that might influence their activity: S2A and N30D for At1a- and S2A, F15L and V267A for At1b-MMP. The sequence of At2-MMP bore only one mutation (T148A). The selected mutant of At4-MMP only had mutations within the predicted[21] cleavable signal peptide: H2G and L22F. The selected clone of At5-MMP contained four substitutions:

R2G, E55K, M222T and S281P. For At3-MMP none of the picked clones included the desired sequence. Even though various efforts were made to optimize PCR for this At-MMP including new primer design, different polymerase enzymes, change of PCR buffer and variation of the PCR program, it was not possible to amplify this gene from cDNA. Due to lack of time, PCR could also not be optimized for the other At-MMPs until non-mutated genes were obtained. All attempts to apply a proof-reading DNA polymerase failed.

These selected inserts were shuttled into the binary vector pTP5 using EcoRI and HindIII as restriction enzymes. This vector comprises three antibiotic resistance sites (gentamycin, kanamycin and rifampicilin) for selection. The plasmids were first inserted into *E. coli* for amplification reasons, then purified and transformed into *Agrobacterium tumefaciens* also by means of electroporation. All steps worked well as can be derived from the colony PCR products of the *Agrobacterium* transformation (Figure 4.9). The clones with the strongest signal were chosen for protein expression as indicated by the purple frames.

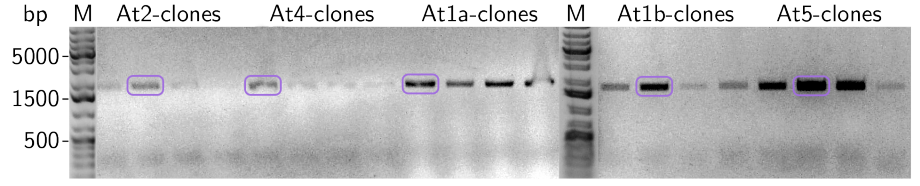

Figure 4.9: Agarose gel of the colony PCR of transformed *Agrobacterium tumefaciens*. The framed clones were later used for agroinfiltration.

Agroinfiltration and At-MMP Expression

Agroinfiltration with coexpression of the silencing inhibitor p19 was done as previously described.[176] The cloned MMPs were transiently overexpressed as C-terminally HA-tagged proteins for detection and purification purpose.

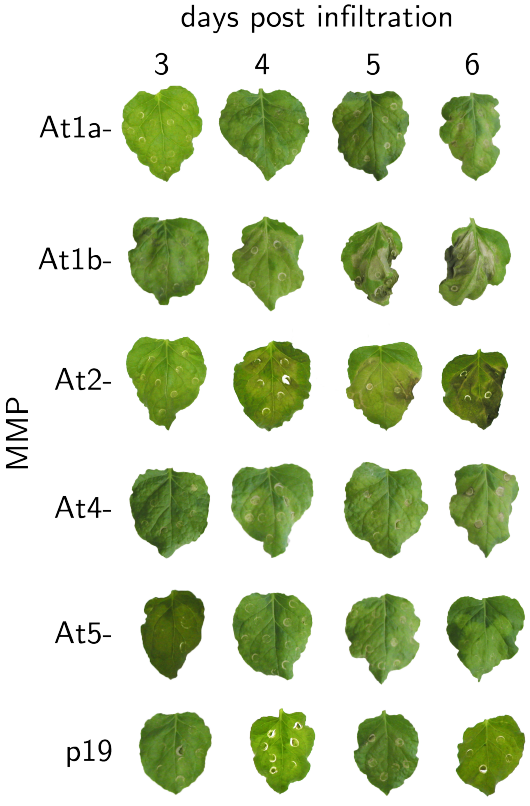

Figure 4.10: Phenotypes of the five expressed At-MMPs and p19 as a control 3–6 days after agroinfiltration.

Four-week-old *Nicotiana* plants were infiltrated with the respective *Agrobacteria* clones and harvested after three to six days post agroinfiltration since *Agrobacterium tumefaciens*-mediated protein expression usually reaches the highest level after two to three days.[177] Phenotypes of the five At-MMPs and p19 as a control were documented by photography of the leaves after harvest (Figure 4.10). In contrast to the p19-expressing leaves, it becomes evident that all At-MMPs caused severe phenotypes with the strongest characteristics for At1b- and At2-MMP. Tissue death was probably related to elevated levels of the respective MMP activity induced by endogenous activation of the pro-At-MMPs. The level of protease activity could also have been influenced by the amount of protein expressed in each leaf which varies from plant to plant and leaf to leaf. Even though all plants were grown under the same conditions, natural variation might still occur.

At4-MMP expressing leaves were analyzed 3–6 days after agroinfiltration by western blotting with αHA-biotin and streptavidin-HRP (Figure 4.11, left panel). The time-dependent evaluation shows that expression reaches the highest level three days after infiltration (Figure 4.11, lane 2–5). By comparing the phenotype of At4-MMP expressing leaves (Figure 4.10) with the blotting results, it becomes clear that leaf tissue damage corresponds with a decrease of protein yield. These results led to the harvest of leaves used for labeling studies 3–4 days after agroinfiltration.

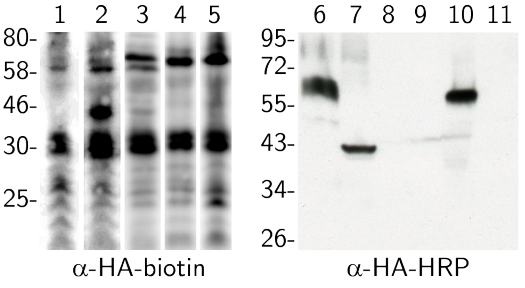

Figure 4.11: Expression analysis of harvested At-MMP-expressing leaves by western blotting. Left panel with αHA-biotin and streptavidin-HRP detection: 1: p19 control; 2: At4-MMP after 3 d, 3: At4-MMP after 4 d, 4: At4-MMP after 5 d, 5: At4-MMP after 6 d. Right panel with αHA-HRP detection: 6: At2-, 7: At4-, 8: At1a-, 9: At1b-, 10: At5-MMP, 11: p19 control.

The αHA-biotin blot exhibits a high amount of background detection. This could be either caused by endogenously biotinylated proteins which bind to streptavidin-HRP, non-specific binding of αHA-biotin or a combination of both. Since cross-detection averts a clear evaluation of HA-tagged At-MMPs, the more expensive but much more specific αHA-HRP conjugate (Figure 4.11, right panel) was used for all further western blots. The αHA-biotin in combination with streptavidin-HRP only detected At4-MMP. In contrast to that, the more specific antibody-HRP conjugate was able to visualize At2- with a mass of about 60 kDa, At4- with a mass of about 42 kDa and At5-MMP with a mass of about 55 kDa (Figure 4.11, lanes 6, 7 and 10). These protein sizes are consistent with the expected molecular masses of glycosylated proteases with aglycon masses of 41, 35 and 39 kDa for the HA-tagged proteins without the presumably cleavable[21] signal peptide. The expression of both mutated At1-MMP proteins was not visible by western blotting even though the respective

overexpressing leaves exhibited strong phenotypes (compare Figure 4.10). This might be due to a lower solubility of At1-MMPs in the extraction buffer compared to At2-, At4- and At5-MMPs. Another explanation could be the C-terminal cleavage of the HA-tag which would completely avert binding of α-HA conjugates.

4.5 Photochemical Affinity-Based Labeling of At-MMPs

To investigate whether plant MMPs are susceptible to the marimastat-based tool **3**, extracts of leaves transiently expressing At-MMPs were incubated and UV-crosslinked with probe **3**. Preincubation with an excess of marimastat **42** prior to labeling with probe **3** was used as an indicator for labeling specificity. Extracts of leaves overexpressing the silencing inhibitor p19 served as a control for the detection of endogenously biotinylated proteins.

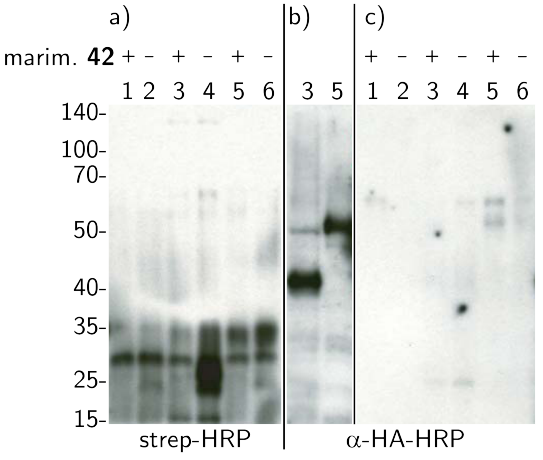

Figure 4.12: Western blot analysis of At4- and At5-MMP labeling by probe **3**. a) streptavidin-HRP after labeling; b) αHA-HRP before labeling; c) αHA-HRP after labeling. 1: p19 with marimastat, 2: p19, 3: At4-MMP with marimastat, 4: At4-MMP, 5: At5-MMP with marimastat, 6: At5-MMP.

Streptavidin-based detection of labeled proteins revealed specific, marimastat-sensitive signals of 25 kDa in At4-MMP and 35 kDa for At5-MMP leave lysates (Figure 4.12a, lanes 3/4 and 5/6). These signals did not appear in extracts of leaves not overexpressing At-MMPs (Figure 4.12a, lanes 1/2). A 30 kDa signal appears in all lanes and represents an endogenously biotinylated protein (Figure 4.12a, lanes 1–6).

The αHA-HRP western blot proves that there were full-length At4- and At5-

MMPs in the leave lysates before labeling (Figure 4.12b). However, after labeling these signals have disappeared in all samples (Figure 4.12c). A possible explanation could be a complete extraction by probe **3** but since the bands also disappeared in the samples which were pretreated with marimastat as a specificity control protein degradation most probably occurred.

The molecular mass of the labeled proteins is about 15 kDa lower than that of the full-length pro-At-MMP detected before labeling (compare Figure 4.12a, lanes 4 and 6 with 4.12b, lanes 3 and 5). The reduced sizes of labeled At-MMPs compared to the full-length protein masses is in agreement with the fact that plant MMPs are active as processed 20–36 kDa isoforms. At1-MMP, for example, is active as a 27 kDa protein,[21] soybean MMP (SMEP1) was isolated as a 19 kDa active protease,[151] cucumber MMP is active as 22 and 18 kDa isoforms,[153] and tobacco MMP is active as 36 and 22 kDa isoforms.[171]

Similarly, the 62 kDa human MMP-2 produces a 43 kDa isoform that lacks part of the protease domain C-terminal to the HEXGH domain[172] and the 82 kDa human MMP-9 produces a 35 kDa mature proteases.[173] The mechanisms of post-translational regulation in MMPs are not completely understood yet and the physiological functions of the various active isoforms are still under discussion. C-terminal truncation may alter substrate specificity as the C-terminal domain is important for substrate binding.[10,172,173] These aspects should be further investigated by time-dependent labeling of At-MMP lysates and addition of various protease inhibitors to determine when cleavage occurs as well as the class of protease which is responsible for MMP truncation.

To unambiguously confirm the identity of the probe **3**-labeled proteins, we enriched the labeled proteins on magnetic streptavidin beads. The samples were digested on-bead with trypsin and eluted peptides were

analyzed by LC-MS/MS (Figure 4.13). At4-MMP was identified from the At4-MMP-expressing sample, with 21 spectral counts covering 48 % of the protein sequence (Figure 4.13). One peptide of the endogenous MMP from *N. benthamiana* (NMMP)[157] was also identified in this sample (Figure 4.13). From the At2-MMP containing samples, three At2-MMP peptides were identified with moderate scores (Figure 4.13) even though the streptavidin blot did not show biotinylated proteins apart from the 30 kDa protein abundant in all samples (data not shown). Two peptides were identified from the At5-MMP sample which cover 8 % of the At5-MMP sequence (Fig. 4.13).

At2-MMP:
MVSSVVFGFLSLFLVVSPASAWFFPNSTAVPPSLRNTTRVFWDAFSNFTGCHHGQNVDGLYRIKKYFQ
RFGYIPETFSGNFTDDFDDILKAAVELYQTNFNLNVTGELDALTIQHIVIPRCGNPDVVNGTSLMHGG
RRKTFEVNFSRAHLHAVKR**YTLFPGEPR**WPRNRRDLTYAFDPK**NPLTEEVK**SVFSRAFGRWSDVTALN
FTLSESFSTSDITIGFYTGDHGDGEPFDGVLGTLAHAFSPPSGKFHLDADENWVVSGDLDSFLSVTAA
VDLESVAVHEIGHLLGLGHSSVEESIMYPTIITGKRKVDLTNDDVEGIQYLYGANPNFNGTTSPPSTT
KHQRDTGGFSAAWRIDGSSRSTIVSLLLSTVGLVLWFLPYPYDVPDYA

At4-MMP:
MGHHHHPCNRKPFTTIFSFFLFYLNLHNQQIIEARNPSQFTTNPSPDVSIPEIKR**HLQQYGYLPQNKE**
SDDVSFEQALVRYQK**NLGLPITGKPDSDTLSQILLPR**CGFPDDVEPK**TAPFHTGK**KYVYFPGRPRWTR
DVPLKLTYAFSQENLTPYLAPTDIRRVFRRAFGKWASVIPVSFIETEDYVIADIK**IGFFNGDHGDGEP**
FDGVLGVLAHTFSPENGRLHLDKAETWAVDFDEEKSSVAVDLESVAVHEIGHVLGLGHSSVKDAAMYP
TLKPRSKKVNLNMDDVVGVQSLYGTNPNFTLNSLLASETSTNLADGSRIRSQGMIYSTLSTVIALCFL
NWYPYDVPDYA

NMMP:
MRIPLFIAIVLVLSLSPASAHFFPNISSIPPLLKPNNTAWDAFHKLLGCHAGQKVDGLAKIKKYFYNF
GYISSLSNFTDDFDDALESALKTYQQNFNLNTTGVLDAPTIEHLIRPRCGNADVVNGTSTMNSGKPSA
GSQNIHTVAHFSFFPGRPRWPESNR**DLTYAFLPQNGLTDNIK**SVFSRAFDRWSEVTPLTFTEIASFQS
ADIKIGFFAGDHNDGEPFDGPMGTLAHAFSPPGGHFHLDGDENWVIDGAPIVEGNFFSILSAVDLESV
AVHEIGHLLGLGHSSVEDSIMFPSLAAGTRRVELANDDIQGVQVLYGSNPNFTGPNTVLTPTHENDTN
GALKFGSLWVHVVVAFFLSFLRLI

At5-MMP:
MGTLLLTILIFFFTVNPISAKFYTNVSSIPPLQFLNATQNAWETFSKLAGCHIGKNINGLSKLKQYFR
RFGYITTTGNCTDDFDDVLQSAINTYQKNFNLKVTGKLDSSTLRQIVKPRCGNPDLIDGVSEMNGGKI
LRTTEKYSFFPGKPRWPKRKRDLTYAFAPQNNLTDEVKRVFSRAFTRWAEVTPLNFTR**SESILR**ADIV
IGFFSGEHGDGEPFDGATGTLAHASSPPTGMLHLDGDEDWLISNGEISRRILPVTTVVDLESVAVHEI
GHLLGLGHPSVEDAIMFPAISGGDRKVELAK**DDIEGIQHLYGGNPNGDGGGSKPSR**ESQSTGGDSVRR
WRGWMISLSSIATCIFLISVYPYDVPDYA

Figure 4.13: Protein sequences of the four At-MMPs which were identified in LC-MS/MS analyses of probe **3**-labeled leaf lysates. The predicted[21] signal peptide is underlined, **identified peptides**, **peptides identified in marimastat control**.

Importantly, no peptides were found for At2-MMP, At5-MMP as well as NMMP and only two peptide spectral counts for At4-MMP if the samples were preincubated with an excess of marimastat **42** (Figure 4.13). These findings confirm that labeling is specific since it can be efficiently competed by addition of marimastat **42**; the original hMMP inhibitor. It is interesting to note that of all five *Arabidopsis* MMPs, only At4-MMP lacks a C-terminal transmembrane domain. This property correlates with the observation that At4-MMP causes the strongest signal in the western blots of leaf lysates (Figure 4.12c) as well as in the labeling experiments (Figure 4.12a). These observations indicate that further adjustments of the protein extraction procedure from the overexpressing leaves are needed to detect the other MMPs more efficiently.

The peptide coverage indicates that the labeled At4-MMP retained most of its prodomain. The presence of a prodomain in a labeled MMP implies that it was not inhibiting protease activity efficiently during the labeling procedure. Otherwise, the active site zinc would have been coordinated by the cysteine switch motif of the prodomain so that it could not have been available to bind the hydroxamate moiety in probe **3**. The presence of a prodomain in active MMPs is not unprecedented. The active isoform of human MMP-9 also contains part of the prodomain with the cysteine switch.[174] Furthermore, inhibition of human MMPs by TIMP-1 traps the protease in a prodomain-containing isoform.[175] Therefore, the detection of part of the prodomain does not exclude MMP activity.

The same labeling workflow as described above was applied to the At-MMP-expressing leave lysates using probe **44**. However, no At-MMP labeling was detected by streptavidin blotting or LC-MS/MS analysis (data not shown). The inferior labeling performance of the benzophenone-bearing probe **44** is supported by the literature. In a comparative study of the labeling efficiencies of metalloprotease probes with benzophenone

and trifluoromethyldiazirine as reactive groups, no labeling of spiked metalloprotease in crude lysates was observed for a benzophenone probe in contrast to a clear signal for a diazirine probe.[16]

4.6 Conclusion

Transient expression of At-MMPs was successfully induced to generate enriched leaf lysates which served as model proteomes to transfer affinity-based proteomics for the first time to plant proteins. Probe **3** was developed in cooperation with caprotec bioanalytics GmbH, Berlin. It specifically labels plant MMPs from *Arabidopsis thaliana* and most probably also *Nicotiana benthamiana*. It could be shown that trifluoromethyldiazirine **3** is a more efficient photocrosslinker than benzophenone **44** for this application which is in good correlation with previous reports.[16] Labeling of At-MMPs was optimized using At-MMP overexpressing *Nicotiana* leaf lysates. These protocols can now be used to detect endogenous MMPs in different proteomes and thereby derive evidence concerning their role in plant physiology.

4.7 Experimental Section

4.7.1 Probe Evaluation

IC_{50} Determination of Human MMP-2

Inhibition of 2 nM recombinant hMMP-2 by concentrations in the range 0.2–2000 nM of of probe **3** was assessed using 5.5 μM of the fluorogenic MMP-2/MMP-7 substrate in a final volume of 100 μL. Liberated fluorophore was excited at 330 nm and fluorescence was detected at 405 nm. Percent residual MMP activity was determined based on measured fluo-

rescence for a given inhibitor concentration in comparison to uninhibited enzyme. The measurements were done in triplicates which were repeated twice. GraphPad Prism 4.0 was used to evaluate the data and calculate IC_{50} values.

Labeling of Human MMP-9

100 ng hMMP-9 in MMP buffer were incubated with 1 μM probe **3** in the presence or absence of 500 μM marimastat in a final volume of 100 μL for 5 min on ice. The samples were UV-irradiated for 4 min at 2 °C in a 200 μL-PCR tube strip using the caproBox (caprotec bioanalytics GmbH, Berlin). 25 μL 5 $\times$ wash buffer was added to each of the samples. After homogenization, 20 μL 10 mg/mL streptavidin-coated magnetic beads were added and the samples were incubated for 3 h at 4 °C keeping the beads in suspension by rotation. The beads were collected using the caproMag and the supernatant was discarded. The beads were washed with 200 μL for each washing step: 6 $\times$ with 1 $\times$ wash buffer (diluted from the 5 $\times$ wash buffer), once with water, 6 $\times$ with 80 % (v/v) ACN and once with water. On-bead tryptic digestion was performed overnight at rt under vigorous shaking (>2000 rpm) using 0.5 μg trypsin in 10 μL 50 mM ammonium bicarbonate. The beads were magnetically collected at the side of the tube inner wall, the supernatant containing the peptides was transferred into a new tube, dried in a vacuum centrifuge, and stored at -20 °C. The peptides were analyzed by Dr. O. Gräbner (caprotec bioanalytics GmbH, Berlin) via LC-MS/MS using the LTQ Orbitrap XL mass spectrometer (Thermo Fisher Scientific, Germany). The MS/MS data were analyzed by SEQUEST and X!Tandem.

4.7.2 Expression of At-MMPs

Polymerase Chain Reaction

PCR was conducted as described in section 5.3.4. For DNA amplification of At-MMP genes total cDNA (extracted from *Arabidopsis thaliana* col-0 by Dr. Sommer at MPI, Cologne) and the following primers were used:
At1-MMP:
forward primer: 5′-GATCCATGGCTCGTAATTTAATCTATAGAAGAAACAGAGCTC-3′
reverse primer: 5′-GCATCTGCAGCTAAGCGTAATCTGGAACATCGTATGGGTATAGGA-AAAGAATCAAACCAACAACCAAC-3′
At2-MMP:
forward primer: 5′-ATGGTCTCGAGCGTTTTCGGGTTTTTATCGCTTTTC-3′
reverse primer: 5′-GCATCTGCAGCTAAGCGTAATCTGGAACATCGTATGGGTACGGTA-AGAACCACAAGACCAATC-3′
At3-MMP:
forward primer: 5′-GATCCATGGTGAGGATTTGTGTTTTCATGGTT-3′
reverse primer: 5′-GCATCTGCAGCTAAGCGTAATCTGGAACATCGTATGGGTACACTA-AATACAAAAATAATCCAAATATAATCCA-3′
At4-MMP:
forward primer: 5′-GATCCATGGGGCATCATCATCATCATCCATGCAATC-3′
reverse primer:5′-GCATCTGCAGCTAAGCGTAATCTGGAACATCGTATGGGTACCAATT-AAGAAAACAGAGAGCGATAACA-3′
At5-MMP:
forward primer: 5′-GATCCATGGGAACACTTCTTCTAACGATTTTGATCTTCTTC-3′
reverse primer: 5′-GCATCTGCAGCTAAGCGTAATCTGGAACATCGTATGGGTAAACAGA-AATCAAGAATATACACGTGGCA-3′

Transformation

Restriction enzyme digestion, ligation and transfection was conducted as described in section 5.3.5. with the following enzymes:
At2-MMP: XhoI and PstI
At1-MMP, At3-MMP, At4-MMP, At5-MMP: NcoI and PstI

The ligation was done with the digested cDNA from PCR and the pFK26[168] plasmid. Transfection of the pFK26 vectors with inserts into *E. coli* cells was done by electroporation and positive clones were screened by colony PCR (5.3.4) with the plasmid specific primer r112[168] and the respective gene specific primer. The cells were grown in presence of Ampicillin.

pFK26 plasmids containing the inserts were digested and ligated into the binary vector pTP5[168] plasmid using the quick digestion and ligation method (5.3.5). *E. coli* transfection was done by electorporation and the bacteria were grown in presence of 50 μg/mL kanamycin. The plasmids were purified and used for *Agrobacterium tumefaciens* transformation via electroporation as described in section 5.3.5. *A. tumefaciens* were grown in presence of kanamycin, rifampicilin and gentamycin.

Agroinfiltration of *Nicotiana benthamiana* leaves

A. tumefaciens were cultivated as described in section 5.3.3 and infiltrated as detailed in section 5.3.6. After harvest, the leaves were photographed, frozen in liquid nitrogen and stored at -80 °C until use. *N. benthamiana* leaf lysates were prepared by grinding leaves in millipore water. The extract was cleared by centrifugation at 13,000 rpm using a bench centrifuge and diluted with water to give a protein concentration of 1 mg/mL. Expression was monitored by western blotting as described in section 5.3.1 using either αHA-biotin and streptavidin-HRP or αHA-HRP for detection.

4.7.3 Labeling of At-MMPs with Probe 3

For Streptavidin Blotting Conducted by Dr. F. Kaschani

N. benthamiana leaf lysates were prepared by grinding leaves in 0.4 M borate buffer, pH 7.6.[178] The extract was cleared by centrifugation and diluted with cross-linking buffer to give a protein concentration of 1 mg/mL. 100 μL of the samples were transferred to a 96-well plate and pretreated with marimastat **42** in DMSO (500 μM final concentration) or DMSO for 10 min. After addition of probe **3** (1 μM final concentration), crosslinking was started by placing a hand-held UV lamp (exposing with wavelengths of 275 and 375 nm) on top of the 96-well plate. The samples were irradiated for 20–30 min on ice. The reaction was stopped by addition of 25 μL 4 $\times$ sample buffer and heating samples to 90 °C for 5 min. 10–15 μL sample was separated by 1D-SDS-GE and blotted onto PVDF membrane. Protein blots were incubated with mouse α-HA antibody and α-mouse-HRP or streptavidin-HRP in 4 % BSA in TBS-T. Membranes were washed extensively in between antibodies and prior to detection of signals with ECL.

For Enrichment on Streptavidin Beads

For enrichment of proteins labeled with probe **3**, 100 μL At-MMP-expressing *Nicotiana benthamiana* leaf lysates in MMP buffer were treated as described above for hMMP-9. The MS/MS data were analyzed by Dr. O. Gräbner (caprotec bioanalytics GmbH, Berlin) using SEQUEST and X!Tandem searching a combined database containing tobacco and *N. benthamiana* proteins which was supplemented with the HA-tagged *Arabidopsis* MMPs.

Table 4.1: Results of LC-MS/MS analysis after labeling At2-, At4- and At5-MMP expressing leaf lysates with probe **3**.

Peptide Sequence	Sequest XCorr Score
At2-MMP	
(K)NPLTEEVK(S)	2.36
(R)DLTYAFDPK(N)	1.93
(R)YTLFPGEPR(W)	1.91
At4-MMP	
(R)LHLDKAETWAVDFDEEK(S)	6.47
(R)HLQQYGYLPQNKESDDVSFEQALVR(Y)	5.73
(R)LHLDKAETWAVDFDEEK(S)	5.58
(R)DVPLKLTYAFSQENLTPYLAPTDIR(R)	4.96
(R)DVPLKLTYAFSQENLTPYLAPTDIRR(V)	4.55
(K)NLGLPITGKPDSDTLSQILLPR(C)	4.45
(K)LTYAFSQENLTPYLAPTDIRR(V)	4.27
(R)HLQQYGYLPQNK(E)	4.23
(K)LTYAFSQENLTPYLAPTDIR(R)	4.14
(K)IGFFNGDHGDGEPFDGVLGVLAHTFSPENGR(L)	3.90
(K)ESDDVSFEQALVR(Y)	3.69
(K)NLGLPITGKPDSDTLSQILLPR(C)	3.41
(R)HLQQYGYLPQNK(E)	3.13
(K)SSVAVDLESVAVHEIGHVLGLGHSSVK(D)	2.57
(K)ESDDVSFEQALVR(Y)	2.47
(K)NLGLPITGKPDSDTLSQILLPR(C)	2.38
(K)DAAMYPTLKPR(S)	2.26
(K)DAAmYPTLKPR(S)	2.05
(K)DAAmYPTLKPR(S)	2.03
(K)TAPFHTGK(K)	1.34

(Y)AFSQENLTPYLAPTDIR(R)	
NMMP	
(R)DLTYAFLPQNGLTDNIK(S)	2.86
At4-MMP neg. control	
(K)ESDDVSFEQALVR(Y)	3.64
(K)NLGLPITGKPDSDTLSQILLPR(C)	2.50
At5-MMP	
(K)DDIEGIQHLYGGNPnGDGGGSKPSR(E)	5.26
(R)SESILR(A)	1.33

5 General Experimental Section

5.1 Synthesis: Analytical Methods, Solvents, and Reagents

Chromatography

Column chromatography was conducted as flash chromatography with silica gel (0.040-0.063 mm, Macherey-Nagel) under slight application of pressure. Thin layer chromatography was performed with Silica gel 60 F_{254}, non-modified on aluminum plates (Merck). Detection was achieved by UV light (254 nm, Desaga MinUVIS), with 5 % (w/v) ninhydrine in EtOH (dipping, heating), and with 5 % (w/v) $(NH_4)_6Mo_7O_{24}{\cdot}4\,H_2O$, 0.2 % ($w/v$) $Ce(SO_4)_2$, 5 % (w/v) H_2SO_4 in water (dipping, heating). Analytical RP-HPLC: Pump: Thermo Separation Products P4000, detector: Thermo Separation Products UV 6000 LP (detection at λ = 220 nm/254 nm), controller: Thermo Separation Products SN 4000, column: Phenomenex Jupiter 4 μm Proteo 90 C18, 4.6·250 mm), eluent A: 5 % (v/v) H_2O, 95 % (v/v) ACN, 0.1 % (v/v) TFA, eluent B: 95 % (v/v) H_2O, 5 % (v/v) ACN, 0.1 % (v/v) TFA, flow: 1 mL/min, method:

Table 5.1: Method for analytical HPLC.

Time [min]	Eluent A [%]	Eluent B [%]
0	0	100
3	0	100
35	100	0
40	100	0
45	0	100

Preparative RP-HPLC: Pump: Thermo Separation Products P4000, detector: Thermo Separation Products UV1000 (detection at λ = 220 nm), controller: Thermo Separation Products SN4000, column: Phenomenex Jupiter 10 μm Proteo 90 C12, 21.2·250 mm), eluent A: 5 % (v/v) H_2O, 95 % (v/v) ACN, 0.1 % (v/v) TFA, eluent B: 95 % (v/v) H_2O, 5 % (v/v) ACN, 0.1 % (v/v) TFA, flow: 10 mL/min, method:

Table 5.2: Method for preparative HPLC.

Time [min]	Eluent A [%]	Eluent B [%]
0	0	100
3	0	100
35	100	0
40	100	0
45	0	100

Spectroscopy

NMR spectra were recorded on a Bruker DRX-500 (^{1}H-NMR: 500.1 MHz, ^{13}C-NMR: 125.8 MHz). Deuterated chloroform with TMS as internal standard was mostly used as solvent. Other deuterated solvents were referenced to the residual solvent peak.[169]

Mass Spectrometry

MALDI-ToF: PerSeptive Biosystems Voyager-DE, LSI nitrogen laser: λ = 337 nm, 1.20 m flight tube, 20 kV acceleration voltage, delay time: 90–150 ms, grid voltage: 93–95 %, guide wire voltage: 0.05 %, scans: 25–100, low mass gate: 300 Da, calibration: instrument default calibration, software: Voyager Instrument Control Panel Version 5.10, Data Explorer Version 4.0.0.0 (Applied Biosystems), matrix: 2,5-dihydroxybenzoic acid.
ESI-MS: Bruker Daltonik Esquire 3000, ion source: standard ESI/APCI source, sample introduction: direct infusion by syringe pump, nebulizer and dry gas: nitrogen, Bruker Nitrogen Generator NGM 11, cooling and collision gas: helium.
ESI-FT-ICR: Bruker Daltonik APEX III, magnet: 7.0 T 160 mm bore superconducting magnet, infinity cell, ion source: nano-ESI, nebulizer and dry gas: nitrogen, Bruker Nitrogen Generator NGM 11, cooling and collision gas: helium.

Solvents

All solvents were purchased in p.a. quality. Solvents of lower quality were purified by distillation. Anhydrous solvents were obtained as follows: Et_2O: Na/Ph_2CO, DCM: CaH_2, DMF: ninhydrine. Water for HPLC and all aqueous solutions was obtained from a Millipore MilliQ ultrapure water system (>18 $M\Omega{\cdot}cm^{-1}$). Acetonitrile for HPLC was purchased in Lichrosolv quality from Merck.

Reagents and Chemicals

Chemicals were purchased from Acros, Merck, Sigma-Aldrich, VWR, Alfa Aesar and Fluorochem. All materials were used without further purification except for the following: sulfuryl chloride: freshly distilled, zinc

dust: stirred in 1 M HCl, filtered, and washed with water, methanol, and DCM.

5.2 Biochemical Material

Material and Laboratory Equipment

2D-SDS-PAGE	SE Ruby, Höfer
96-well plate for Bradford assay and sulfatase inhibition studies	Tissue Culture Plate, Sarstedt
96-well plate for MMP activity assays	Bicro Well, NUNC
Bench centrifuge	miniSpin, Eppendorf
caproBox	caprotec bioanalytics GmbH, Berlin
caproMag	caprotec bioanalytics GmbH, Berlin
CCD-camera	LAS-3000, Fujifilm
Centrifuge	5810 R, with swing-out rotor A-4-62 and fixed-angle rotor F-34-6-38, Eppendorf
DNA purification kit	plasmid purification kit, Qiagen
Electroporator	Electroporator 2510, Eppendorf
Fluorogenic MMP-2/MMP-7 substrate	Calbiochem
Immobiline DryStrips pH 3–10NL, 18 cm	GE Healthcare
Incubator	Hood: TH-15, Shaker: KS-15, Edmund Bühler GmbH
In-gel fluorescence detection	λ_{ex} = 460 nm, detection filter: FL-Y515, LAS-3000, Fujifilm

Isoelectric focusing	Ettan^{TM}IPGphor II Isoelectric Focusing System, GE Healthcare
LC-MS/MS nano-column	15 cm $\times$ 75 μm, Acclaim PepMap^{TM} C18, 100 , Dionex
LC-MS/MS pump	1D-NanoLC Eksigent Technologies
LC-MS/MS spectrometer	LCQ Deca, Thermo Fisher Scientific
LC-MS/MS nanospray needle	uncoated, 15 μm tip, New Objective
Magnetic Streptavidin beads	Dynabeads MyOne Streptavidin C1, Invitrogen Dynal
Microplate reader	infinite M200, software: i-Control 1.4, Tecan
p19-expressing *A. tumefaciens* culture	supplied by Dr. R.A.L. van der Hoorn, MPI, Cologne
pH Electrode	Inlab 420 pH electrode, Mettler Toledo
pH-Meter	MP220 pH Meter, Mettler Toledo
Pipettes	10, 20, 100, 200, 1000, 5000, Eppendorf
Plasmid purification kit	Nucleospin, Macherey & Nagel
Plasmids	pFK26 and pTP5 were supplied by Dr. R.A.L. van der Hoorn, MPI, Cologne
Power supply	EPS 601, Amersham Biosciences
Primer	Operon
PVDF membrane	BioTrace^{TM} PVDF Membrane, Pall Life Sciences
SDS-PAGE, small gel chamber	Xcell sure lock, Novex Mini-Cell, Invitrogen
SDS-PAGE, big gel chamber	SE Ruby, Höfer
Sonifier	Model 450, Branson
Spectrometer	Heλios γ, Spectronic Unicam

Thermomixer	Thermomixer compact, Eppendorf
Water filtration system	Milli-Q, Millipore
Western blotting chamber	custom-made, Bielefeld University
Whatman filter paper	GE Healthcare

Buffers and Solutions

Buffers were solved and diluted using water obtained from a Millipore MilliQ ultrapure water system. pH adjustment was achieved with 1 M HCl and NaOH solutions. All buffers were filtered (pore size 0.22 μm) and degassed. All chemicals were used in p.a. or BioChemika quality.

3 × sample buffer	200 mM Tris·HCl pH 6.8, 25 % (w/v) glycerine, 6 % (w/v) SDS, 0.06 % (w/v) bromophenol blue, 5 % (v/v) β-mercaptoethanol
4 % stacking gel buffer (for 2 big gels)	4.81 mL water, 2.10 mL stacking buffer, 83.5 μL 10 % (w/v) SDS in water, 0.84 mL 40 % acrylamide/*N*,*N*'-methylenebisacrylamide 29:1, 8.35 μL TEMED, 0.50 mL 1.5 % (w/v) APS in water
5 × wash buffer	250 mM Tris HCl, pH 7.5, 5 mM EDTA, 5 M NaCl, 42.5 μM octyl-β-D-glucopyranoside
10 × Ammonium buffer	10 × Ammonium buffer 15 mM $MgCl_2$, Amplicon

10 % resolving gel buffer (for 2 big gels)	15.38 mL water, 9.37 mL resolving gel buffer, 375 μL 10 % (w/v) SDS in water, 9.37 mL 40 % acrylamide/*N,N'*-methylenebisacrylamide 29:1, 18.7 μL TEMED, 3.00 mL 1.5 % (w/v) APS in water
15 % resolving gel buffer (for 2 big gels)	12.38 mL water, 11.25 mL resolving gel buffer, 450 μL 10 % (w/v) SDS in water, 16.88 mL 40 % acrylamide/*N,N'*-methylenebisacrylamide 29:1, 22.5 μL TEMED, 3.60 mL 1.5 % (w/v) APS in water
Agarose sealing solution	190 mM glycine, 25 mM Tris·HCl, 0.1 % (w/v) SDS, 0.0002 % (w/v) bromophenol blue
Blotting buffer	100 mL methanol, 100 mL 10 $\times$ SDS electrophoresis buffer, 800 mL water
Bradford assay buffer	Coomassie Protein Assay Reagent, Thermo Scientific
Colloidal coomassie stain	0.02 % Coomassie BB-G250, 5 % (w/v) $AlSO_4 \cdot 14\ H_2O$, 10 % (v/v) EtOH, 2 % (v/v) *o*-phosporic acid
Coomassie stain	Imperial Protein Stain, Thermo Scientific
Cross-linking buffer	25 mM Tris pH 7.5, 60 μM $ZnCl_2$
Developing solution	15 g Na_2CO_3, 5 mL sensitizing solution, 125 μL 37 % formaldehyde, 250 mL water
EcoRI Buffer	EcoRI Buffer, New England Biolabs

Enhanced Chemiluminescence	Luminol reagent 1, Luminol reagent 2, Roth
Equilibration buffer I	6 M urea, 75 mM Tris·HCl pH 8.8, 29.3 % (v/v) glycerine, 2 % (w/v) SDS, 0.002 % (v/v) bromophenol blue, 1 % (w/v) DTT
Equilibration buffer II	6 M urea, 75 mM Tris·HCl pH 8.8, 29.3 % (v/v) glycerine, 2 % (w/v) SDS, 0.002 % (v/v) bromophenol blue, 2.5 % (w/v) iodoacetamide
Fixing solution	500 mL ethanol, 100 mL acetic acid, 400 mL water, 500 μL 37 % formaldehyde
Infiltration buffer	10 mM MES, pH 5, 10 mM $MgCl_2$, 1 mM acetosyringone
LB medium	1 % (w/v) tryptone, 1 % (w/v) NaCl, 0.5 % (w/v) yeast extract, pH 7.0
MMP buffer	50 mM Tris·HCl pH 7.5, 0.2 M NaCl, 5 mM $CaCl_2$, 0.02 % (w/v) Brij 35
MMP-2/MMP-7 Substrate, Fluorogenic	Calbiochem
Oil PlusOne Dry Strip Cover Fluid	GE Healthcare
PBS buffer	10 mM $Na_2HPO_4 \cdot H_2O$, 1.8 mM KH_2PO_4, 2.7 mM KCl, 140 mM NaCl, pH 7.2
Rehydration buffer	0.5 % (v/v) IPG-buffer pH 3–10 in DeStreak^{TM} rehydration solution, GE Healthcare

Resolving gel buffer	1.5 M Tris·HCl, pH 8.8
SDS electrophoresis buffer	190 mM glycine, 25 mM Tris·HCl, 0.1 % (w/v) SDS
Sensitizing solution	100 mg $Na_2S_2O_3 \cdot 5\ H_2O$, 500 mL water
Stacking gel buffer	0.5 M Tris·HCl, pH 6.8
Staining solution	400 mg $AgNO_3$, 150 μL 37 % formaldehyde, 200 mL water
Stop solution	60 mL acetic acid, 220 mL ethanol, 220 mL water
T4 DNA Ligase buffer	Promega
TAE buffer	40 mM Tris·HCl, 40 mM acetic acid, 1 mM EDTA, pH 8.0
TBS buffer	50 mM Tris·HCl pH 7.5, 150 mM NaCl, 0.02 % (w/v) Brij 35
TBS-T buffer	0.1 % (v/v) Tween-20 in TBS buffer

Proteins

αHA proteins	Monoclonal Anti-HA-Biotin (Mouse, Clone HA-7, 1:2500), Sigma-Aldrich; Anti-HA-HRP (3F10, 1:2000), Roche; α-HA antibody (Mouse, 8:10000), Sigma
α-mouse-HRP	α-Mouse-HRP (Rabbit, 6:10000), Pierce
ARSA, ARSB	Supplied as purified enzyme by Prof. T. Dierks, BCI, Bielefeld University
ARSG	Supplied as purified enzyme by Dr. M.-A. Frese, BCI, Bielefeld University
BSA	PAA Laboratories GmbH

hMMP-2	Proenzyme, Human, Recombinant, CHO Cells, Calbiochem
hMMP-2	Proenzyme, Human, Rheumatoid, Synovial, Fibroblast 1:1-complex with TIMP-2, Calbiochem
hMMP-9	Proenzyme, Human, Recombinant, CHO Cells, Calbiochem
Ligase	T4 DNA Ligase, Promega
KARS	Supplied as purified enzyme by M. Schröder, OCIII, Bielefeld University
PARS	Supplied as purified enzyme by Dr. S. R. Hanson, TSRI, La Jolla
Prepurified KARS	Expressed in *E. coli* and purified by ion exchange chromatography, Biochemistry Practical Course 2008, Bielefeld University, Germany [83]
Protein Marker	Prestained Protein Marker, Broad Range, New England Biolabs
Protein Marker	SeeBlue® Plus, Invitrogen
Proteinase inhibitor cocktail	proteinase inhibitor cocktail 1:100, Sigma
Restriction endonucleases	XhoI, PstI, NcoI, HindIII, EcoRI, New England Biolabs
Streptavidin-HRP	Ultrasensitive streptavidin-HRP (1:5000), Sigma-Aldrich
Taq DNA polymerase	Taq polymerase, Amplicon
Trypsin	sequencing grade, Roche; Seq. Grade Modified Trypsin, Porcine, Promega

5.3 General Biochemical Methods

5.3.1 Electrophoresis

Agarose Gel Electrophoresis

Gels were prepared by dissolving 1 % (w/v) agarose in TEA buffer. The agarose was melted in a microwave, ethidium bromide was added to a final concentration of 0.5 μg/mL, and the solution was poured into a sealed gel casting platform. The DNA samples to be resolved were mixed with respective volumes of DNA loading buffer. The electrophoresis was performed in a gel chamber filled with TEA at a voltage of 120 V for 20 min.

SDS-GE[179]

Protein samples were separated according to protein size by SDS-GE under denaturing conditions. Small gels (8 × 7 cm) were cast into disposable cassettes. For big gels (15 × 13 cm) glass plates with spacers were used as described in the manual. Resolving gels were allowed to polymerize for 1–3 h before the stacking gels were cast on top.

Samples for SDS-GE were mixed with corresponding volumes of 3 × sample buffer and denatured for 5 min at 95 °C, briefly centrifuged and loaded on the gel. Electrophoresis of small gels was performed at constant voltage of 125 V per gel for 60 min in SDS electrophoresis buffer. Big gels were run at 100 V per gel for 15 min and 200 V per gel for 3 h. Proteins were then either blotted, stained with Coomassie or colloidal Coomassie stain. Briefly, gels were washed 3 × 5 min with water and stained overnight. Destaining was achieved by washing with water. For dilute samples, MALDI-ToF compatible silver staining was used: Gels were fixed for at least 60 min in fixing solution and then washed twice for 25 min each in ethanol/water = 1:1. The gels were incubated for 1 min in

sensitizing solution and then washed 3 × 20 s in water. Staining was done for 20 min in staining solution followed by washing with water (3 × 20 s). The gel was transferred to a new container and then developed in developing solution for about 3–5 min, until the desired staining was almost achieved. The gel was quickly washed with one change of water and then stop solution was added for at least 10 min. Afterwards the gel was washed 3 × 10 min with water.

2D-GE

Protein samples were diluted with 310-330 μL rehydration buffer to give a final volume of 340 μL and submitted to isoelectric focusing on Immobiline dry strips as described in the manual. The following program was used for focusing: 1. Step: 10 V, 1 h; 2. Step: 30 V, 12 h; 3. Step: 500 V, 1 h; 4. Gradient: 1000 V, 8 h; 5. Gradient: 8000 V, 3 h; 6. Step: 8000 V, 2 h; 7. Step: 100 V, until further use of strips.

Subsequently, the strips were equilibrated for 15 min each in equilibration buffers I and II before being placed on a 10 % SDS gel. The strips were sealed with agarose sealing solution and electrophoresis was conducted as described above for big gels.

Western Blotting

Following 1D- or 2D-GE, proteins were transferred to PVDF membranes for protein detection via specific interactions of an antibody or streptavidin-biotin binding. The gel, the membrane and two sheets of Whatman paper were equilibrated in blotting buffer, and piled on an electrophoresis chamber for semi-dry transfer. Proteins were blotted at a constant current of 1 mA/cm^2 for 66 min. After blotting the membrane was blocked in 4 % (w/v) BSA in TBS-T for 5 min at rt on a rotator. Streptavidin-HRP, αHA-Biotin or αHA-HRP was added and incubated for 60 min at rt or

overnight at 4 °C. The membrane was washed 5 × 5 min at rt with TBS-T. Then, either streptavidin-HRP was applied, incubated and washed as described, or, protein signals were immediately detected by ECL. Equal volumes of each luminol reagent were premixed and applied to the membrane. The signals were visualized using a CCD-camera.

5.3.2 Protein Analysis

Determination of Protein Concentration

Protein concentrations were measured using Bradford assay buffer as described in the supplied manual. Briefly, 5 μL of each protein sample were mixed with 150 μL of assay buffer and absorbance was detected at 595 nm. Values were normalized using a buffer blank and protein concentrations were calculated from a reference curve using BSA as a standard. All assays were performed in triplicates.

Protein Precipitation

Acetone precipitation: The protein sample was resuspended in four volumes of ice-cold acetone and incubated for 60 min at -20 °C. The precipitated proteins were pelleted by centrifugation at 4 °C for 30 min at 10,000 g. The supernatant was discarded and the pellet was allowed to dry under a stream of N_2.

Trichloroacetic acid (TCA) precipitation: One volume of 100 % (w/v) TCA was added to four volumes of protein sample and incubated for 10 min at 4 °C. The sample was centrifuged at 13,000 rpm in a bench centrifuge for 5 min. The supernatant was removed and the pellet was washed three times with 200 μL of ice-cold acetone. The protein pellet was dried under a stream of N_2.

In-Gel Tryptic Digestion

Protein bands or spots were cut out from coomassie stained gels and divided into 1 mm^3 pieces. The gel slabs were washed with 250 μL of ACN/H_2O = 1:1 (5 min), ACN/50 mM NH_4HCO_3 = 1:1 (30 min), ACN/ 10 mM NH_4HCO_3 = 1:1 (2 h) and then dried under a stream of N_2. 15 μL 10 mM NH_4HCO_3 and 1 μL trypsin were added and incubated for 2 h at 37 °C. Another 20 μL of 10 mM NH_4HCO_3 were added to prevent drying of the gel pieces. The digests were incubated overnight at 37 °C. The samples were removed from the gel pieces, lyophilized, and stored at -20 °C until LC-MS/MS measurement.

Identification of Proteins by LC-MS/MS

All measurements of sulfatase samples were conducted by B. Müller (Technical Faculty, Bielefeld University). The lyophilized samples were dissolved in 10 μL 5 % ACN/0.1 % TFA, and submitted to nano-LC-MS/MS analysis using a nano-column coupled to the mass spectrometer via a fused silica capillary (50 μm) and a nanospray needle. Eluents: A = 95 % (v/v) H_2O, 5 % (v/v) ACN, 0.1 % (v/v) FA; B = 20 % (v/v) H_2O, 80 % (v/v) ACN, 0.1 % (v/v) FA. Method: flow rate 200 nL/min, gradient (A:B): 0–5 min: 98:2, 5–40 min: 98:2–50:50. Ionization and sample uptake by the mass spectrometer were conducted with a spray/needle voltage of 1.2 kV and a capillary voltage of 30 V at 170 °C. Relevant precursor ions were selected automatically for MS/MS-acquisition using the X-calibur software^{TM} (Thermo Fisher Scientific). Peptide fragmentation was initiated by collision energy (30 % CE, activation time: 30 ms) in the ion-trap MS. All MS/MS-spectra were converted to mzXML-files using ReAdW 4.0.2 (Seattle Proteome Center). Protein identification was performed with MASCOT MS/MS ion search (Matrixscience) against the

SwissProt-database. Search parameters: taxonomy: proteobacteria, instrument: ESI-TRAP, 2 missed cleavage sites, variable modifications: oxidation (M), carbamidomethyl (C), labeling with probe **1c**, peptide tolerance: 1000 ppm, MS/MS tolerance: 800 mmu, peptide charge: +1,+2,+3 monoisotopic, significance threshold (p<): 0.05, automatic scoring. Proteins were annotated with the in-house program QuPE[126] (FDR threshold: 0.05, minimal number of hits: 2).

5.3.3 Bacteria Cultivation

E.coli: LB medium containing 10 μg/mL ampicilin or 50 μg/mL kanamycin was agitated at 37 °C.
Agrobacterium tumefaciens: LB medium containing 50 μg/mL rifampicilin, 50 μg/mL kanamycin and 10 μg/mL gentamycin was agitated at 28 °C.

Glycerol stocks

Glycerol stocks of bacteria were prepared from 500 μL of a fresh overnight culture which was mixed with 500 μL of 50 % (v/v) glycerol. The glycerol cultures were stored at -80 °C until use.

5.3.4 Polymerase Chain Reaction

All PCR samples were set up in a volume of 70 μL, containing 53 μL millipore water, 2 μL cDNA, 7.5 μL 10 $\times$ Ammonium buffer, 1 μL each of 10 μM forward and reverse primers, 1.5 μL 10 mM dNTPs and 1 μL *Taq* DNA polymerase. Cycling parameters were 2 min at 94 °C, 20 s at 94 °C, 25 s at 56 °C, 2 min at 72 °C, with 26 cycles and a final step of 5 min at 72 °C. The resulting DNA fragments were resolved by preparative agarose gel electrophoresis and purified using the DNA purification kit.

For this purpose, cDNA bands were quickly excised from the gel under UV irradiation. The gel slabs were weighed and the weight was multiplied by the percentage of the original agarose gel: for 100 mg·% 300 μL buffer QG were added and incubated at 37 °C for 15 min to solubilize the cDNA. The resulting solution was applied to the purification column, washed with 500 μL QG buffer, 750 μL PE+EtOH buffer and then dried by centrifugation (11,000 rpm for 3 min). The DNA was eluted by incubation with 30 μL EB for 2 min at rt and subsequent centrifugation at 13,000 rpm for 3 min.

For colony PCR, eight colonies of each agar plate were picked with a sterile yellow pipet tip which was then put into a 96-well plate well containing 50 μL sterile water. PCR samples of a total volume of 25 μL contained 15.2 μL millipore water, 5 μL of the picked colony in water, 2.5 μL 10 $\times$ Ammonium buffer, 0.75 μL of each primer, 0.5 μL 10 mM dNTPs and 0.3 μL *Taq* DNA polymerase. Cycling parameters were 2 min at 94 °C, 20 s at 94 °C, 25 s at 56 °C, 2 min at 72 °C, with 26 cycles and a final step of 5 min at 72 °C.

5.3.5 Transformation of Bacteria

Restriction Enzyme Digestion and Ligation

15 μL of the purified cDNA (insert) and 5 μL of the purified plasmids were digested in a total volume of 60.6 μL containing 6 μL 10 $\times$ NE3 buffer, 0.5 μL of each restriction enzyme and 0.6 μL BSA 100 $\times$ purified. The digestion proceeded for 2 h at 37 °C without agitation. The digests were then purified using the DNA purification kits. The samples were first diluted with a fivefold volume of PBI buffer and then applied to the purification columns. The columns were washed twice with 750 μL PE buffer and dried by centrifugation (13,000 rpm, 2 min). The digests were

eluted after incubation with 30 μL EB for 2 min at rt and subsequent centrifugation at 13,000 rpm for 2 min.

Ligation was done in a total volume of 30 μL with 4 μL of the digested plasmid, 3 μL of the digested insert and 1 μL ligase in T4 DNA Ligase buffer. After 60 min of incubation 1 μL of ligase was added and the ligation was allowed to proceed for another 60 min. The DNA was then precipitated by first adding 3 μL of 3 M NaOAc, pH 5.2 followed by 30 μL of *iso*propanol, a short incubation on ice and centrifugation at 13,000 rpm and 4 °C for 30 min. The pellet was carefully washed once with 70 % (v/v) EtOH and then taken up in 10 μL millipore water.

Quick Digestion and Ligation Method

Plasmids were digested in a total volume of 100 μL. 5 μL of the plasmid with insert and 5 μL of the new plasmid were mixed with 10 μL of EcoRI Buffer, 1.5 μL HindIII, 1.5 μL EcoRI and 77 μL water. The samples were incubated for 2 h at 37 °C and then for 15 min at 72 °C. The DNA was precipitated by addition of 5 μL 3 M NaOAc and 100 μL *iso*propanol and incubation for 15 min on ice. The DNA was pelleted by centrifugation at 13,000 rpm for 30 min and 4 °C. The pellet was washed once with 50 μL 70 % (v/v) EtOH and centrifuged again at 13,000 rpm for 10 min and 4 °C. The pellet was taken up in the ligase mix (3 μL T4 DNA Ligase buffer, 1 μL Ligase and 26 μL water) and incubated for 2 h at rt. The DNA was precipitated again as described after the digestion step. The DNA was taken up in 10 μL water.

Electroporation of Bacteria

Competent *E. coli* (DH10B, Invitrogen) or *A. tumefaciens* (GV3101) bacteria were transformed with purified plasmid DNA using electroporation (1800 V).[170] For each transformation reaction 50 μL cells were thawed

on ice, mixed with 3 μL of the purified plasmids and incubated on ice for 1 min. The cells were then transferred to a sterile UV cuvette and inserted into the electroporator. Immediately after electroporation, 1 mL of LB medium was added and the bacteria were incubated for 1 h at 37 °C before spreading them on agar plates containing the respective antibiotics. The success of transformation was monitored by colony PCR and agarose gel electrophoresis. The three most promising clones were selected for plasmid purification and nucleotide sequencing.

Plasmid Purification

For plasmid purification with the plasmid purification kit, an overnight culture was pelleted by centrifugation at 1670 g at 4 °C for 20 min. The pellet was taken up in 250 μL A1 Buffer and transferred into an Eppendorf tube. 250 μL of A2 Buffer were added, the mixture was inverted well and incubated for 4 min at rt. 300 μL A3 Buffer were added, the tubes were inverted and centrifuged for 15 min at 13,000 rpm. The supernatant was applied to the column and spun down for 1 min at 11,000 rpm. The column was subsequently washed with 500 μL AW and 600 μL A4 Buffer with centrifugation for 1 min at 11,000 rpm each. The column was dried by centrifugation for 2 min at 11,000 rpm. The plasmids were eluted by incubation with 50 μL AE Buffer for 2 min at rt and then spun down for 1 min at 11,000 rpm. 20 μL of the eluate was submitted to sequencing.

5.3.6 Transient Expression of Proteins in *N. benthamiana* by *A. tumefaciens* Infiltration

Overnight *A. tumefaciens* cultures were centrifuged at 1500 g for 20 min and 4 °C. The bacteria were resuspended in infiltration buffer and incubated for 2 h at rt. The OD_{600} was adjusted to 2 and the cultures ex-

pressing At-MMPs were mixed in a 1:1 ratio (v/v) with p19-expressing *A. tumefaciens*. *N. benthamiana* leaves of four week-old plants were infiltrated with the bacteria suspension and allowed to grow (14 h light, 10 h dark) for 3–6 days. Only p19-expressing cultures were used for control plants.

6 Conclusion

Activity- and affinity-based proteomics methods as applied in this work offer unprecedented opportunities to characterize enzymes using their respective activity or affinity profiles (Figures 6.1 and 6.2).

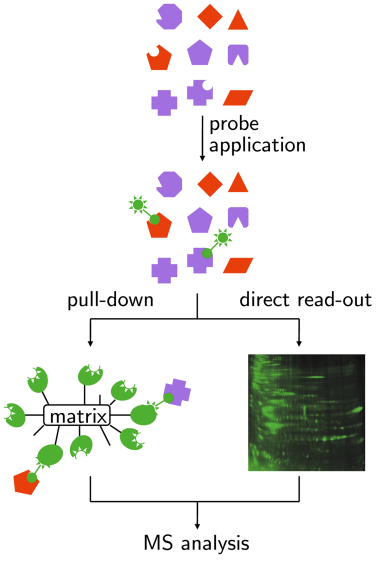

Figure 6.1: The activity-based proteomics workflow as applied to the investigation of sulfatases. Samples were labeled and then either analyzed via 2D-GE tryptic digestion and MS-based fingerprint analysis or enriched, tryptically digested and identified via MS.

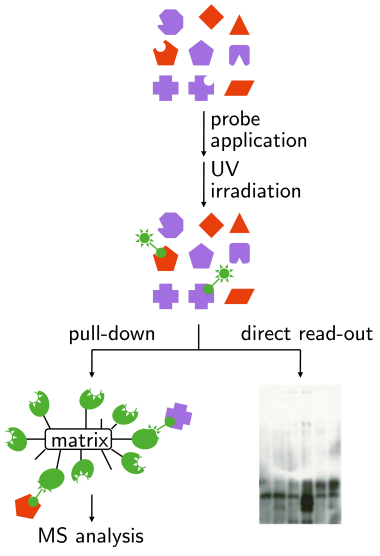

Figure 6.2: Affinity-based proteomics approach as applied to leaf lysates expressing At-MMPs. Samples were labeled, irradiated and then investigated by streptavidin blotting as well as enriched, tryptically digested, and the bound proteins were identified via LC-MS/MS.

The output of these techniques can be manifold: novel enzymes are identified from crude lysates or changes in the activity of individual enzymes

and enzyme families can be monitored. Thereby, the physiological roles that enzymes play in cells and/or organisms are elucidated. In this work, two enzyme classes were investigated: sulfatases by activity-based proteomics and matrix metalloproteases by affinity-based proteomics.

Since sulfatases are key players in diseases such as cancer and inflammation as well as hereditary disorders, activity-based proteomics provides important methods to attain information about their catalytic integrity in these processes. Sulfatase-directed QM traps were examined based on masked monofluoromethylphenyl sulfates as quinone methide precursors for sulfatases. The sulfatase-directed probe **1a**[40,107] was found to have mechanism-dependent irreversible inactivation properties against aryl sulfatases in comparison to previously designed difluoromethylphenyls.[9] MFPS **1c** was active against aryl sulfatases operating at neutral and basic pH, including bacterial PARS and KARS and human STS; however, they were not active against the human lysosomal enzyme ARSG (active under acidic conditions).

Sulfatases

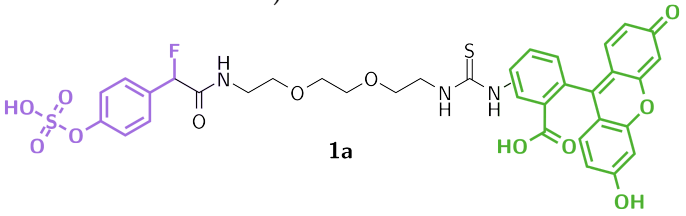

1a

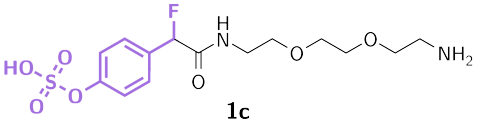

1c

Figure 6.3: Structures of MFPS QM precursor probe **1a** with fluorescein as reporter group and MFPS inhibitor **1c**.

Despite good inactivation and reasonable reactivity toward the enzyme class, ^{19}F-NMR experiments of MFPS **1c** with purified PARS and KARS demonstrated that sulfatase inactivation occurs only after an excess of QM traps are enzymatically generated. This leads to multiple enzyme

labeling events as shown by LC-MS/MS analysis of **1c**-labeled KARS and PARS, presumably through non-specific QM capture of the enzymes.

The activity of fluorescent MFPS probe **1a** in complex proteomes confirmed that the sulfatase-directed QM traps required enzymatic activation, but lead to non-specific labeling of many different enzyme classes. Furthermore, QM trapping sites on the bacterial sulfatase PARS are most probably on solvent exposed regions of the enzyme as investigated by LC-MS/MS of tryptic digests of **1c**-labeled PARS. Unfortunately, such behavior does not meet the stringent requirements for activity-based proteomics, which must be able to decisively report on the activity of a specific enzyme class by turnover-dependent labeling in the context of the greater proteome.[33] Therefore, it can be concluded that quinone methide probes are not suitable for activity-based proteomics studies of sulfatases, since selective labeling of their target enzymes is too slow and diffusion of the activated species takes place.

In search for a different suicide inhibitor which could be incorporated into the presented modular probe synthesis, alkynylated cyclic sulfamates **2b** and **2c** as well as azido-reporter groups **37** and **39** were synthesized and biochemically evaluated.

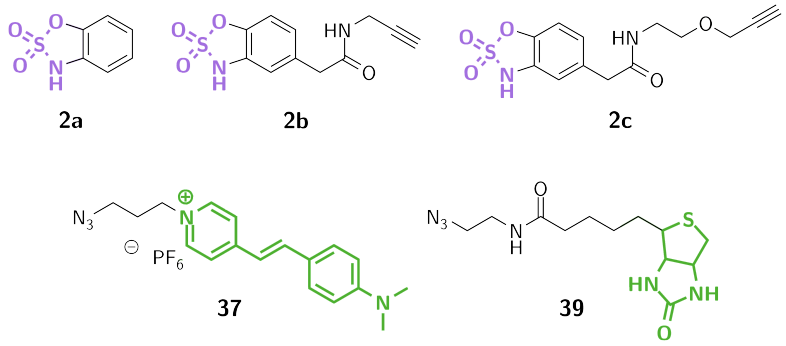

Figure 6.4: Cyclic sulfamates **2a**, **b** and **c** and reporter groups **37** and **39**.

Apparently, CySAs target and modify the active site FGly residue. This was shown by labeling PARS with CySA **2a** which impairs labeling of the

aldehyde-targeting fluorescence dye Alexa Fluor® 488 hydroxylamine. Even though the CySA labeling mechanism leads to a product robust enough to be detected after SDS-GE, it escapes a direct characterization by LC-MS/MS which only shows a decrease of the FGly-bearing PARS fragment after CySA **2a** labeling. First 1D- and 2D-GE labeling studies are promising to further pursue the investigation of sulfatase activity by cyclic sulfamates with the molecular tools now in hands.

Fluorescence microscopy could now be employed to visualize sulfatase activity in tissue samples. This might prove a valuable method for sulfatase deficiency diagnostics in the future. It would also be possible to screen cell lysates to identify novel sulfatases.

Matrix metalloproteases

Matrix metalloproteases are a newly described family of plant proteins with interesting physiological roles in growth and development as well as pathogen defense.[21,156,158] Probe **3** which is based on the human MMP inhibitor marimastat **42** was developed in cooperation with caprotec bioanalytics GmbH, Berlin and proved to be a high-affinity photoreactive probe for hMMPs.

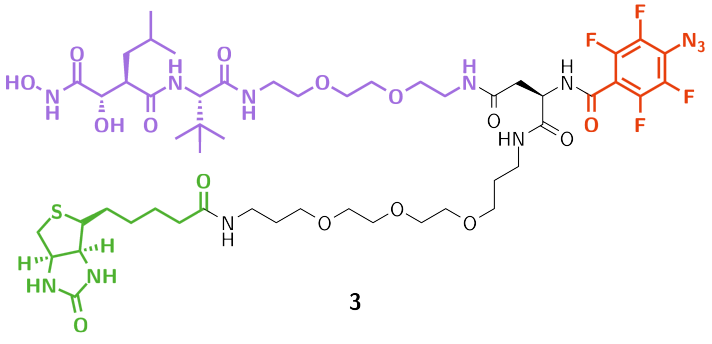

Figure 6.5: Photoreactive Marimastat-based affinity probe with **biotin** as the reporter group.

To apply this probe to plant MMPs, four *Arabidopsis thaliana* MMPs were transiently overexpressed in *Nicotiana benthamiana* leaves via agroinfiltration. Marimastat-probe **3** was successfully applied to label overexpressed At2-, At4- and At5-MMP, and additionally an endogenous *Nicotiana benthamiana* MMP in total leaf extracts by means of streptavidin blotting and LC-MS/MS analysis. This labeling was marimastat-sensitive

which is a strong indicator for the specificity of binding. Affinity-based photoreactive capturing was thereby successfully applied to plant samples for the first time. The labeling of NMMP should be further pursued: MMPs have only once been identified from an endogenous source before (synovial fluid of an arthritis patient which contains elevated levels of active hMMPs).[20]

Since most At-MMPs are transmembrane proteins, their signals should be increased by optimizing the protein extraction protocol to enrich for membrane proteins. Application of the developed probe and the established workflow will hopefully contribute to the elucidation of the role and post-translational regulation of plant MMPs during plant-pathogen interactions and other biological processes.

Bibliography

[1] M.C. Hagenstein, N. Sewald, *J. Biotechnol.* **2006**, *124*, 56–73.

[2] D.K. Nomura, J.Z. Long, S. Niessen, H.S. Hoover, S.-W. Ng, B.F. Cravatt, *Cell* **2010**, *140*, 49–61.

[3] M.Bantscheff, D. Eberhard, Y. Abraham, S. Bastuck, M. Boesche, S. Hobson, T. Mathieson, J. Perrin, M. Raida et al., *Nat. Biotechnol.* **2007**, *25*, 1035–1044.

[4] N. Jessani, S. Niessen, B.Q. Wei, M. Nicolau, M. Humphrey, Y. Ji, W. Han, D.Y. Noh, J.R. 3rd Yates, S.S. et al., *Nat. Methods* **2005**, *2*, 691–697.

[5] A.Y. Strongin, *Cancer Metastasis Rev.* **2006**, *25*, 87–98.

[6] G. Parenti, B. Meroni, A. Ballabio, *Curr. Opin. Genet. Dev.* **1997**, *7*, 386–391.

[7] S.R. Hanson, M.D. Best, C.-H. Wong, *Angew. Chem.* **2004**, *116*, 5858–5886, *Angew. Chem. Int. Ed.* **2004**, *43*, 5736–5763.

[8] C.-L. Lu, C.-T. Ren, S.-H. Wu, C.-Y. Chu, L.-C. Lo, *ChemBioChem* **2007**, *8*, 2187–2190.

[9] S.R. Hanson, L.J. Whalen, C.-H. Wong, *Bioorg. Med. Chem.* **2006**, *14*, 8386–8395.

[10] H. Birkedal-Hansen, W.G.I. Moore, M.K. Bodden, L.J. Windsor, B. Birkedal-Hansen, A. DeCarlo, J.A. Engler, *Crit. Rev. Oral Biol. Med.* **1993**, *2*, 197–250.

[11] J.G. Erhardt, H.K. Biesalski, L.C. Malaba, N.E. Craft, *Clin. Chem.* **2003**, *2*, 339–340.

[12] A. Saghatelian, N. Jessani, A. Joseph, M. Humphrey, B.F. Cravatt, *Proc. Natl. Acad. Sci. USA* **2004**, *101*, 10000–10005.

[13] S.A. Sieber, S. Niessen, H.S. Hoover, B.F. Cravatt, *Nat. Chem. Biol.* **2006**, *5*, 274–281.

[14] M.A. Leeuwenburgh, P.P Geurink, T. Klein, H.F. Kauffman, G.A. van der Marel, R. Bischoff, H.S. Overkleeft, *Org. Lett.* **2006**, *8*, 1705–1708.

[15] P.P. Geurink, T. Klein, L. Prèly, K. Paal, M.A. Leeuwenburgh, G.A. van der Marel, H.F. Kauffman, H.S. Overkleeft, R. Bischoff, *Eur. J. Org. Chem.* **2010**, *11*, 2100–2112.

[16] E.W.S. Chan, S. Chattopadhaya, R.C. Panicker, X. Huang, S.Q. Yao, *J. Am. Chem. Soc.* **2004**, *126*, 14435–14446.

[17] A. David, D. Steer, S. Bregant, L. Devel, A. Makaritis, F. Beau, A. Yiotakis, V. Dive, *Angew. Chem.* **2007**, *119*, 3339–3341, *Angew. Chem. Int. Ed.* **2007**, *46*, 3275–3277.

[18] K. Jenssen, K. Sewald, N. Sewald, *Bioconj. Chem.* **2004**, *15*, 594–600.

[19] M. Collet, J. Lenger, K. Jenssen, H.P. Plattner, N. Sewald, *J. Biotechnol.* **2006**, *129*, 316–328.

[20] J.R. Freije, T. Klein, J.A. Ooms, J.P. Franke, R. Bischoff, *J. Prot. Res.* **2006**, *5*, 1186–1194.

[21] J.M. Maidment, D. Moore, G.P. Murphy, G. Murphy, I.M. Clark, *J. Biol. Chem.* **1999**, *274*, 34706–34710.

[22] V. Kähäri, U. Saarialho-Kere, *Ann. Med.* **1999**, *31*, 34–45.

[23] Janina Lenger, *Diplomarbeit* **Juni 2006**, *Synthese und Anwendung einer Sonde für Matrix-Metalloproteasen in der funktionellen Proteomik*, Universität Bielefeld.

[24] Hannes Patrik Plattner, *Dissertation* **April 2009**, *Molekulare Werkzeuge für die Bioanalytik*, Universität Bielefeld.

[25] P.Q. James, *Rev. Biophys.* **1997**, *30*, 279–331.

[26] A.J. Link, J. Eng, D.M. Schieltz, E. Carmack, G.J. Mize, D.R. Morris, B.M. Garvik, J.R. 3rd Yates, *Nat. Biotechnol.* **1999**, *17*, 676–682.

[27] G. MacBeath, *Nat. Genet.* **2002**, *32 (suppl.)*, 526–532.

[28] Y. Liu, M.P. Patricelli, B.F. Cravatt, *Proc. Natl. Acad. Sci. USA* **1999**, *96*, 14694–14699.

[29] D. Greenbaum, K.F. Medzihradszky, A. Burlingame, M. Bogyo, *Chem. Biol.* **2000**, *7*, 569–581.

[30] A. Borodovsky, H. Ovaa, N. Kolli, T. Gan-Erdene, K.D. Wilkinson, H.L. Ploegh, B.M. Kessler, *Chem. Biol.* **2002**, *9*, 1149–1159.

[31] D.S. Johnson, K. Ahn, S. Kesten, S.E. Lazerwith, Y. Song, M. Morris, L. Fay, T. Gregory, C. Stiff et al., *Bioorg. Med. Chem. Lett.* **2009**, *19*, 2865–2869.

[32] T. Böttcher, M. Pitscheider, S.A. Sieber, *Angew. Chem.* **2010**, *122*, 2740-2759, *Angew. Chem. Int. Ed.* **2010**, *49*, 2680–2698.

[33] B.F. Cravatt, A.T. Wright, J.W. Kozarich, J. W. *Annu. Rev. Biochem.* **2008**, *77*, 383–414.

[34] M. Fonovic, M. Bogyo, *Expert Rev. Proteomics* **2008**, *5*, 721–730.

[35] M. Uttamchandani, J. Li, H. Sun, S.Q. Yao, *ChemBioChem* **2008**, *9*, 667–675.

[36] M.J. Evans, B.F. Cravatt, *Chem. Rev.* **2006**, *106*, 3279–3301.

[37] E. Sabidó, T. Tarragó, S. Niessen, B.F. Cravatt, E. Giralt, *ChemBioChem* **2009**, *10*, 2361–2366.

[38] D. Greenbaum, A. Baruch, L. Hayrapetian, Z. Darula, A. Burlingame, K.F. Medzihradszky, M. Bogyo, *Mol. Cell. Proteomics* **2002**, *1*, 60–68.

[39] I. Staub, S.A. Sieber, *J. Am. Chem. Soc.* **2009**, *131*, 6271–6276.

[40] J. Lenger, M. Schröder, E.C. Ennemann, B. Müller, C.-H. Wong, T. Noll, T. Dierks, S.R. Hanson, N. Sewald, *Bioorg. Med. Chem.*, doi:10.1016/j.bmc.2011.04.044.

[41] K.T. Barglow, B.F. Cravatt, *Angew. Chem.* **2006**, *118*, 7568–7571, *Angew. Chem. Int. Ed.* **2006**, *45*, 7408–7411.

[42] J.P. Alexander, B.F. Cravatt, *J. Am. Chem. Soc.* **2006**, *128*, 9699–9704.

[43] D.A. Bachovchin, S.J. Brown, H. Rosen, B.F. Cravatt, *Nat. Biotechnol.* **2009**, *27*, 387–394.

[44] N. Schaschke, I. Assfalg-Machleidt, T. Laßleben, C.P. Sommerhoff, L. Moroder, W. Machleidt, *FEBS Lett.* **2000**, *482*, 91–96.

[45] I. Staub, S.A. Sieber, *J. Am. Chem. Soc.* **2008**, *130*, 13400–13409.

[46] T. Böttcher, S.A. Sieber, *Angew. Chem.* **2008**, *120*, 4677–4680, *Angew. Chem. Int. Ed.* **2008**, *47*, 4600–4603.

[47] K.A. Kalesh, L.P. Tan, K. Lu, L. Gao, J. Wang, S.Q. Yao, *Chem. Comm.* **2010**, *46*, 589–591.

[48] L.-C. Lo, C.-H. Lo, K.D. Janda, *Bioorg. Med. Chem. Lett.* **1996**, *6*, 2117–2120.

[49] L.-C. Lo, H.-Y. Wang, Z.-J. Wang, *J. Chin. Chem. Soc.* **1999**, *46*, 715–718.

[50] L.-C. Lo, T.-L. Pang, C.-H. Kuo, Y.-L. Chiang, H.-Y. Wang, J.-J. Lin, *J. Prot. Res.* **2002**, *1*, 35–40.

[51] C.-S. Tsai, Y.-K. Li, L.-C. Lo, *Org. Lett.* **2002**, *4*, 3607–3610.

[52] Q. Zhu, X. Huang, G.Y.J. Chen, S.Q. Yao, *Tet. Lett.* **2003**, *44*, 2669–2672.

[53] Q. Zhu, A. Girish, S. Chattopadhaya, S.Q. Yao, *ChemComm* **2004**, 1512–1513.

[54] R. Srinivasan, X. Huang, S.L. Ng, S.Q. Yao, *ChemBioChem* **2006**, *7*, 32–36.

[55] L.-C. Lo, Y.-L. Chiang, C.-H. Kuo, H.-K. Liao, Y.-J. Chen, J.-J. Lin, *Biochem. Biophys. Res. Comm.* **2005**, *326*, 30–35.

[56] C.-P. Lu, C.-T. Ren, Y.-N. Lai, S.-H. Wu, W.-M. Wang, J.-Y. Chen, L.-C. Lo, *Angew. Chem.* **2005**, *117*, 7048–7052, *Angew. Chem. Int. Ed.* **2005**, *44*, 6888–6892.

[57] T. Komatsu, K. Kikuchi, H. Takakusa, K. Hanaoka, T. Ueno, M. Kamiya, Y. Urano, T. Nagano, *J. Am. Chem. Soc.* **2006**, *128*, 15946–15947.

[58] Y.-M. Li, M. Xu, M.-T. Lai, Q. Huang, J.L. Castro, J. Dimuzio-Mower, T. Harrison, C. Lellis, A. Nadin et al., *Nature* **2000**, *405*, 689–694.

[59] J. Lenger, F. Kaschani, T. Lenz, C. Dalhoff, H. Köster, N. Sewald, R.A.L. van der Hoorn, *Bioorg. Med Chem.*, submitted.

[60] S. Chattopadhaya, E.W.S Chan, S.Q. Yao, *Tet. Lett.* **2005**, *46*, 4053–4056.

[61] M.C. Hagenstein, J.H. Mussgnug, K. Lotte, R. Plessow, A. Brockhinke, O. Kruse, N. Sewald, *Angew. Chem.* **2003**, *115*, 5793–5796, *Angew. Chem. Int. Ed.* **2003**, *42*, 5635–5638.

[62] H. Nagase, J.F. Jr. Woessner, *J. Biol. Chem.* **1999**, *31*, 21491–21494.

[63] R. Nakai, C.M. Salisbury, H. Rosen, B.F. Cravatt, *Bioorg. Med. Chem.* **2009**, *17*, 1101–1108.

[64] Y. Hatanaka, Y. Sadanake, *Curr. Top. Med. Chem.* **2002**, *3*, 271–288.

[65] A.M. Sadaghiani, S.H.L. Verhelst, M. Bogyo, M. *Curr. Opin. Chem. Biol.* **2007**, *11*, 1–9.

[66] B.M. Kessler, D. Tortorella, M. Altun, A.F. Kisselev, E. Fiebiger, B.G. Hekking, H.L. Ploegh, H.S. Overkleeft, *Chem. Biol.* **2001**, *8*, 913–929.

[67] D.S. Kirkpatrick, S.A. Gerber, S.P. Gygi, *Methods* **2005**, *25*, 265–273.

[68] O. Hekmat, S. He, R.A.J. Warren, S.G. Withers, *J. Prot. Res.* **2008**, *7*, 3282–3292.

[69] M.P. Patricelli, D.K. Giang, L.M. Stamp, J.J. Burbaum, *Proteomics* **2001**, *9*, 1067–1071.

[70] M. Verdoes, B.I. Florea, U. Hillaert, L.I. Willems, W.A. van der Linden, M. Sae-Heng, D.V. Filippov, A.F. Kisselev, G.A. van der Marel, H.S. Overkleeft, *ChemBioChem* **2008**, *9*, 1735–1738.

[71] G. Blum, R.M. Weimer, L.E. Edgington, W. Adams, M. Bogyo, *PLoS ONE* **2009**, *4*(7), 1–10, e6374.

[72] J. Lee, M. Bogyo, *ACS Chem. Biol.* **2010**, *5*, 233–243.

[73] A.E. Speers, G.C. Adam, B.F. Cravatt, *J. Am. Chem. Soc.* **2003**, *125*, 4686–4687.

[74] R. Orth, S.A. Sieber, *J. Org. Chem.* **2009**, *74*, 8476–8479.

[75] D. Maurel, S. Banala, T. Laroche, K. Johnsson, *ACS Chem. Biol.* **2010**, *5*, 507–516.

[76] E. Weerapana, A.E. Speers, B.F. Cravatt, *Nat. Prot.* **2007**, *2*, 1414–1425.

[77] P. Bojarova, S.J. Williams, *Cur. Opin. Chem. Biol.* **2008**, *12*, 573–581.

[78] M. Sardiello, I. Annunziata, G. Roma, A. Ballabio, *A. Hum. Mol. Genet.* **2005**, *14*, 3203–3217.

[79] T. Dierks, B. Schmidt, K. von Figura, *Proc. Natl. Acad. Sci. USA* **1997**, *94*, 11963–11968.

[80] B. Schmidt, T. Selmer, A. Ingendoh, K. von Figura, *Cell* **1995**, *82*, 271–278.

[81] T. Selmer, A. Hallmann, B. Schmidt, M. Sumper, K. von Figura, *Eur. J. Biochem.* **1996**, *238*, 341–345.

[82] T. Dierks, C. Miech, J. Hummerjohann, B. Schmidt, M. A. Kertesz, K. von Figura, *J. Biol. Chem.* **1998**, *273*, 25560–25564.

[83] C. Miech, T. Dierks, T. Selmer, K. von Figura, B. Schmidt, *J. Biol. Chem.* **1998**, *273*, 4835–4837.

[84] G. Diez-Roux, A. Ballabio, *Annu. Rev. Genomics Hum. Genet.* **2005**, *6*, 355–379.

[85] G. Lukatela, N. Krauss, K. Theis, T. Selmer, V. Gieselmann, K. von Figura, W. Saenger, *Biochemistry* **1998**, *37*, 3654–3664.

[86] C.S. Bond, P.R. Clemens, S.J. Ashby, C.A. Collyer, S.J. Harrop, J.J. Hopwood, J.M. Guss, *Structure* **1997**, *5*, 277–289.

[87] F.G. Hernandez-Guzman, T. Higashiyama, W. Pangborn, Y. Osawa, D. Ghosh, *J. Biol. Chem.* **2003**, *278*, 22989–22997.

[88] I. Boltes, H. Czapinska, A. Kahnert, R. von Bülow, T. Dierks, B. Schmidt, K. von Figura, M.A. Kertesz, I. Uson, *Structure* **2001**, *9*, 483–491.

[89] R. Recksiek, T. Selmer, T. Dierks, B. Schmidt, K. von Figura, *J. Biol. Chem.* **1998**, *273*, 6096–6103.

[90] C.L.L. Chai, W.A. Loughlin, G. Lowe, *Biochem. J.* **1992**, *287*, 805–812.

[91] K.S. Dodgson, G.F. White, J.W. Fitzgerald, *Sulfatases of Microbial Origin*, CRC, Boca Raton, **1982**.

[92] P. Bojarová, E. Denehy, I. Walker, K. Loft, D.P. De Souza, L.W.L. Woo, B.V.L. Potter, M.J. McConville, S.J. Williams, *ChemBioChem* **2008**, *9*, 613–623.

[93] S. Ahmed, K. James, C.P. Owen, C.K. Patel, L. Samspon, *Bioorg. Med. Chem. Lett.* **2002**, *9*, 1279–1282.

[94] T. Utsumi, N. Yoshimura, S. Takeuchi, M. Maruta, K. Maeda, N. Harada, *J. Steroid. Biochem. Mol. Biol.* **2000**, *73*, 141–145.

[95] K.W. Selcer, H. Kabler, J. Sarap, Z. Xiao, P.K. Li, *Steroids* **2002**, *67*, 821–826.

[96] P. Nussbaumer, A. Billich, *Med. Res. Rev.* **2004**, *24*, 529–576.

[97] N.M. Howarth, A. Purohit, M.J. Reed, B.V.L. Potter, *J. Med. Chem.* **1994**, *37*, 219–221.

[98] W. Elger, S. Schwarz, A. Hedden, G. Reddersen, B. Schneider, *J. Steroid Biochem. Mol. Biol.* **1995**, *55*, 395–403.

[99] S.J. Stanway, A. Purohit, L.W.L. Woo, S. Sufi, D. Vigushin, R. Ward, R.H. Wilson, F.Z. Stanczyk, N. Dobbs et al., *Clin. Cancer Res.* **2006**, *12*, 1585–1592.

[100] H.H. Tsai, D. Sunderland, G.R. Gibson, C.A. Hart, J.M. Rhodes, *Clin. Sci* **1992**, *82*, 447–454.

[101] A. Ratzka, H. Vogel, D.J. Kliebenstein, T. Mitchel-Olds, J. Kroymann, *Proc. Natl. Acad. Sci. USA* **2002**, *99*, 11223–11228.

[102] P. Bojarová, S.J. Williams, *Bioorg. Med. Chem. Lett.* **2009**, *19*, 477–480.

[103] V. Ahmed, Y. Liu, S.D. Taylor, *ChemBioChem* **2009**, *10*, 1457–1461.

[104] R. Kitz, I.B. Wilson, *J. Biol. Chem.* **1962**, *237*, 3245–3249.

[105] Q. Wang, U. Dechert, F. Jirik, S.G. Withers, *Biochem. Biophys. Res. Commun.* **1994**, *200*, 577–583.

[106] T.L. Born, J.K. Myers, T.S. Widlanski, F. Rusnak, *J. Biol. Chem.* **1995**, *270*, 25651–25655.

[107] Thomas Kramer, *Diplomarbeit* **Sept. 2007**, *Molekulare Werkzeuge zur Charakterisierung von Sulfatasen*, Universität Bielefeld.

[108] B. Hanney, Y. Kim, M.R. Krout, R. S. Meissner, H.J. Mitchell, J. Musselmann, J.J. Perkins, J. Wang, (Merck & CO., Inc.), US 7,268,153 B2, **2007**.

[109] R. Paul, G.W. Anderson, *J. Am. Chem. Soc.* **1960**, *82*, 4596–4600.

[110] Z. Li, E. Mintzer, R. Bittman, *J. Org. Chem.* **2006**, *71*, 1718–1721.

[111] M. Verdoes, U. Hillaert, B.I. Florea, M. Sae-Heng, M.D.P. Risseeuw, D.V. Filippov, G.A. van der Marel, H.S. Overkleeft, *Bioorg. Med. Chem. Lett.* **2007**, *17*, 6169–6171.

[112] Personal communication by Martijn Verdoes at 7^{th} HUPO 2008, Amsterdam.

[113] T.W. Green, P.G.M. Wuts, *Protective groups in organic synthesis*, 3rd ed. Wiley, New York, **1999**, p.286.

[114] A. Töhl, O. Eberhard, *Chem. Ber.* **1893**, *26*, 2940–2945.

[115] P. Kéle, X. Le, M. Link, K. Nagy, A. Herner, K. Lőrincz, S. Béni, O.S. Wolfbeis, *Org. Biomol. Chem.* **2009**, *7*, 3486–3490.

[116] P. Kéle, G. Mezö, D. Achatz, O.S. Wolfbeis, *Angew. Chem.* **2009**, *121*, 350–353, *Angew. Chem. Int. Ed.* **2009**, *48*, 344–347.

[117] T. Mayer, M.E. Maier, *Eur. J. Org. Chem.* **2007**, *28*, 4711–4720.

[118] S. Bräse, C. Gil, K. Knepper, V. Zimmermann, *Angew. Chem.* **2005**, *117*, 5320–5374, *Angew. Chem. Int. Ed.* **2005**, *44*, 5188–5240.

[119] A.E. Speers, B.F. Cravatt, *Chem. Biol.* **2004**, *11*, 535–546.

[120] T.R. Chan, R. Hilgraf, K.B. Sharpless, V.V. Fokin, *Org. Lett.* **2004**, *6*, 2853–2855.

[121] C. Szameit, C. Miech, M. Balleinigner, B. Schmidt, K. von Figura, T. Dierks, T. *J. Biol. Chem.* **1999**, *274*, 15375–15381.

[122] M.-A. Frese, S. Schulz, T. Dierks, *J. Biol. Chem.* **2008**, *17*, 11388–11395.

[123] M. Mariappan, S.L. Gande, K. Radhakrishnan, B. Schmidt, T. Dierks, K. von Figura, *J. Biol. Chem.* **2008**, *283*, 11556–11564.

[124] J.D. Sellars, M. Landrum, A. Congreve, D.P. Dixon, J.A. Mosely, A. Beeby, R. Edwards, P.G. Steel, *Org. Biomol. Chem.* **2010**, *8*, 1610–1618.

[125] Personal communication by Michaela Wachs and Stefanie Weiland, BCI, Bielefeld University.

[126] S.P. Albaum, H. Neuweger, B. Fränzel, S. Lange, D. Mertens, C. Trötschel, D. Wolters, J. Kalinowski, T. Nattkemper, A. Goesmann, *Bioinformatics* **2009**, *25*, 3128–34.

[127] http://www.invitrogen.com/site/us/en/home/References/Molecular-Probes-The-Handbook/Reagents-for-Modifying-Groups-Other-Than-Thiols-or-Amines/Hydrazines-Hydroxylamines-and-Aromatic-Amines-for-Modifying-Aldehydes-and-Ketones.html, 10/04/2010.

[128] J. Conary, A. Nauerth, G. Burns, A. Hasilik, K. von Figura, *Eur. J. Biochem.* **1986**, *158*, 71–76.

[129] T. Sorsa, L. Tjäderhane, Y.T. Konttinen, A. Lauhio, T. Salo, H.M. Lee, L.M. Golub, D.L. Brown, P. Mänylä, *Ann. Med.* **2006**, *38*, 306–321.

[130] G. Murphy, H. Nagase, *Nat. Clin. Pract. Rheumatol.* **2008**, *4*, 128–135.

[131] K. Kessenbrock, V. Plaks, Z. Werb, *Cell* **2010**, *141*, 52–67.

[132] http://merops.sanger.ac.uk/cgi-bin/famsum?family=M10, 12/03/2011.

[133] R.P.T. Somerville, S.A. Oblander, S.S. Apte, *Genome Biology* 2003, 4, 216.1–216.11.

[134] H. Sato, T. Takino, Y. Okada, J. Cao, A. Shinagawa, E. Yamamoto, M. Seiki, *Nature* **1994**, *370*, 61–65.

[135] Y. Itoh, M. Kajita, H. Kinoh, H. Mori, A. Okada, M. Seiki, *J. Biol. Chem.* **1999**, *274*, 34260–34266.

[136] H.E. Van Wart, H. Birkedahl-Hansen, *Proc. Natl. Acad. Sci. USA* **1990**, *87*, 5578–5582.

[137] H. Birkedahl-Hansen, *Curr. Opin. Cell Biol.* **1995**, *7*, 728–735.

[138] C. Chang, Z. Werb, *Trends Cell Biol.* **2001**, *11*, S37–S43.

[139] G. Preece, G. Murphy, A. Ager, *J. Biol. Chem.* **1996**, *271*, 11634–11640.

[140] M. Suzuki, G. Raab, M.A. Moses, C.A. Fernandez, M. Klagsbrun, *J. Biol. Chem.* **1997**, *272*, 31730–31737.

[141] G.A. McQuibban, G.S. Butler, J.H. Gong, L. Bendall, C. Power, I. Clark-Lewis, C.M. Overall, *J. Biol. Chem.* **2001**, *276*, 43503–43508.

[142] E. Levi, R. Fridman, H.Q. Miao, Y.S. Ma, A. Yayon, I. Vlodavsky, *Proc. Natl. Acad. Sci. USA* **1996**, *93*, 7069–7074.

[143] C.L. Wilson, A.J. Ouellette, D.P. Satchell, T. Ayabe, Y.S. Lopez-Boado, J.L. Stratman, S.J. Hultgren, L.M. Matrisian, W.C. Parks, *Science* **1999**, *296*, 113–117.

[144] A.J. Gearing, S.J. Thorpe, K. Miller, M. Mangan, P.G. Varley, T. Dodgeon, G. Ward, C. Turner, R. Thorpe, *Immunol. Lett.* **2002**, *81*, 41–48.

[145] K. Wada, H. Sato, H. Kinoh, M. Kajita, H. Yamamoto, M. Seiki, *Gene* **1998**, *211*, 57–62.

[146] E. Llano, A.M. Pendas, P. Aza-Blanc, T.B. Kornberg, C. Lopez-Otin, *J. Biol. Chem.* **2000**, *275*, 35978–35985.

[147] T. Lepage, C. Gache, *EMBO J.* **1990**, *9*, 3003–3012.

[148] A.A. Leontovich, J. Zhang, K. Shimokawa, H. Nagase, M.P. Sarras Jr., *Development* **2000**, *127*, 907–920.

[149] A. Hallmann, P. Amon, K. Godl, M. Heitzer, M. Sumper, *Plant J.* **2001**, *26*, 583–593.

[150] T. Kinoshita, H. Fukuzawa, T. Shimade, T. Saito, Y. Matsuda, *Proc. Natl. Acad. Sci. USA* **1992**, *89*, 4693–4687.

[151] J.S. Graham, J. Xiong, J.W. Gilikin, *Plant Physiol.* **1991**, *97*, 786–792.

[152] G. McGreehan, W. Burkhart, R. Anderegg, J.D. Becherer, J.W. Gilikin, J.S. Graham, *Plant Physiol.* **1992**, *99*, 1179–1183.

[153] V.G.R. Delorme, P.F. McCabe, D.-J. Kim, C.J. Leaver, *Plant Physiol.* **2000**, *123*, 917–927.

[154] J.-P. Combier, T. Vernié, F. de Billy, F.E. Yahyaoui, R. Mathis, P. Gamas, *Plant Physiol.* **2007**, *144*, 703–716.

[155] S.M. Ratnaparkhe, E.M.U. Egertsdotter, B.S. Flinn, *Planta* **2009**, *230*, 339–354.

[156] A. Schiermeyer, H. Hartenstein, M.K. Mandal, B. Otte, V. Wahner, S. Schillberg, *BMC Plant Biology* **2009**, *9*, 83.

[157] S. Kang, S.-K. Oh, J.-J. Kim, D. Choi, K.-H. Baek, *Plant Pathol. J.* **2010**, *26*, 402–408.

[158] D. Golldack, O.V. Popova, K.-J. Dietz, *J. Biol. Chem.* **2002**, *277*, 5541–5547.

[159] Y. Liu, C. Dammann, M.K. Bhattacharyya, *Plant Physiol.* **2001**, *127*, 1788–1797.

[160] D. Kim, S. Mobashery, *Curr. Med Chem.* **2001**, *8*, 959–965.

[161] D. Rasnick, J.C. Powers, *Biochemistry* **1978**, *17*, 4363–4369.

[162] S. Brown, M.M. Bernardo, Z.-H. Li, L.P. Kotra, Y. Tanaka, R. Fridman, S. Mobashery, *J. Am. Chem. Soc.* **2000**, *122*, 3410–3411.

[163] H. Köster, D.P. Little, P. Luan, R. Muller, S.M. Siddiqi, S. Marappan, P. Yip, *Assay Drug Dev. Technol.* **2007**, *5*, 381–90.

[164] R.P. Beckett, A.H. Davidson, A.H. Drummond, P. Huxley, M. Whittaker, *Drug Discov. Today* **1996**, *1*, 16–26.

[165] P. Geurink, T. Klein, M. Leeuwenburgh, G. van der Marel, H. Kauffman, R. Bischoff, H. Overkleeft, *Org. Biomol. Chem.* **2008**, *6*, 1244–1250.

[166] S. Bregant, C. Huillet, L. Devel, A.-S. Dabert-Gay, F. Beau, R. Thai, B. Czarny, A. Yiotakis, V. Dive, *J. Prot. Res.* **2009**, *8*, 2484–2494.

[167] Jens Conradi, *Diplomarbeit* **Dez. 2007**, *Klonierung, Expression und funktionelle Studien von Arabidopsis thaliana Matrix-Metalloproteinasen*, Universität Bielefeld.

[168] M. Shabab, T. Shindo, C. Gu, F. Kaschani, T. Pansuriya, R. Chintha, A. Harzen, T. Colby, S. Kamoun, R.A.L. Van der Hoorn, *Plant Cell* **2008**, *20*, 1169–1183.

[169] H.E. Gottlieb, V. Kotlyar, A. Nudelman, *J. Org. Chem.* **1997**, *21*, 7512–7515.

[170] E. Neumann, M. Schaefer-Ridder, Y. Wang, P.H. Hofschneider, *J. EMBO* **1982**, *1*, 841–845.

[171] M.K. Mandal, R. Fischer, S. Schillberg, A. Schiermeyer, *Planta* **2010**, *232*, 899–910.

[172] E.W. Howard, E.C. Bullen, M.J. Banda, *J. Biol. Chem.* **1991**, *266*, 13064–13069.

[173] C. Ries, T. Pitsch, R. Mentele, S. Zahler, V. Egea, H. Nagase, M. Jochum, *Biochem. J.* **2007**, *495*, 547–558.

[174] S. Triebel, J. Bläser, H. Reinke, V. Knäuper, H. Tschesche, *FEBS* **1992**, *298*, 280–284.

[175] N.D. Rawlings, A.J. Barrett, A. Bateman, *Nucleic Acids Res.* **2010**, *38*, D227–D223.

[176] R.A.L. Van der Hoorn, F. Laurent, R. Roth, P.J.G.M. De Wit, *Mol. Plant-Microbe Interact.* **2000**, *13*, 438–446.

[177] M. Wydrow, E. Kozubek, P. Lehmann, *Acta Biochim. Pol.* **2006**, *53*, 289–298.

[178] P. Cornelis, M.C. Dupont-de Patoul, *Phytochemistry* **1975**, *14*, 397–401.

[179] U. K. Laemmli, *Nature* **1970**, *227*, 680-685.